



**HAL**  
open science

## Validation of non-equilibrium kinetics in CO<sub>2</sub> –N<sub>2</sub> plasmas

C Fromentin, T Silva, T Dias, E Baratte, O Guaitella, V Guerra

► **To cite this version:**

C Fromentin, T Silva, T Dias, E Baratte, O Guaitella, et al.. Validation of non-equilibrium kinetics in CO<sub>2</sub> –N<sub>2</sub> plasmas. Plasma Sources Science and Technology, 2023, 32 (5), pp.054004. 10.1088/1361-6595/acce64 . hal-04514662

**HAL Id: hal-04514662**

**<https://polytechnique.hal.science/hal-04514662>**

Submitted on 15 May 2024

**HAL** is a multi-disciplinary open access archive for the deposit and dissemination of scientific research documents, whether they are published or not. The documents may come from teaching and research institutions in France or abroad, or from public or private research centers.

L'archive ouverte pluridisciplinaire **HAL**, est destinée au dépôt et à la diffusion de documents scientifiques de niveau recherche, publiés ou non, émanant des établissements d'enseignement et de recherche français ou étrangers, des laboratoires publics ou privés.

# Validation of non-equilibrium kinetics in CO<sub>2</sub>-N<sub>2</sub> plasmas

C. Fromentin<sup>1</sup>, T. Silva<sup>1</sup>, T. C. Dias<sup>1</sup>, E. Baratte<sup>2</sup>, O. Guaitella<sup>2</sup> and V. Guerra<sup>1</sup>

<sup>1</sup> Instituto de Plasmas e Fusão Nuclear, Instituto Superior Técnico, Universidade de Lisboa, Portugal

<sup>2</sup> Laboratoire de Physique des Plasmas (UMR 7648), CNRS, Univ. Paris Saclay, Sorbonne Université, École Polytechnique, France

## Abstract

This work explores the effect of N<sub>2</sub> addition on CO<sub>2</sub> dissociation and on the vibrational kinetics of CO<sub>2</sub> and CO under various non-equilibrium plasma conditions. A self-consistent kinetic model, previously validated for pure CO<sub>2</sub> and CO<sub>2</sub>-O<sub>2</sub> discharges, is further extended by adding the kinetics of N<sub>2</sub>. The vibrational kinetics considered include levels up to  $v = 10$  for CO,  $v = 59$  for N<sub>2</sub> and up to  $v_1 = 2$  and  $v_2 = v_3 = 5$ , respectively for the symmetric stretch, bending and asymmetric stretch modes of CO<sub>2</sub>, and account for electron-impact excitation and de-excitation (e-V), vibration-to-translation (V-T) and vibration-to-vibration energy exchange (V-V) processes. The kinetic scheme is validated by comparing the model predictions with recent experimental data measured in a DC glow discharge operating in pure CO<sub>2</sub> and in CO<sub>2</sub>-N<sub>2</sub> mixtures, at pressures in the range 0.6 - 4 Torr (80.00 – 533.33 Pa) and a current of 50 mA. The experimental results show a higher vibrational temperature of the different modes of CO<sub>2</sub> and CO and an increased dissociation fraction of CO<sub>2</sub>, that can reach values as high as 70 %, when N<sub>2</sub> is added to the plasma. On the one hand, the simulations suggest that the former effect is the result of the CO<sub>2</sub>-N<sub>2</sub> and CO-N<sub>2</sub> V-V transfers and the reduction of quenching due to the decrease of atomic oxygen concentration; on the other hand, the dilution of CO<sub>2</sub> and dissociation products, CO and O<sub>2</sub>, reduces the importance of back reactions and contributes to the higher CO<sub>2</sub> dissociation fraction with increased N<sub>2</sub> content in the mixture, while the N<sub>2</sub>(B<sup>3</sup>Π<sub>g</sub>) electronically excited state further enhances the CO<sub>2</sub> dissociation.

## I. Introduction

To reach climate neutrality (balance between greenhouse gas emission sources and sinks [1]) and limit the irreversibility, severity and likelihood of climate hazards and their widespread impacts on human and natural ecosystems [2,3], by holding the temperature increase below 2°C in line with the Paris Agreement [4], breakthrough innovations are required. Some existing and under-development technologies for CO<sub>2</sub> valorisation in the world are briefly reviewed in [5]. The conversion of CO<sub>2</sub> into value-added chemicals and liquid fuels, via the CO<sub>2</sub> Capture and Utilization (CCU) approach is a potential way to not only decrease the CO<sub>2</sub> emissions, but also generate more economic value, reduce the dependence of fossil fuels and create the possibility to recycle CO<sub>2</sub> and close the carbon cycle [6]. The dissociation of CO<sub>2</sub> into CO is the critical step of any CCU process. Indeed, CO<sub>2</sub> is, thermodynamically, a very stable molecule so there are large energy barriers to overcome for its conversion. A very promising approach to achieve efficient dissociation of CO<sub>2</sub> is the use of non-thermal plasmas (NTPs) [7–18] benefiting from non-equilibrium conditions where high energy electrons coexist with cold ions and neutrals. The kinetics of nonequilibrium processes can be stimulated by vibrational excitation of molecules in the plasma [19]. Depending mainly on the electron temperature [20], NTPs can selectively transfer energy from the electrons (gaining energy from the electric field) to the heavy particles in the plasma to initiate certain chemical processes like the dissociation of CO<sub>2</sub> with lower energy compared to conventional methods [21]. CO<sub>2</sub> dissociation has been the focus of many studies, exploring electron-impact [22–24], vibrationally driven [19,24–27] and thermal [28–30] dissociation routes.

In the last few years, a combination of computational simulations and experimental campaigns have contributed to a better understanding of CO<sub>2</sub>-containing discharges [31–38] and to the development of the corresponding “reaction mechanisms”, i.e., a set of reactions and rate coefficients validated

against benchmark experiments. In particular, our modelling results were validated step-by-step against experimental data obtained using direct current (DC) glow discharges (plasmas sustained by high voltages inside a pair of electrodes) and advanced plasma diagnostics, namely Fourier Transform Infrared (FTIR) absorption spectroscopy [36] and optical emission spectroscopy (OES) [39]. By selecting specific working conditions in low-pressure glow discharges, the accuracy of the Electron Energy Distribution Function (EEDF) calculations, electron-impact vibrational excitation and de-excitation (e-V), vibration-to-vibration (V-V) and vibration-to-translation (V-T) energy transfer processes coefficients, and the rate coefficients of the main plasma processes could be tested in low CO<sub>2</sub> excitation regime. Our previous modelling research works were focused on:

- (i) The electron-neutral scattering cross sections for CO<sub>2</sub> [40] and CO [41],
- (ii) The validation of the electron-impact dissociation cross sections of CO<sub>2</sub> [22],
- (iii) The study of the time-resolved evolution of the lower vibrationally excited CO<sub>2</sub> levels during the afterglow of CO<sub>2</sub> discharges, validating a set of V-V and V-T processes involving the lower  $\sim 70$  states and the corresponding rate coefficients [32],
- (iv) The extension of the model by including the e-V processes and studying the effect of electrons on the distribution of vibrationally excited CO<sub>2</sub> levels in pulsed and continuous glow discharges [33] to understand the transfer of electron energy toward CO<sub>2</sub> vibrations,
- (v) The study of the dynamics of gas heating in the afterglow of pulsed CO<sub>2</sub> and CO<sub>2</sub>-N<sub>2</sub> glow discharges, further validating the V-V and V-T mechanisms and rate coefficients [35],
- (vi) The preliminary study of the N<sub>2</sub> influence on CO<sub>2</sub> the vibrational distribution functions in pulsed glow discharges using a simplified kinetic scheme [34],
- (vii) The development of a reaction mechanism for ‘vibrationally cold CO<sub>2</sub> plasmas’ taking into account the CO<sub>2</sub> dissociation products in CO<sub>2</sub> discharges in conditions where the vibrational kinetics can modify the EEDF but has no direct influence on chemical reactions [42],
- (viii) The elucidation of the role of the electronically excited metastable state CO(*a*<sup>3</sup>Π<sub>r</sub>) in CO<sub>2</sub> dissociation and CO recombination [36,38,42,43],
- (ix) The study of the CO<sub>2</sub> dissociation under Martian environment for oxygen production [31,44],
- (x) The inclusion of a self-consistent description of the CO<sub>2</sub> and CO vibrational kinetics involving the dissociation products, namely CO, O<sub>2</sub>, O validated in CO<sub>2</sub> and CO<sub>2</sub>-O<sub>2</sub> discharges [38].

Herein we extend the study of the coupled electron, vibrational and chemical kinetics developed in [31–34,38,42], already tested and validated in CO<sub>2</sub>-containing discharges and afterglows and for various operating conditions, with the addition and validation of the N<sub>2</sub> electron, vibration and chemical kinetics. For this purpose we include 59 vibrational levels of N<sub>2</sub>, as was initiated in [31,34]. The V-T and V-V processes for these levels with CO<sub>2</sub> and N<sub>2</sub> molecules and the dissociation products are included, as well as the heavy-particle reactions involving nitrogen species. The model predictions are compared with measurements in DC discharges ignited in different CO<sub>2</sub>-N<sub>2</sub> mixtures.

Several reasons motivate the study of CO<sub>2</sub>-N<sub>2</sub> low temperature plasmas. N<sub>2</sub> represents a large fraction in most industrial flue gas [45] along with other impurities like oxygen and water, so the influence it may have on the kinetics and chemistry of the plasma must be investigated, as done previously for O<sub>2</sub> [38] and H<sub>2</sub>O [46,47]. Moreover, the combined presence of nitrogen and oxygen species is bound to lead to the formation of N<sub>x</sub>O<sub>y</sub> by-products which are dangerous compounds [48] but could also be an intermediary for nitrogen fixation [49,50]. Furthermore, by varying the N<sub>2</sub> content in CO<sub>2</sub>-N<sub>2</sub> mixtures we enlarge the parameter space and can have a thorough validation of the model and gain a deeper understanding of the kinetics of CO<sub>2</sub> plasmas. In the context of in situ resource utilization (ISRU) on Mars, studying the effect of N<sub>2</sub> on CO<sub>2</sub> dissociation is relevant given the presence of N<sub>2</sub> in the Martian atmosphere (96 % CO<sub>2</sub> – 2 % Ar – 2 % N<sub>2</sub>). Decomposition of CO<sub>2</sub> under Martin environment would

promote the local production of breathable O<sub>2</sub>, fertilizers and transportation fuel on Mars [31,44,51–54], where the conditions are optimal for CO<sub>2</sub> dissociation by plasmas [31]. Moreover, once oxygen has been made available, extracted from CO<sub>2</sub> thanks to membranes for instance [52], N<sub>2</sub> from the Martian atmosphere can be used for the local production of N<sub>x</sub>O<sub>y</sub> essential for the synthesis of fertilizers on site [54]. Finally, our model for the simulation of CO<sub>2</sub>-N<sub>2</sub> DC discharges is a first step towards the simulation of CO<sub>2</sub>/N<sub>2</sub>/H<sub>2</sub>O mixtures as investigated in [55–57] where the chemistry induced by atmospheric pressure DC discharges above a water surface is studied. Since this mixture represents a model of prebiotic atmosphere of the Earth, it is interesting for the study of amino acids formation and for the verification of the theory of the origins of life. Some recent works have studied CO<sub>2</sub>-N<sub>2</sub> mixtures, with a focus on the entry problems [58–62], the characterisation of electrical discharges in CO<sub>2</sub>/Ar/N<sub>2</sub> mixtures [31,63–65] and the CO<sub>2</sub> conversion [63,66–71].

Current research on plasma-based CO<sub>2</sub> conversion in presence of N<sub>2</sub> is done mainly with dielectric barrier discharges (DBD) [67,69,72,73], microwave plasmas (MW) [68,74], ns pulse discharges [75–77] and DC glow discharges [34,66,78,79] where CO<sub>2</sub> dissociation pathways and energy efficiency are analysed. It has been shown that the admixture of N<sub>2</sub> has a beneficial impact on the CO<sub>2</sub> decomposition by plasmas [34,70]. Several reasons can be assigned to this effect: the enhancement of the reduced electric field, the effect of electronically and vibrationally excited states on CO<sub>2</sub> dissociation directly [66,80] or via changes of the EEDF [24,26,31,42], and the dilution with N<sub>2</sub> limiting the influence of back reaction mechanisms producing CO<sub>2</sub> from CO [34]. Favouring the excitation of the asymmetric vibrational mode of CO<sub>2</sub> by adding N<sub>2</sub> is well known in the context of CO<sub>2</sub>-N<sub>2</sub> maser/laser systems extensively studied in the 60s [81–84]. The selective excitation of the asymmetric mode of CO<sub>2</sub> by nearly resonant vibrational energy transfers from N<sub>2</sub> was reported to enhance lasing power. Indeed, the first excited level of N<sub>2</sub> has an energy very close to the first asymmetric level of CO<sub>2</sub> ( $\Delta E = 18 \text{ cm}^{-1} = 2.23 \cdot 10^{-3} \text{ eV}$ ), which is smaller than the typical average kinetic energy  $kT$  [85], allowing nitrogen to easily exchange vibration quanta with the asymmetric mode of CO<sub>2</sub>. This near-resonant transfer can be beneficial for vibrational dissociation of CO<sub>2</sub> as vibrationally excited CO<sub>2</sub> can undergo molecular dissociation through the so-called ladder climbing mechanism or by electron-impact stepwise processes. The anharmonicity of the molecule creates a preferential excitation of molecules in higher vibrational levels compared to those in lower levels, in V-V collisions, which leads to an overpopulating of the higher vibrational levels [86,87] and possible dissociation of highly vibrating CO<sub>2</sub> molecules without a significant amount of kinetic energy required. This purely vibrational mechanism requires  $\sim 5.5 \text{ eV}$  and the products are obtained in the ground state, whereas the CO<sub>2</sub> dissociation by direct electron-impact excitation requires more than 7 eV and leads to the formation of an O atom in an electronically excited state [21]. The asymmetric mode  $\nu_3$  is of major interest here to reach an efficient dissociation by molecular collisions. While in principle any highly excited mode can lead to dissociation, the excited vibrational levels corresponding to the asymmetric stretch has a relatively long lifetime and its relaxation is thus much slower than that of the symmetric stretch and bending modes [84].

To establish a reaction mechanism for vibrationally excited CO<sub>2</sub>-N<sub>2</sub> plasmas a DC glow discharge is used here as it generates a stable (axially) homogeneous plasma (in the positive column) and is accessible to different diagnostics [21]. Despite its evident limitations, namely, fairly low energy efficiency and CO<sub>2</sub> dissociation fractions, these plasma sources are optimal for validation of volume averaged 0D self-consistent kinetic models with detailed and complex kinetics and therefore for the fundamental study of CO<sub>2</sub>-containing plasmas. The CO<sub>2</sub>, CO and NO densities and the vibrational kinetics are diagnosed by FTIR absorption spectroscopy, and actinometry is used to determine the O atom density and loss frequency.

The paper is structured as follows. After the introduction, Section 2 briefly gives information on the experimental set-up and the diagnostics used. This is followed in Section 3 by a description of the model and the kinetic scheme used to study the CO<sub>2</sub>-N<sub>2</sub> discharge. Moreover, in this section we report rate coefficients for electron-impact reactions and vibration-translation and vibration-vibration exchanges involving CO<sub>2</sub>, N<sub>2</sub> and the dissociation products. The comparison between the experiments

and the simulations is presented and discussed in section 4 to gain further insight into the underlying kinetics. Finally, perspectives and conclusions are reported in section 5.

## II. Experiments

Experiments are performed in non-thermal plasmas sustained by a continuous DC glow discharge, operating at pressures in the range  $P = 0.6 - 4$  Torr and discharge current  $I = 50$  mA, in a cylindrical Pyrex tube of radius  $R = 1$  cm. Two tube lengths are used throughout this study, 23 cm for the Fourier transform infrared (FTIR) measurements and 67 cm for the actinometry and reduced field measurements. The experimental setup and diagnostics used are very similar to those described in [36,88,89]. In this section we provide a less detailed but essential description of the experiments.

For all measurements, the pressure, flow and current are imposed. The experiments are conducted both in pure  $\text{CO}_2$  and in a  $\text{CO}_2\text{-N}_2$  mixture (Air Liquide Alphagaz 1 standard for both  $\text{CO}_2$  and  $\text{N}_2$ ). The gas flows are controlled using mass flow controllers (Bronkhorst F-210CV) and a total gas flow of 7.4 sccm has been used in the present experiments as done previously in [31,34,36,38,88,89]. The electric field in the positive column of the discharge is estimated by measuring the voltage drop between two tungsten pins placed 20 cm apart and pointing radially inside the reactor. Since the positive column can be considered homogeneous, the electric field measurement is representative of the average field in the plasma bulk. The error on the reduced electric field,  $E/N$ , was calculated taking into account the uncertainty on the  $T_{\text{rot}}$  (see below) used for the calculation of the plasma density  $N$ .

In situ FTIR absorption spectroscopy was used to determine the different vibrationally excited states densities of  $\text{CO}_2$  and  $\text{CO}$  from which are deduced the characteristic vibrational temperatures of  $\text{CO}$  and of the different modes of  $\text{CO}_2$ , namely, bending, symmetric stretching and asymmetric stretching modes, corresponding to  $T_1$ ,  $T_2$  and  $T_3$  respectively [20]. The detected IR spectra contain several lines of  $\text{CO}$  and  $\text{CO}_2$  vibrational transitions which are fitted using a MATLAB® algorithm, according to the procedure described in [36,88]. The measurements further give information on the rotational temperature of both  $\text{CO}_2$  and  $\text{CO}$  which is assumed to be representative of the gas temperature [89]. By default, the fit assumes a Treanor vibrational distribution for the three vibrational modes of  $\text{CO}_2$  [36,88,90] and bending and symmetric modes are assumed to be in equilibrium i.e.  $T_1 = T_2 = T_{1,2}$  and this assumption was confirmed in [33,37,89]. During the experiments, an FTIR resolution of  $0.2 \text{ cm}^{-1}$  is used and the error on the different temperatures was estimated to be 30 K and 27 K for  $T_{\text{rot}}$  and  $T_{1,2}$  respectively, 67 K for  $T_3$  and 357 K for  $T_{\text{CO}}$  at 5 Torr, 50 mA and in pure  $\text{CO}_2$  [36]. As an outcome of the fitting procedure, the dissociation fraction

$$\alpha = \frac{[\text{CO}]}{[\text{CO}] + [\text{CO}_2]}, \quad (1)$$

where  $[\text{CO}]$  and  $[\text{CO}_2]$  represent the gas phase concentrations of  $\text{CO}$  and  $\text{CO}_2$  molecules, respectively, is also obtained. Due to the small dimensions of the sample chamber of the FTIR spectrometer (Bruker V70??), these measurements are done in the 23 cm long reactor. The temperatures for the same pressure and current are assumed to be the same in both reactors due to the fast timescales of temperature evolution in comparison with the residence times in our experimental conditions [89]. Finally, note that the measured vibrational temperatures are only representative of the populations of the lower vibrational levels and do not bring any information regarding the populations of the higher ones, which may deviate from equilibrium Boltzmann and/or Treanor distributions and are modified by the presence of  $\text{N}_2$ .

Downstream measurements, in which the same plasma reactor is placed upstream a measurement cell installed in the FTIR sample compartment, were also performed, similarly to what has been done by Morillo-Candas *et al.* [91]. Indeed, due to the small fraction of  $\text{N}_x\text{O}_y$  species in the discharge, we had to use a multipass cell placed after the plasma reactor, to increase the optical path to 5 m. Thanks to this configuration, we could reach sufficient sensitivity to observe  $\text{NO}$  and nitrogen dioxide ( $\text{NO}_2$ ) absorption lines and capturing a wavenumber range of  $950\text{--}3350 \text{ cm}^{-1}$  ensured the simultaneous

measurement of NO, NO<sub>2</sub> as well as CO<sub>2</sub> and CO absorption bands. The NO<sub>2</sub> signal was at the noise level, so that the uncertainty obtained on the NO<sub>2</sub> density was so large that the data obtained are not reliable and therefore not provided here.

O atom densities and wall loss frequencies are measured in pure CO<sub>2</sub> by actinometry in a 67 cm length tube [89]. The absolute O atom densities obtained rely on several parameters for which large discrepancies exist in the literature which leads to an error estimation for this specie density above 30% [89,91]. The loss probability of O atoms at the wall,  $\gamma_{\text{O}}$ , is given in [89] as a function of pressure, for a current of 50 mA, and is deduced from the experimental determination of O atom loss frequencies, in pure CO<sub>2</sub>, and was extrapolated at lower pressure. The values are summarized in Table 1.

Table 1: O loss probabilities from [89] obtained experimentally, in pure CO<sub>2</sub>, for a discharge current of 50 mA and used in our calculations. \*Extrapolated value.

Pressure (Torr)	O loss probability $\gamma_{\text{O}}$
0.6	$8.87 \cdot 10^{-4*}$
0.8	$6.50 \cdot 10^{-4}$
1	$5.33 \cdot 10^{-4}$
2	$4.50 \cdot 10^{-4}$
3	$4.91 \cdot 10^{-4}$
4	$5.33 \cdot 10^{-4}$

Overall, the set of measurements provides the gas temperature, vibrational temperatures of CO and the various modes of CO<sub>2</sub>, the reduced field E/N, the fraction of atomic oxygen, [O]/N, and the densities of O(<sup>3</sup>P), CO(X<sup>1</sup> $\Sigma^+$ ), CO<sub>2</sub>(X<sup>1</sup> $\Sigma^+_{\text{g}}$ ) and NO(X<sup>2</sup> $\Pi_r$ ) which are compared with the simulation results for the validation of the model described in section IV. The density of the gas, N, is calculated from the ideal gas law with the pressure and gas temperature obtained with the FTIR measurements.

### III. Model

The development and validation of self-consistent models constitute a powerful tool to access quantities that are not available experimentally, to obtain insight into the processes occurring in the plasma, to interpret the experimental results and to predict the behaviour of important physical and chemical quantities in different plasma systems. In particular, 0D kinetic models can describe a detailed plasma chemistry with a significant number of processes included and therefore can provide very useful information on the main source and loss mechanisms of the species of interest like CO and NO. However, the reliability of these models depends strongly on the accuracy of the cross sections and/or rate coefficients used to describe the energy transfers, electron-impact mechanisms and heavy-particle chemical reactions.

The calculations are done with the LisbOn KInetics (LoKI) simulation tool developed in-house under MATLAB® and solving a Boltzmann-chemistry global model [92,93]. Since electrons play an important role in low-temperature plasmas, an accurate description of the electron energy distribution function (EEDF) and macroscopic electron parameters, including rate coefficients of electron-impact processes, is required. This is achieved here using the open-source Boltzmann solver LoKI-B, which numerically solves a space-independent form of the two-term electron Boltzmann equation (EBE) for non-magnetised non-equilibrium low-temperature plasmas, excited by DC or HF electric fields [92] or time-dependent (non-oscillatory) electric fields [94], in different gases or gas mixtures. Moreover, to get a self-consistent description of both electron and heavy species, the homogeneous EBE is coupled with the Chemical solver LoKI-C corresponding to a system of zero-dimensional state-to-state rate-balance equations describing the creation and loss of the most important neutral and charged heavy-particles. The relevant information regarding the model is summarized in this section and a figure of the workflow can be found in [42].

The electron, chemical and vibrational kinetics are coupled into a self-consistent scheme for which the reduced electric field,  $E/N$ , corresponds to steady-state conditions where the total rate of production of electrons in ionization events compensates exactly their total loss rate due to ambipolar diffusion to the wall and electron-ion recombination or, in other words, when the densities of negative and positive charges are the same, satisfying the quasi-neutrality condition. Moreover, it is guaranteed, thanks to the coupling between LoKI-B and LoKI-C, that the EEDF and electron parameters are obtained taking into account the self-consistently calculated concentrations of the parent gas and for a value of reduced electric field also self-consistently obtained. Vice-versa, all the rate coefficients of the electron-impact reactions depend on this self-consistent EEDF.

The electron density,  $n_e$ , is such that the current ( $I$ ) given as input calculated with:

$$I = \pi R^2 |q_e| n_e v_e, \quad (2)$$

must give the experimental current intensity of 50 mA; where  $q_e$  is the elementary charge of electrons and  $v_e$  is the electron drift velocity obtained from the EBE solution. The diffusion of neutral species, including the vibrationally excited species, is taken as in [34,95], and is based on the formula of Chantray [96] to obtain the loss rate of species interacting with the wall due to the combined effect of transport (due to diffusion) and reaction at the wall (with a certain wall recombination/deactivation probability  $\gamma$ ). The diffusion of charged-particles is described by classical ambipolar diffusion [95] and the effect of the negative ions on the electron density radial profiles is taken into account [97,98]. The gas flow is used as input parameter to the model, where we assume a simple mechanism of renewal of gas: new  $\text{CO}_2/\text{N}_2$  particles enter the reactor while the species produced in the plasma exit at the outlet assuming conservation of atoms in the plasma mixture [42].

Together with the discharge current ( $I$ ) given in (2), the input parameters of the model are the gas pressure ( $P$ ), the flow, the initial gas mixture and reactor dimensions (tube length and radius). The loss probability of O atoms at the wall,  $\gamma_O$ , is also an input parameter and is deduced from the experimental determination of O atom loss frequencies (cf. Table 1). Additionally, in the present simulations the gas temperature obtained experimentally is also used as input parameter. The self-consistent calculation of  $T_g$  is possible, using a thermal balance equation [35,95,99] but the study of heat transfer mechanisms is not the focus of this work.

### III.1 Chemistry

Most of the required electron scattering cross-section data can be found at the open-access website LXCat [100,101]. For this work, we use the IST-Lisbon database [100] including complete sets of electron scattering cross sections (CS) with neutral species in the ground-state (GS) based on [95,102,103] for  $\text{N}_2$ , [104] for N, [38,40] for  $\text{CO}_2$ , [41] for CO, and [105,106] for  $\text{O}_2$  and O. They are defined as sets of cross sections giving a good description of the main electron energy and momentum losses, yielding electron swarm parameters in agreement with available measured data, when used in a two-term Boltzmann solver [100]. In  $\text{CO}_2\text{-N}_2$  plasmas, CO,  $\text{O}_2$  and O may be present with significant concentrations, therefore, besides  $\text{CO}_2$  and  $\text{N}_2$ , cross sections for electron impact on these three plasma species are of importance. The CS describe the elastic momentum-transfer due to electron collision with the GS, the excitation of electronic and vibrational states from GS and ionisation. The sets of electron scattering cross sections from ground-states  $\text{CO}_2$ ,  $\text{N}_2$ , CO and  $\text{O}_2$  are complemented by additional collisional data, essentially for collisions from their vibrationally excited states, as well as from some of their electronically excited states. They can be found in the IST-Lisbon database [100] but are not part of the complete sets. The list of all the e-V processes and corresponding cross sections for  $\text{CO}_2$  are reported in the Supplementary Information of [38]. Notice that the superelastic processes are considered and the corresponding cross sections are deduced from the direct processes using the Klein-Rosseland relation [107]. Due to the lack of data, the dissociation cross sections via electron impact from vibrationally excited states are considered with a threshold shift, while keeping

the same amplitude as for dissociation from the ground-state [31]. The same procedure is used for ionization from vibrationally excited CO and CO<sub>2</sub> molecules as well as attachment for CO<sub>2</sub>.

The vibrational excitation of oxygen is included in the calculation of the EEDF, assuming a Boltzmann distribution at T<sub>g</sub> for vibrational levels up to 4, but not in the Chemistry module as a strong depopulation of the Vibrational Distribution Function (VDF) in the first vibrational levels was observed experimentally [108] and in the calculations of [109,110]. Vibrationally excited O<sub>2</sub> molecules do not seem to have a direct influence neither in the EEDF nor in the chemistry [111] but may have a relevant contribution to gas heating, due to V–T deactivation by atomic oxygen, affecting indirectly the discharge [98].

For the description of the rotational excitation and deexcitation of the ground-state N<sub>2</sub> and O<sub>2</sub> by electron impact, we adopt the continuous (CAR) approach, using the GCAR rotational operator [95,112], whereas a discrete approach that considers a set of cross sections for rotational transitions involving the states CO (X<sup>1</sup>Σ<sup>+</sup>, v = 0, J = 0-17) published also in the IST-Lisbon database is used for CO.

The species considered in the plasma chemistry of the model include: ground-state, vibrationally and/or electronically excited CO, CO<sub>2</sub>, O<sub>2</sub>, N<sub>2</sub>, NO, NO<sub>2</sub> and CN molecules CO(X<sup>1</sup>Σ<sup>+</sup>, v=0:10), CO(a<sup>3</sup>Π<sub>r</sub>), CO<sub>2</sub>(X<sup>1</sup>Σ<sup>+</sup><sub>g</sub>, v<sub>1</sub><sup>max</sup>=2; v<sub>2</sub><sup>max</sup>=v<sub>3</sub><sup>max</sup>=5), O<sub>2</sub>(X<sup>3</sup>Σ<sub>g</sub><sup>-</sup>), O<sub>2</sub>(a<sup>1</sup>Δ<sub>g</sub>), O<sub>2</sub>(b<sup>1</sup>Σ<sub>g</sub><sup>+</sup>), O<sub>2</sub>(A<sup>3</sup>Δ<sub>u</sub>, A<sup>3</sup>Σ<sub>u</sub><sup>+</sup>, c<sup>1</sup>Σ<sub>u</sub><sup>-</sup>), N<sub>2</sub>(X<sup>1</sup>Σ<sub>g</sub><sup>+</sup>, v=0:59), N<sub>2</sub>(A<sup>3</sup>Σ<sub>u</sub><sup>+</sup>), N<sub>2</sub>(B<sup>3</sup>Π<sub>g</sub>), N<sub>2</sub>(C<sup>3</sup>Π<sub>u</sub>), N<sub>2</sub>(w<sup>1</sup>Δ<sub>u</sub>), N<sub>2</sub>(a<sup>1</sup>Π<sub>g</sub>), N<sub>2</sub>(a<sup>1</sup>Σ<sub>u</sub><sup>-</sup>), NO(X<sup>2</sup>Π<sub>r</sub>), NO(A<sup>2</sup>Σ<sup>+</sup>), NO(B<sup>2</sup>Π<sub>r</sub>), NO<sub>2</sub>(X<sup>2</sup>A<sub>1</sub>), NO<sub>2</sub>(a<sup>4</sup>A<sub>2</sub>), CN(X<sup>2</sup>Σ<sup>+</sup>) and CN(B<sup>2</sup>Σ<sup>+</sup>); ground-state and electronically excited oxygen and nitrogen atoms, O(<sup>3</sup>P), O(<sup>1</sup>D), N(<sup>4</sup>S), N(<sup>2</sup>D), N(<sup>2</sup>P), ground-state carbon C(<sup>3</sup>P), ground-state ozone and vibrationally excited ozone, O<sub>3</sub>, O<sub>3</sub>\*; and positive and negative ions, O<sup>+</sup>, O<sub>2</sub><sup>+</sup>, O<sup>-</sup>, CO<sub>2</sub><sup>+</sup>, CO<sup>+</sup>, N<sub>2</sub><sup>+</sup>, N<sub>2</sub><sup>+</sup>(B<sup>2</sup>Σ<sub>u</sub><sup>+</sup>), N<sup>+</sup>, N<sub>4</sub><sup>+</sup>, N<sub>3</sub><sup>+</sup> and NO<sup>+</sup>. For O<sub>3</sub>\* we consider a single effective vibrationally excited state [113]. O<sub>2</sub>(A<sup>3</sup>Δ<sub>u</sub>, A<sup>3</sup>Σ<sub>u</sub><sup>+</sup>, c<sup>1</sup>Σ<sub>u</sub><sup>-</sup>) is an effective sum of the Herzberg states. Our model does not take into account directly the kinetics of N<sub>2</sub>(W<sup>3</sup>Δ<sub>u</sub>). However, it is considered indirectly in the kinetics of the N<sub>2</sub>(B<sup>3</sup>Π<sub>g</sub>) state since the collisional data measured in flow systems actually provide the relaxation coefficients for the coupled states as a whole [114]. Besides, the N<sub>2</sub>(B<sup>3</sup>Π<sub>g</sub>) state is populated by the radiative cascade N<sub>2</sub>(B<sup>1</sup>Σ<sub>u</sub><sup>-</sup>) → N<sub>2</sub>(B<sup>3</sup>Π<sub>g</sub>), on the assumption that the N<sub>2</sub>(B<sup>1</sup>Σ<sub>u</sub><sup>-</sup>) is only populated by electron impact and radiatively depopulated (i.e., the populating rate of the N<sub>2</sub>(B<sup>3</sup>Π<sub>g</sub>) state due to this mechanism is that for creating the N<sub>2</sub>(B<sup>1</sup>Σ<sub>u</sub><sup>-</sup>) by electron impact) [114,115]. The rate coefficients of heavy-particle reactions are adopted from literature and based on the kinetic schemes of O<sub>2</sub> [98] based on [111,116,117], CO<sub>2</sub> [42], N<sub>2</sub> [114], N<sub>x</sub>O<sub>y</sub> [95] and CN [118] while the rate coefficients of the electron impact reactions are calculated from the energy-dependent cross sections, in combination with the EEDF. For the kinetics of oxygen, the set proposed in [98] is adopted without modifications except for the exclusion of vibrational states in the heavy-species chemistry. We also added the three-body reaction:



with the rate coefficients taken from [68].

### III.1.1 Quenching of N<sub>2</sub>(A) and N<sub>2</sub>(B)

Reactions involving N<sub>2</sub>(A<sup>3</sup>Σ<sub>u</sub><sup>+</sup>), referred to as N<sub>2</sub>(A), and the triplet levels N<sub>2</sub>(B<sup>1</sup>Σ<sub>u</sub><sup>-</sup>), N<sub>2</sub>(B<sup>3</sup>Π<sub>g</sub>), and N<sub>2</sub>(W<sup>3</sup>Δ<sub>u</sub>), considered here as a single effective state N<sub>2</sub>(B) [119], are relevant for the study of active nitrogen, shock waves and flames [120,121]. Several authors claim that the presence of these species improves the CO<sub>2</sub> dissociation [66–68,71,121] and therefore these studies regained interest more recently for the study of N<sub>2</sub>-containing CO<sub>2</sub> discharges. According to [66,121], the most important electronically excited nitrogen state for CO<sub>2</sub> conversion is N<sub>2</sub>(B) with the rate coefficients being roughly gas kinetic [122] for N<sub>2</sub>(B) quenched by CO<sub>2</sub> and CO, as can be seen in Table 2, where a brief survey of reported rate coefficients for reactions involving N<sub>2</sub>(B) and CO<sub>2</sub> or CO is given.



The rate coefficient for CO<sub>2</sub> dissociation due to quenching with N<sub>2</sub>(A) is much smaller than with N<sub>2</sub>(B) and is two orders lower than those by products of CO<sub>2</sub> dissociation like CO [123]. Indeed, CO is a more efficient acceptor of the electronic energy from N<sub>2</sub>(A) [124–127]. Several rate coefficients found in the literature for the quenching of N<sub>2</sub>(A) with CO and CO<sub>2</sub> are compiled in Table 3.

The relative importance of N<sub>2</sub>(A) and N<sub>2</sub>(B) metastable states for CO<sub>2</sub> dissociation seem to depend on the operating conditions. For discharges with high electron energy like DBD N<sub>2</sub>(A) was claimed to be important [67,71] for CO<sub>2</sub> dissociation while for a microwave discharge, with lower electron average energy, it was shown that N<sub>2</sub>(A) was of minor importance [68]. However, the study done in the DBD [67] used a value for the rate coefficient for the N<sub>2</sub>(A) quenching by CO<sub>2</sub> taken from [71], which is two orders of magnitude higher than what is commonly found in literature (see Table 3).

It is worth noting that in the collisional quenching of electronically excited N<sub>2</sub> molecules the branching ratio of the quenching products remains uncertain and can affect the modeling predictions in the most significant way [80]. Finally, it is necessary to note that an important feature of many reaction involving N<sub>2</sub>(A,B) is a dependence of the rate coefficients and products ratios on the vibrational levels [120,122,123,128] and that the actual measurements of rate coefficients can be a mix of vibrational levels [123].

process	[120,129]	[71,121,129]	[66,122]	[71]	[120]
N <sub>2</sub> (B) + CO <sub>2</sub> → N <sub>2</sub> +CO+O	1.5·10 <sup>-10</sup> (a)	8.5·10 <sup>-11</sup> (b)			
N <sub>2</sub> (B) + CO <sub>2</sub> → products			<b>2·10<sup>-10</sup></b> (a)		
N <sub>2</sub> (B) + CO <sub>2</sub> → N <sub>2</sub> +CO <sub>2</sub>				1·10 <sup>-11</sup>	
N <sub>2</sub> (B) + CO <sub>2</sub> → N <sub>2</sub> +CO <sub>2</sub>				1.9·10 <sup>-10</sup>	
N <sub>2</sub> (B)+CO → products			<b>2·10<sup>-10</sup></b> (a)		8.5·10 <sup>-11</sup>

Table 2: Rate coefficients in cm<sup>3</sup>s<sup>-1</sup> for processes involving the quenching of N<sub>2</sub>(B), measured at (a) 300 K and (b) 196 K. In bold, values used in the model for section IV.2.

process	[71]	[123]	[126]	[120]
N <sub>2</sub> (A) + CO <sub>2</sub> → N <sub>2</sub> +CO+O	1.54·10 <sup>-12</sup>			
N <sub>2</sub> (A) + CO <sub>2</sub> → products		<b>1.98·10<sup>-14</sup></b> (c)		
N <sub>2</sub> (A) + CO <sub>2</sub> → N <sub>2</sub> +CO <sub>2</sub>	9.9·10 <sup>-15</sup>			
N <sub>2</sub> (A) + CO → products		<b>1.7·10<sup>-12</sup></b> (c)	2.5·10 <sup>-11</sup>	2.5·10 <sup>-12</sup>

Table 3: Rate coefficients in cm<sup>3</sup>s<sup>-1</sup> for processes involving the quenching of N<sub>2</sub>(A), (c) measured at 298 K. In bold, values used in the model for section IV.2.

The quenching processes of N<sub>2</sub>(A) and N<sub>2</sub>(B) are investigated in section IV.2. The values of the rate coefficients used for this study corresponding to the quenching of N<sub>2</sub>(A) with CO<sub>2</sub> and CO are, respectively, 1.98·10<sup>-14</sup> cm<sup>3</sup>s<sup>-1</sup> and 1.7·10<sup>-12</sup> cm<sup>3</sup>s<sup>-1</sup> [123] and are assumed to occur via the following processes:



For the quenching of N<sub>2</sub>(B) with CO<sub>2</sub> and CO, considered as follows:



we use the values reported in Piper [122] and used as well in Naidis & Babaeva [66], namely 2·10<sup>-10</sup> cm<sup>3</sup>s<sup>-1</sup> for both processes.

### III.2 Vibrational kinetics

The vibrational kinetics include excitation/de-excitation mechanisms due to electron-impact collisions (e-V), energy transfer via vibrational–translational (V-T), vibrational–vibrational (V-V) interactions and wall loss of vibrational quanta (W). The VDFs of CO<sub>2</sub>, N<sub>2</sub> and CO are obtained from the solution of the rate-balance equations describing the creation and loss of each individual vibrational level,

accounting for these e-V, V-V, V-T, W processes, as well as chemical reactions like electron-impact dissociation from vibrationally-excited molecules and dissociation in pure vibrational mechanisms. The pure CO<sub>2</sub> subsystem was recently addressed in [38], where expressions for the V-T and V-V involving CO<sub>2</sub>, CO, O<sub>2</sub> and O, rate coefficients are suggested. The vibrational energy transfers in the nitrogen system have been extensively studied in the past, due to the key role of vibrations in nitrogen plasmas [95,97,109,110,114,115,130]. The rate coefficients used for the pure N<sub>2</sub> subsystem are given in [34,95] and the calculation of the V-T and V-V rate coefficients were benchmarked from the calculations of Billing *et al.* [131,132]. The reader is referred to these papers for further details and figures representing these rate coefficients. The rate coefficients were scaled using either the Schwartz, Slawsky, and Herzfeld (SSH) theory [133] (SSH) or the theory from Sharma and Brau (SB) [134,135] (SB), which are summarized in [32] for the case of CO<sub>2</sub>. A comprehensive description of the SSH scaling law can be found in [16]. In regards of rate coefficients used for inverse reactions, we have used the principle of detailed balance [136] for the various V-T and V-V transitions. We only consider dissociation by electron impact from vibrationally excited CO<sub>2</sub> molecules as the higher levels are not significantly populated in our conditions. In other words, we do not consider dissociation through the pure vibrational path (CO<sub>2</sub>(v\*) + CO<sub>2</sub> → CO + O + CO<sub>2</sub>), but only stepwise dissociation by electron impact on vibrationally excited CO<sub>2</sub>. The validity of this assumption is shown and discussed in [38,42].

In the following subsections, we start by discussing the description of the vibrational levels considered and the e-V processes. We then review our current choice of rate coefficients for the relevant mechanisms in CO<sub>2</sub>-N<sub>2</sub> plasmas, namely CO<sub>2</sub>-N<sub>2</sub>, CO<sub>2</sub>-CO and N<sub>2</sub>-CO V-V exchanges and different V-T processes. Finally, we report the probabilities of deactivation of vibrationally excited species and atomic oxygen recombination at the walls.

### III.2.1 Energy levels and e-V processes

The model considers 59 vibrational levels of N<sub>2</sub>, up to the energy of ~10 eV. They are included in the model following the formula given in [137]:

$$\frac{E_{N_2}}{hc} = \sum_{i=1}^5 a_i \left( v + \frac{1}{2} \right)^i, \quad (4)$$

with the coefficients  $a_i$  in cm<sup>-1</sup> equal to 2378.1, -18.516, 0.26662,  $-6.2127 \cdot 10^{-3}$  and  $3.4215 \cdot 10^{-5}$ , respectively, for  $i=1-5$ . The energies of the individual CO<sub>2</sub> vibrational levels are calculated according to the anharmonic oscillator approximation [138] and more details can be found in [38]. The CO vibrational energy levels are calculated by the formula of the anharmonic Morse oscillator [114] as done in [38]. By convention, the ground-state energy is set to 0 eV for CO<sub>2</sub>, CO and N<sub>2</sub>.

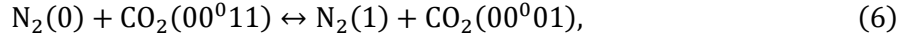
As carefully described in [33,40] and briefly reviewed in [38,99], the cross sections for electron-impact excitation (e-V) of CO<sub>2</sub> vibrations are obtained from a direct deconvolution of the available lumped cross sections, according to the statistical weights of the various levels, and the missing cross sections are generated following the approach from [38], based on a modified form of the semi-empirical Fridman's approximation [21]. For the electron-impact excitation of the CO vibrations, we have adopted the cross sections from [139] for the vibrational excitation and de-excitation which are largely based on resonant excitation data from Laporta and co-workers [140], and where contributions from non-resonant collisions for the transition  $e + \text{CO}(v=0) \leftrightarrow e + \text{CO}(v=1)$ , taken from [141], are also included. Finally, the e-V mechanisms for N<sub>2</sub> are described as follows: (i) in the electron kinetics calculations, e.g. when solving the electron Boltzmann equation, by adopting electron-scattering cross sections for the reactions  $e + \text{N}_2(\text{X},v) \rightarrow e + \text{N}_2(\text{X},v')$  ( $1 \leq v \leq v' \leq 10$ ), obtained by applying a threshold shift to the excitation cross sections for the corresponding vibrational transitions from the ground-state  $\text{N}_2(\text{X},v = 0)$ ; (ii) in the chemistry model calculations, by using electron rate coefficients satisfying the scaling law:

$$k_{v,v+v'} = \frac{k_{0,v'}}{1 + 0.15v'}, \quad (5)$$

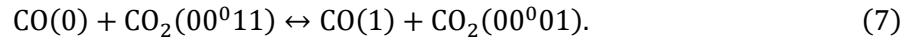
For  $1 \leq v' \leq 10, 1 \leq v \leq 59$  and where  $k_{0,v'}$  are the rate coefficients for vibrational transition from  $N_2$  in the ground state to the first 10 vibrational states. This scaling law given by Colonna in [142] was validated in [103] and used in [34,95,143].

### III.2.2 $CO_2-N_2$ and $CO_2-CO$ V-V exchanges

The transfer between vibrationally excited nitrogen and the asymmetric stretching mode of  $CO_2$ , is very efficient and may potentially have a positive effect on  $CO_2$  dissociation via the ladder climbing mechanism [21].  $CO_2$  is known to couple very strongly to  $N_2$  via



since the energy difference between the first vibrationally excited levels is only  $18 \text{ cm}^{-1}$  [135]. For details on the notation used for the  $CO_2$  vibrations, the reader is referred to [32,37,38]. The hypothesis regarding the selective excitation of the upper laser level of  $CO_2$  lasers by resonant transfer of vibrational energy from  $N_2$  molecules, necessary to obtain the population inversion in the  $CO_2-N_2$  laser system, is widely accepted by the scientific community [82,83,85]. Moreover, even though the equivalent reaction between  $CO_2$  and  $CO$  is not as close to energy resonance as for  $N_2$ ,  $CO$  molecules can transfer a considerable amount of energy to the  $v_3$  vibration via (7) because the difference between the energies of the vibrational level of  $CO$  and the  $(00^011)$  level of  $CO_2$  is  $170 \text{ cm}^{-1}$  which is typically smaller than the average kinetic energy  $kT$  [81],



The importance of these two processes comes from the large populations of vibrationally excited  $CO$  and  $N_2$  molecules present in the discharge, most likely due to direct electronic excitation, followed by the transfer of energy to the vibrational levels of  $CO_2$ . This is supported by experimental data on the cross sections of collisions between electrons and heavy species ( $CO$  and  $N_2$ ), reported in [144]. Indeed, according to Schulz, the electron-impact excitation cross sections of the vibrational levels of  $CO$  and  $N_2$  are unusually large because of the resonance effect of the short-lived negative  $CO^-$  and  $N_2^-$  ions [145]. The excitation cross section of the first levels of  $CO$  and  $N_2$  ( $\sim 5 \cdot 10^{-16} \text{ cm}^2$ ) is one order of magnitude higher compared to the excitation of  $CO_2$  in the first asymmetric stretch mode level by electron impact [33,40], for electrons of 2 eV energy, typical of our discharge.

Since the energy defect is about 10 times larger for  $CO$  than for  $N_2$  it might be anticipated that  $CO$  is not as effective as  $N_2$  in exciting the vibration of  $CO_2$ . Furthermore since the  $CO$  molecule has a dipole moment, it has also a spontaneous decay whereas  $N_2$  can only decay via collisions with the wall or with other molecules [85]. It appears, however, that the additional dipole-dipole attractive forces between  $CO_2$  and  $CO$  more than compensate for this disparity, as the  $CO_2-CO$  transfer can even be more efficient than the  $CO_2-N_2$  transfer. This could come from the observation that near resonant V-V transfer processes are more likely to occur when the vibrational modes involved are infrared active [146].

The  $CO_2-CO$  V-V rate coefficient comes from our previous work [38] and is based on [147], while the rate coefficient for  $CO_2-N_2$  V-V used in the present work is taken from [148]. We compare in Figure 1 the rate coefficients used in this work for the processes (6) and (7) with experimental data available in literature obtained with laser-excited vibrational fluorescence and shock tube techniques by Taylor *et al.* [149], Rosser *et al.* [150], Taylor & Bitterman [151], Stephenson *et al.* [146], Moore *et al.* [152], Starr & Hancock [153], Rosser *et al.* [154], Blauer and Nickelson [148]. Although there are considerable data for  $CO_2-N_2$ , a large scatter can be observed. Above 1000 K there are similarities between the  $CO_2-CO$  and  $CO_2-N_2$  V-V rate coefficients as might be expected based on the similarities between  $N_2$  and  $CO$  molecules. At lower temperatures, however, the situation may seem puzzling.

The positive temperature dependence for the CO<sub>2</sub>-CO V-V rate coefficient is the reverse of that found for CO<sub>2</sub>-N<sub>2</sub>. It is clear that the Schwartz, Slawsky, and Herzfeld (SSH) theory [133] cannot explain the low-temperature behaviour for CO<sub>2</sub>-N<sub>2</sub>, as this theory predicts an increase of the reaction rates with temperature. Sharma and Brau (SB) [134,135] have explained the negative temperature dependence of the CO<sub>2</sub>-N<sub>2</sub> V-V energy exchange, at low temperatures, on the basis of the long range force between the dipole moment of CO<sub>2</sub> and the quadrupole moment of N<sub>2</sub>, being more important than the short range repulsive forces normally used in vibrational relaxation theories. Such an interaction is more important at low temperatures and for processes of near energy resonance.

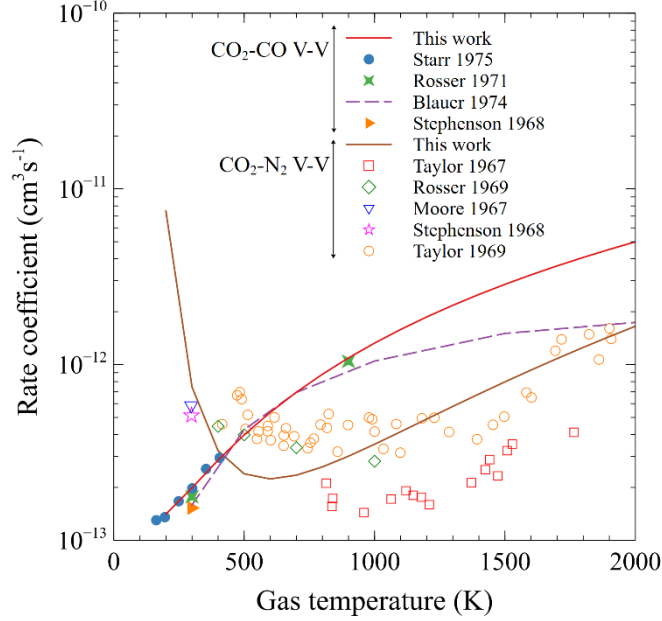
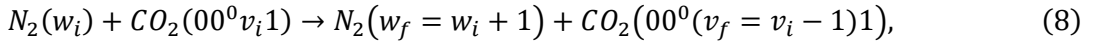


Figure 1: Comparison of the rate coefficients used in this work with experimental data for the near-resonant V-V exchange between the mode  $v_3$  of CO<sub>2</sub> and N<sub>2</sub> and CO,  $CO_2(00^011) + N_2/CO(v=0) \rightarrow CO_2(00^001) + N_2/CO(v=1)$ .

Only a few vibrational levels of the CO<sub>2</sub> asymmetric stretching mode are considered in the present model ( $v_3 \leq 5$ ) and for simplicity the rate coefficients for the process



can be considered with the same value as for the low lying levels (*i. e.*  $w_i = 0, v_i = 1$ ) as done in [34]. However, in this work, we scale the rate coefficients for the upper levels since they have a noticeable influence on the results, especially the vibrational temperatures, as verified in section IV (cf. Fig. 12). The rate coefficient for the process (6) with  $w_i = 0, v_i = 1$ , is described by:

$$k(\text{cm}^3\text{s}^{-1}) = 1,66 \cdot 10^{-24} \cdot \exp(a + b \cdot T^{-1/3} + c \cdot T^{-2/3}), \quad (9)$$

where  $a = 43.8$ ,  $b = -306$  and  $c = 1288$  [148] and is represented in Figure 1. The rate coefficient of the reverse process is calculated from the principle of the detailed balance [136], by multiplying the coefficients of the direct process with the Boltzmann factor,  $\exp\left(\frac{-\Delta E}{T_g}\right)$ , where  $T_g$  is the gas temperature and  $\Delta E$  the energy difference in K.

To be able to use the SB and SSH theories separately for the scaling of the rate coefficient from [148] (plotted in Fig. 1), we separate it into two parts, one for the long range corresponding to the ‘SB part’,  $L_{SB}$ , and one for the short range corresponding to the ‘SSH part’,  $S_{SSH}$ . To facilitate the scaling of rate coefficients at low and high temperatures with both theories, the function shown in (9) is then split into SSH and SB parts. The sum of these contributions ( $L_{SB}+S_{SSH}$ ) for the mechanism  $N_2(0) + CO_2(00^011) \rightarrow N_2(1) + CO_2(00^001)$  is given in figure 2 to show that we can recover the original

rate coefficient for the process (6) after the fitting procedure. Note that in this case we have  $a_{SB} = -6.28496$ ,  $b_{SB} = 379.838$ ,  $c_{SB} = -1059.2$ , for  $L_{SB}$ , and  $a_{SSH} = 27.221$ ,  $b_{SSH} = 10.8178$ ,  $c_{SSH} = -224.158$  for  $S_{SSH}$ . We then scale separately the rate coefficients with SB and SSH and add the two contributions to recover the characteristic ‘U shaped’ curve. All the rate coefficients are given in the Supplementary Information and a comprehensive description of the SSH scaling law can be found in [16].

According to the SB theory and retaining only the terms involving the vibrational levels of  $CO_2$  and  $N_2$  (and not the rotational distributions) for the only non-vanishing contribution, namely the interaction of the  $N_2$  quadrupole moment,  $Q$ , with the  $CO_2$  dipole moment,  $\mu$ , an analytical expression for the probability of the transition (8) is [155]:

$$\frac{k_{v_i, w_i}^{v_f, w_f}}{k_{1,0}^{0,1}} = \frac{|\langle w_f | Q | w_i \rangle|^2 * |\langle v_f | \mu | v_i \rangle|^2 * I(z(\Delta E))}{|\langle 1 | Q | 0 \rangle|^2 * |\langle 0 | \mu | 1 \rangle|^2 * I(z(\Delta E_{10}))}, \quad (10)$$

with  $k_{1,0}^{0,1}$  the rate coefficient for the forward direction of the transition (1) and  $|\langle w_f | \mu / Q | w_i \rangle|^2$  the matrix elements of the dipole moment of  $CO_2$  ( $\mu$ ) and quadrupole moments of  $N_2$  ( $Q$ ). They can be approximated by the harmonic oscillator relation [155]:

$$|\langle w_f = n | \mu / Q | w_i = n - 1 \rangle|_{CO_2/N_2}^2 = n * |\langle w_f = 1 | \mu / Q | w_i = 0 \rangle|_{CO_2/N_2}^2, \quad (11)$$

$I(z)$  is the resonance function defined as follows [155]:

$$I(z) = \exp(-z) (0.1339 + 0.1223z + 0.1477z^2 - 0.0283z^3 + 0.0078z^4 - 0.0007z^5), \quad (12)$$

with  $z = \Delta E d \left( \frac{M}{2k_B T_g} \right)^{1/2}$  and  $\Delta E = |E_f - E_i|/\hbar$  is the energy mismatch,  $d$  is the average of the hard sphere diameters of the two molecules,  $E_i$  and  $E_f$  the total energies of the initial states and final states, respectively, of  $CO_2$  and  $N_2$ ,  $M$  the reduced mass of the collision pair and  $\Delta E_{10}$  is the energy mismatch in process (6). By substitution of (11) into (12), we obtain:

$$\frac{k_{v_i, w_i}^{v_f, w_f}}{k_{1,0}^{0,1}} = \frac{w_f * |\langle 1 | Q | 0 \rangle|^2 * v_i * |\langle 0 | \mu | 1 \rangle|^2 * I(w(\Delta E))}{|\langle 1 | Q | 0 \rangle|^2 * |\langle 0 | \mu | 1 \rangle|^2 * I(w(\Delta E_{10}))} = k_{1,0}^{0,1} * \frac{w_f * v_i * I(w(\Delta E))}{I(w(\Delta E_{10}))}. \quad (13)$$

The SB theory is only used for near resonant processes as the resonance function,  $I(w)$ , has a fast decay with increasing  $\Delta E$ . Considering that the resonance function for values above  $50 \text{ cm}^{-1}$  provides  $\sim 8 \cdot 10^{-3}$ , which leads to rate coefficients below  $6 \cdot 10^{-14} \text{ cm}^3 \text{ s}^{-1}$ , we used the SB theory only for the processes which fulfil  $\Delta E < 50 \text{ cm}^{-1}$ . A few rate coefficients are given in Figure 3. When  $\Delta E > 50 \text{ cm}^{-1}$  we only consider the  $S_{SSH}$  contribution to the rate coefficient and we scale using the harmonic oscillator.

Our scaling approach is only valid for  $300 < T_g < 1000 \text{ K}$  as the fitting of  $L_{SB}$  and  $S_{SSH}$  with expression (9) fails outside of this range. Besides, the V-V transfer involving vibrationally excited  $N_2$  molecules and the bending and symmetric modes of  $CO_2$  is not included in the model as the corresponding rate coefficients are three orders of magnitude lower than the transfer with the asymmetric stretching mode in the gas temperature range of interest [300 K; 1000 K] [156,157].

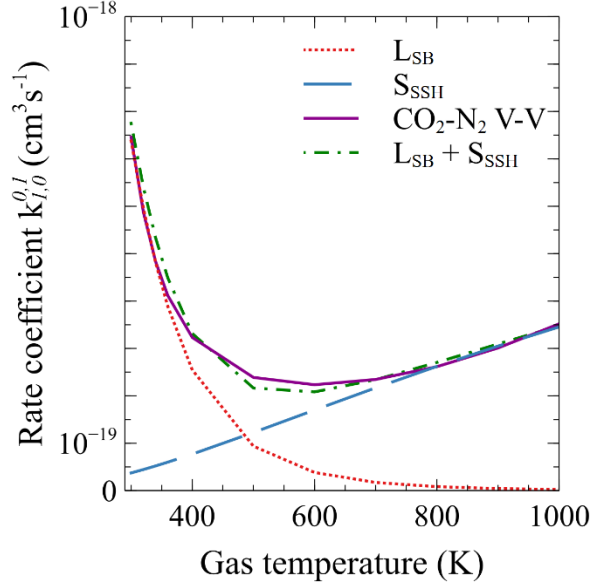


Figure 2: Fitting of the low temperature ( $\cdots$ ) and high temperature ranges ( $--$ ) of the rate coefficient corresponding to the  $\text{CO}_2\text{-N}_2$  V-V transfer,  $\text{N}_2(0) + \text{CO}_2(00^011) \rightarrow \text{N}_2(1) + \text{CO}_2(00^001)$  ( $\leftarrow$ ) from [148] and the sum of these two contributions ( $L_{\text{SB}}+S_{\text{SSH}}$ ) ( $-\cdot-$ ).

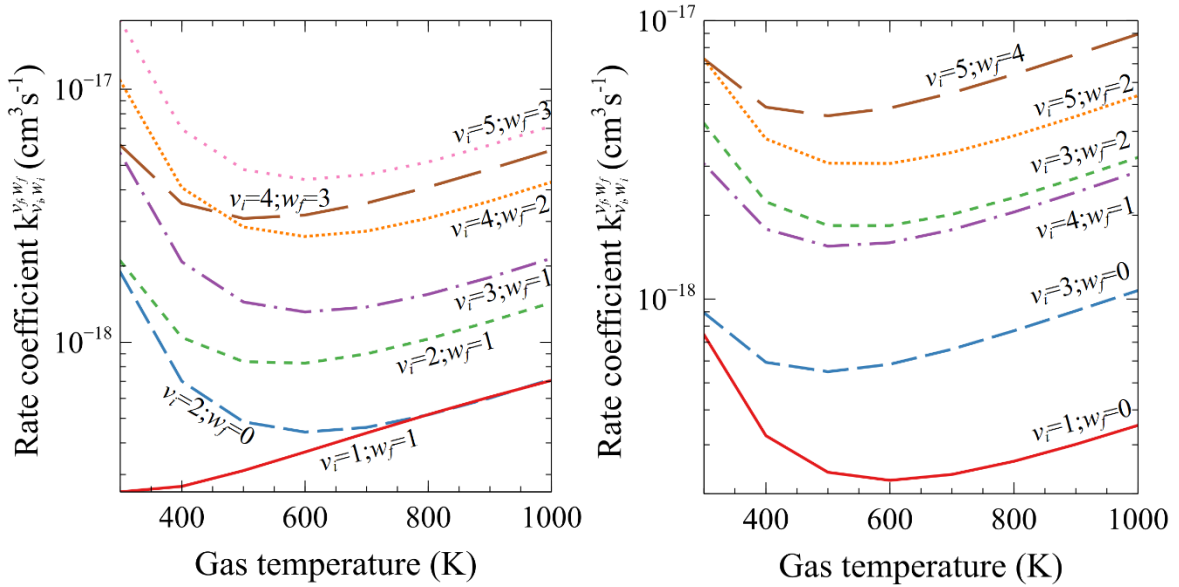


Figure 3: Rate coefficients ( $k_{v_i, w_i}^{v_f, w_f}$ ) of the process  $\text{N}_2(w_i) + \text{CO}_2(00^0 v_i 1) \rightarrow \text{N}_2(w_f = w_i + 1) + \text{CO}_2(00^0 (v_f = v_i - 1) 1)$  scaled with the procedure described in this section as a function of  $T_g$ .

### III.2.3 $\text{N}_2\text{-CO}$ V-V exchanges

The V-V exchange  $\text{N}_2(1) + \text{CO}(0) \rightarrow \text{N}_2(0) + \text{CO}(1)$  has an equivalent importance to the V-V exchange  $\text{N}_2(1) + \text{CO}_2(00^001) \rightarrow \text{N}_2(0) + \text{CO}_2(00^011)$  due to the high density of vibrationally excited CO and  $\text{N}_2$  molecules in the plasma, despite a lower rate coefficient. To obtain accurate rate coefficients we use the analytical expression from Kurnosov *et al.* [158] which seems to be a good approximation to experimental and semiclassical rate coefficients for a large range of near resonant vibrational transitions in the  $\text{N}_2\text{-CO}$  system. This expression takes into account short range repulsive and van der Waals forces (first term) as well as quadrupole-quadrupole interaction (second term):

$$k(v, u | v-1, u+1; T_g) = a \cdot Z \cdot T_g \cdot z(v) \cdot z(u+1) \cdot \exp\left(\frac{\Delta E}{2T_g}\right) \cdot F(y) \cdot F_S + \frac{b}{T_g} \cdot Z \cdot z(v) \cdot |\langle u+1 | q | u \rangle|^2 \cdot \exp\left(\frac{\Delta E}{2T_g}\right) \cdot \exp\left(-\frac{\Delta E^2}{CT_g}\right), \quad (20)$$

with  $Z = (\pi\sigma^2)V_M$  the gas kinetic collision rate coefficient, with  $V_M$  the average relative translational velocity,  $\pi\sigma^2$  the gas kinetic collision cross section.  $\Delta E$  is defined as  $[E_{CO}(u+1) + E_{N_2}(v-1)] - [E_{CO}(u) + E_{N_2}(v)]$  and should be in Kelvin.  $z(v) = \frac{v}{1-v\chi_e}$ , with the anharmonicity factor  $\chi_{eCO} = 0.00612$  and  $\chi_{eN_2} = 0.00607$  and  $F(y)$  and the argument of the adiabatic function  $y$  are defined as (18) and (19).  $F_S$  is Shin's factor

$$F_S = \exp\left[\frac{4}{\pi \cdot \sqrt{T^*}} \cdot y^{\frac{1}{3}} + \frac{16}{3 \cdot \pi^2 \cdot T^*}\right], \quad (21)$$

with  $T^* = \frac{T}{\epsilon_{ST}}$ ,  $|\langle u+1 | q | u \rangle|^2$  is the matrix element of the quadrupole moment of  $N_2$  and  $\epsilon_{ST}$  is the well depth taken to be equal to the Lennard-Jones potential well depth. The semi-empirical parameters in equation (20) were obtained by fitting the rate coefficients from [159,160] in the temperature range  $80 \text{ K} < T_g < 700 \text{ K}$  and assuming that  $|\langle u+1 | q | u \rangle|^2 \approx (u+1)$ ,  $a = 6.6 \times 10^{-8} \text{ K}^{-1}$ ,  $b = 0.04 \text{ K}$ ,  $C = 145 \text{ K}$ . According to [158], the best-fitted interaction length  $L$  used in  $y$  is equal to  $0.185 \text{ \AA}$ . With this value, equation (20) adequately reproduces all the semiclassical data for resonant and non-resonant transitions [158].

The various coefficients are fitted through the exponential expression (9) and the fitting parameters can be found in the Supplementary Information. In Figure 4, we represent the rate coefficients obtained in this work following the procedure from Kurnosov *et al.* [158] for the process  $N_2(1) + CO(0) \rightarrow N_2(0) + CO(1)$  as a function of the gas temperature. Figure 4 shows as well the rate coefficients calculated using a mixed quantum-classical method by Hong *et al.* [161], a fitting of experimental data from Sato *et al.* [162] found in a survey of vibrational relaxation rate coefficients from Blauer & Nickerson [148], calculated by Shin [163] and other rate coefficients determined experimentally by Zittel & Moore [164], Stephenson & Mosburg [165], Starr *et al.* [166], Allen & Simpson [159] Green & Hancock [167] and Mastrocinque *et al.* [160] and found a good agreement with the experiments. Our rate coefficients are valid for  $T_g < 1000 \text{ K}$ . For higher gas temperatures the Quantum-classical rate coefficients calculated by Hong *et al.* [161] should be used instead, as they are in good agreement with the experimental data from Sato *et al.* [162] (not shown here) measured for  $T_g > 1600 \text{ K}$ .

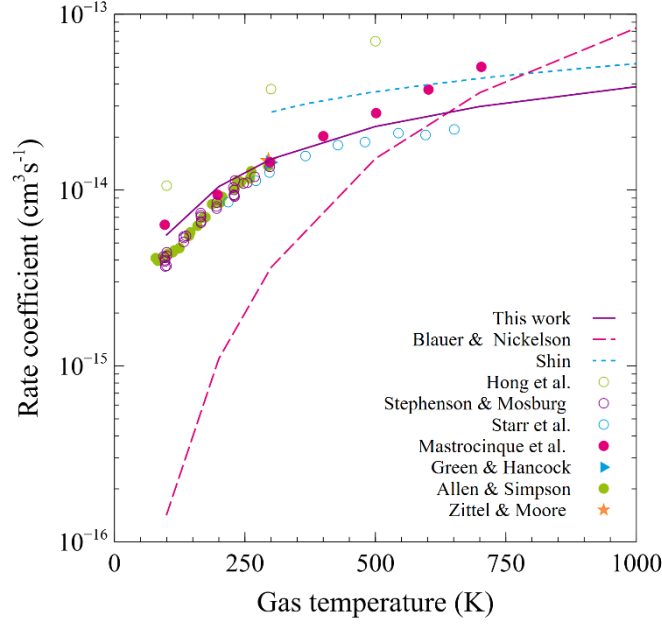


Figure 4: Comparison of the rate coefficients used in this work (—) with experimental data (symbols), fitting at high  $T_g$  (—) and calculation (--) for the near resonant VV exchange between  $N_2$  and  $CO$ ,  $N_2(1) + CO(0) \rightarrow N_2(0) + CO(1)$ .

### III.2.4 $M(v)$ - $M'$ V-T

The rate coefficients for the V-T relaxation from level  $v$  to  $v-1$  of  $N_2$  by collision with  $CO$  are obtained following the work of Plonjes *et al.* [168]. For the  $N_2(v)$ - $N_2$  V-T, the expressions recommended in [95,115,130] were favoured in the present paper as they lead to rate coefficients in a good agreement with the semiclassical calculations from [131,132] in the range  $300 \text{ K} < T_g < 1000 \text{ K}$ . Vibrational dissociation by V-T processes is included as a transition from the last bound vibrational level of  $N_2$  ( $v = 59$  here) to a pseudo-level in the continuum as done in [95,102,130] for  $N_2$  and originally for  $H_2$  in [169]. Note that, Terraz *et al.* [34] extended the applicability to temperatures in the range [200 K; 300 K] compared with the rate coefficients previously used in [95,115,130]. To do so the results from the semi-classical model of [131,132] available only for a few temperatures in the range [200 K ; 8000 K] were fitted as a function of the gas temperature and over two different temperature regimes, according to the exponential form (9). All the details for the determination of the  $N_2(v)$ - $N_2/CO_2$  rate coefficients using this procedure can be found in [34] as well as all the necessary coefficients to calculate the rate coefficients until  $v = 20$  for  $N_2$  (supplementary appendix).

For the other  $M(v)$ - $M'$  V-T rate coefficients we scale them according to the theoretical dependences from the SSH theory on the vibrational levels and gas temperature, as done in [95] for  $N_2(v)$ - $O_2$  and in [34] for  $N_2(v)$ - $CO_2$  energy transfers, calculated from the V-T  $N_2(v)$ - $N_2$ . To illustrate this method, the rate coefficient  $k_{v,v-1}(N_2)$  for deactivation of a vibrational level of  $CO$  by  $N_2$ , corresponding to the process  $CO(v) + N_2 \rightarrow CO(v-1) + N_2$ , is estimated from the rate coefficient for the relaxation of  $CO$  due to  $CO(v)$ - $CO$  collisions,  $k_{v,v-1}(CO)$  [38,170].

$$k_{v,v-1}(N_2)(T_g) = C_{radius} \times C_{mass} \times k_{v,v-1}(CO)(T_g) \times \frac{F(Y_{v,v-1}^{CO-N_2})}{F(Y_{v,v-1}^{CO-CO})}, \quad (14)$$

$$C_{radius} = \left( \frac{r_{CO-N_2}}{r_{CO-CO}} \right)^2 \text{ where } r_{i-j} = \frac{1}{2}(r_i + r_j), \quad (15)$$

with  $r_i$  the diameter of the molecule  $i$  in the hard sphere collision model



$$C_{mass} = \left( \frac{\mu_{CO-N_2}}{\mu_{CO-CO}} \right)^{\frac{1}{2}}, \quad (16)$$

where  $\mu_{i-j} = \frac{m_i \times m_j}{m_i + m_j}$  is the reduced mass of the collision and  $m_i$  the mass of molecule  $i$ .

$F(y)$  is the adiabacity function given by

$$F(y) \begin{cases} \frac{1}{2} \left[ 3 - e^{\frac{2y}{3}} \right] e^{-\frac{2y}{3}}, & y < 21.622 \\ 8 \left( \frac{\pi}{3} \right)^{\frac{1}{2}} y^{\frac{7}{3}} e^{-\frac{2y}{3}}, & y \geq 21.622 \end{cases}, \quad (17)$$

with  $y$  the adiabacity factor

$$y_{v,v-1} = \Delta E_{v,v-1} \times \left( \frac{\pi L}{\hbar} \right) \times \sqrt{\frac{\mu}{2k_B T_g}}, \quad (18)$$

with  $\Delta E_{v,v-1}$  the energy difference between the vibrational levels  $v$  and  $v-1$  of  $N_2$ ,  $k_B$  the Boltzmann constant,  $T_g$  the gas temperature and  $L$  is the 'interaction length' calculated from the expression [16]:

$$L = \frac{1}{\frac{17.5}{r_0}}, \quad (19)$$

with  $r_0$  the Lennard Jones potential distance from [171]. The same approach was adopted in our previous work [38] for  $CO(v)$ -M ( $M=CO_2, O_2$ ) using the rate coefficient from  $CO(v)$ - $CO$  V-T and  $CO_2(v)$ -M' ( $M'=CO, O_2$ ) using the rate coefficient from  $CO_2(v)$ - $CO_2$  V-T.

### III.3 Surfaces processes

An important process in the vibrational kinetics, in our experimental conditions, is the deactivation of vibrationally excited  $CO_2$ ,  $CO$  and  $N_2$  molecules through collisions at the reactor wall. This deactivation of vibrationally excited states is shown to have a significant influence on the vibrational characteristic temperatures, especially for pressures below 1 Torr [38,172]. Due to the lack of experimental values, we set the same value of deactivation probability,  $\gamma_v$ , for any mode of  $CO_2$  i.e.  $\gamma_v(CO_2(v>0)) = 0.2$  for a Pyrex surface (average value from Table 1 of [173]) where the  $CO_2$  molecule is assumed to deactivate to the vibrational ground state. We use a constant value of  $4 \cdot 10^{-2}$  for the deactivation probability for all levels of  $CO$  and  $4.9 \cdot 10^{-4}$  for the deactivation probability for all levels of  $N_2$  both taken from [173]. As opposed to  $CO_2$ , we consider single-quantum transitions for  $CO$  and  $N_2$  as done for  $N_2$  and  $O_2$  in [95], where only one vibrational quantum is lost upon collision with the wall. We also investigate the impact of changing the deactivation probability for the bending, symmetric stretch and mixed modes of  $CO_2$ , from 0.2 to 0.05, on the vibrational temperatures (cf. Section (IV.1, Fig. 9 and 10). Note that the gas mixture might influence the wall de-excitation probability of vibrationally excited molecules. For instance, a linear enhancement of the  $N_2(v)$  wall deactivation probability from  $1.3 \cdot 10^{-3}$  to  $2.6 \cdot 10^{-3}$  with an increase in the admixture of  $CO_2$  (from 0.066 % to 0.5 %) in a low-pressure  $N_2$  plasma was observed for a Pyrex surface [174].

The importance of the  $CO_2$ -O V-T exchanges calls for a verification of the accuracy of the calculation of the atomic oxygen concentration. In turn, the loss of O atoms is mainly controlled by recombination at the walls to form  $O_2$  molecules characterized by the wall O loss/recombination probability,  $\gamma_O$ . In this study,  $\gamma_O$  is assumed to remain constant for the different mixture compositions, equal to the probability measured in pure  $CO_2$  [89] as a function of pressure and at 50 mA (cf. Table 1). Changes in  $\gamma_O$  are not expected to significantly modify the  $CO_2$  dissociation fraction, as shown in

[38,175], but could lead to an increase/decrease in O atom fractions affecting the vibrational temperatures because of the strong CO<sub>2</sub>-O V-T deactivation. It is known that the recombination probability depends on the nature of the gas ignited in the reactor [89,176]. In CO<sub>2</sub>-N<sub>2</sub> plasmas, CO molecules, C and N atoms or even CO<sub>2</sub> molecules are likely to be chemisorbed or physisorbed on the reactor walls, changing the surface configuration and competing for the adsorption sites with O atoms limiting the recombination into O<sub>2</sub>. The possibility of CO adsorbed at the walls was already suggested by Cenian *et al.* [177] where the rate for the O recombination at the wall is assumed to depend on the CO concentration in the gas phase (see reaction 11 in Table 3.1 of [177]). We thus expect  $\gamma_O$  to be lower for a CO<sub>2</sub>-N<sub>2</sub> plasma than for a pure O<sub>2</sub> plasma. However, at present it is difficult to draw any conclusions on the values of  $\gamma_O$  in CO<sub>2</sub>-N<sub>2</sub> with regards to the pure CO<sub>2</sub> case.

## IV. Results

### IV.1 Model validation

In this section, the results of our model are compared with experimental data measured in a CO<sub>2</sub>-N<sub>2</sub> DC discharge for pressures between 0.6 and 4 Torr and a current of 50 mA. The calculated reduced electric field, vibrational temperatures, atomic oxygen and NO fractions and CO<sub>2</sub> dissociation fraction are compared with the ones obtained experimentally. For completeness, tables with the calculated concentrations of all the species considered in the model are given in the Supplementary Information for a few selected conditions.

The model shows a satisfactory quantitative agreement and reproduces very well the dependencies of the measured quantities for different pressures and initial CO<sub>2</sub> fractions in the different CO<sub>2</sub>-N<sub>2</sub> mixtures. Once validated against the benchmark experiments, the model is used for the interpretation of the measured quantities and the identification of the main processes ruling the discharge.

In Figures 5 and 6 we represent E/N and [O]/N, respectively, as a function of pressure for a pure CO<sub>2</sub> plasma and for a CO<sub>2</sub>-N<sub>2</sub> plasma with a ratio of 1:1. A decrease of E/N with increasing pressure can be observed in experiments and simulations for pure CO<sub>2</sub> and for the mixture. There is, in general, a quite good agreement between the model predictions and the experimental values, although the absolute value of E/N is somewhat overestimated in the calculations at the low pressures, especially for the pure CO<sub>2</sub> discharge. A maximum of [O]/N around 1 Torr can be observed in experiments and simulations for pure CO<sub>2</sub> which is mostly due to the O loss frequency showing a minimum at 1 Torr [89]. However, the maximum of experimental [O]/N seems to be shifted for CO<sub>2</sub>-N<sub>2</sub> which is not reproduced in the simulations. Since the simulations consider the same recombination probability for atomic oxygen at the wall via  $O + \text{wall} \xrightarrow{\gamma_O} O_2$ ,  $\gamma_O$ , for pure CO<sub>2</sub> and for the CO<sub>2</sub>-N<sub>2</sub> mixture (cf. section III.2.5), the results suggest that the dependence on pressure of  $\gamma_O$  might be different in the CO<sub>2</sub>-N<sub>2</sub> mixtures than in pure CO<sub>2</sub>. To investigate the importance of this quantity on the [O]/N simulation results, we multiply by two the  $\gamma_O$  and the resulting [O]/N are given in Figures 6 and 7.

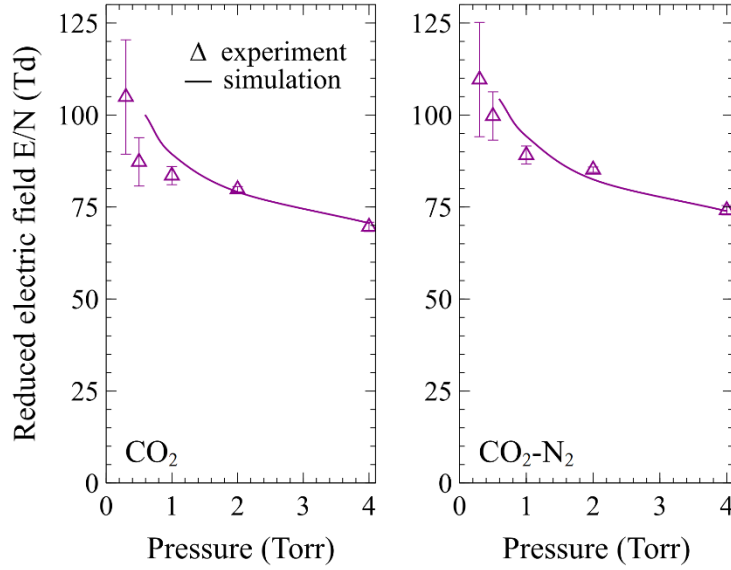


Figure 5: Reduced electric field  $E/N$  as a function of pressure for pure  $\text{CO}_2$  (left) and a 50/50  $\text{CO}_2\text{-N}_2$  mixture, at a current of 50 mA: experiment ( $\Delta$ ) and model calculations (—).

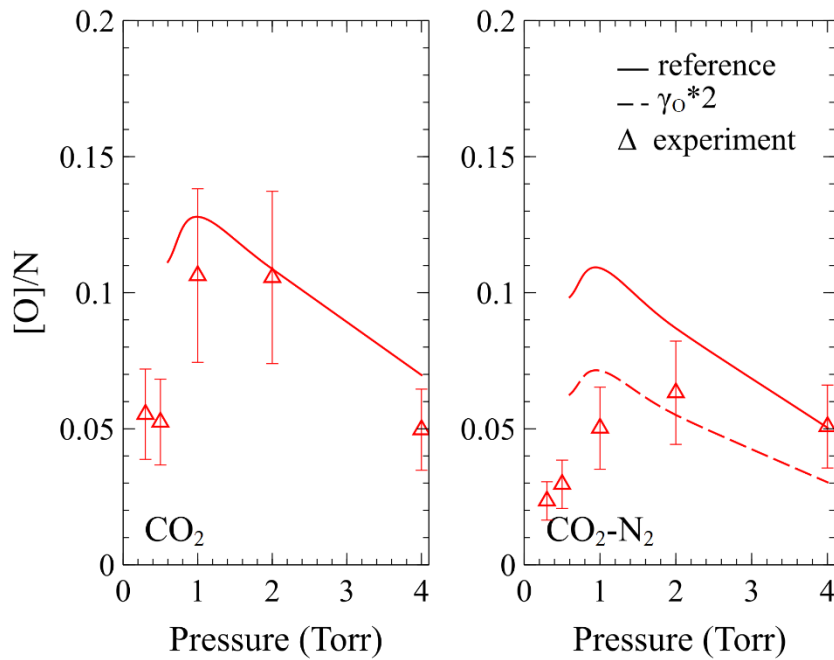


Figure 6: Atomic oxygen fraction,  $[O]/N$ , as a function of pressure for pure  $\text{CO}_2$  (left) and a 50/50  $\text{CO}_2\text{-N}_2$  mixture, at a current of 50 mA: experiment ( $\Delta$ ), model calculations with the default  $\gamma_0$  values from [89] (—) and  $\gamma_0$  values multiplied by two (--).

Figure 7 shows the measured and calculated values of the reduced electric field,  $E/N$ , and the atomic oxygen fraction,  $[O]/N$ , as a function of the  $\text{CO}_2$  initial fraction for a discharge current of 50 mA, at 2 Torr. Overall, the self-consistently calculated reduced electric field variation with the  $\text{CO}_2$  initial fraction agrees well with the experimentally measured  $E/N$ . These results prove that the ionization rates and ion chemistry (transport and charge exchange) are well characterized and that the model can be used as a predictive tool when no experimental data for  $E/N$  are available. The atomic oxygen fraction,  $[O]/N$ , also shows a proper trend with the  $\text{CO}_2$  fraction but remains too high for all conditions except for the pure  $\text{CO}_2$  case. One possibility to justify this discrepancy would be a too strong  $\text{O}_2$  dissociation by electron impact associated with Phelps cross section, as suggested by

several authors [178,179] and further discussed in [38,111]. The agreement could be improved by using Polak's cross section for O<sub>2</sub> dissociation by electron impact [180] as discussed in [38] in the context of CO<sub>2</sub>-O<sub>2</sub> plasmas. Another possibility would be a larger recombination probability at the wall for the different mixtures in comparison to the pure CO<sub>2</sub> case. A dependence of  $\gamma_O$  on the CO<sub>2</sub> fraction in the different CO<sub>2</sub>-N<sub>2</sub> mixtures seems plausible, as discussed in section III.2.5. Upon multiplying  $\gamma_O$  by two, we can observe that [O]/N decreases by 24 % and 38 % for CO<sub>2</sub> initial fractions of 0.1 and 0.9 respectively, leading to a [O]/N too low for CO<sub>2</sub> fractions higher than 0.25 and too high for CO<sub>2</sub> fractions below. From this analysis it can be inferred that [O]/N is very sensitive to the recombination probability of atomic oxygen  $\gamma_O$  at the wall and that to obtain a good agreement between the simulations and experiment the  $\gamma_O$  should increase with the N<sub>2</sub> fraction.

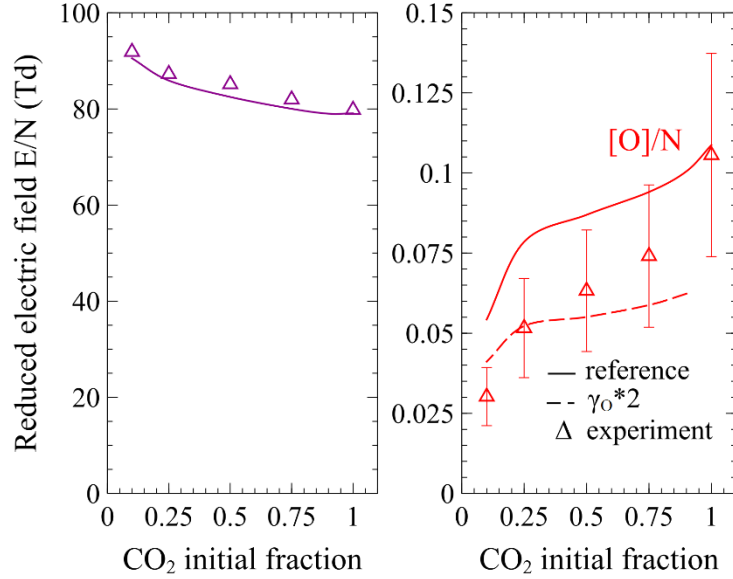


Figure 7: Measured and calculated reduced electric field,  $E/N$ , and atomic oxygen fraction,  $[O]/N$ , of a CO<sub>2</sub>-N<sub>2</sub> discharge as a function of the CO<sub>2</sub> fraction in the initial mixture, at 2 Torr and 50 mA: from experiment ( $\Delta$ ) and model calculations with the default  $\gamma_O$  values from [89] (—) and  $\gamma_O$  values multiplied by two (---).

Our state-to-state model also provides the populations of each individual vibrational levels of the different modes of CO<sub>2</sub> and of CO and N<sub>2</sub>. The vibrational temperature is then calculated assuming a Treanor distribution [90], as:

$$T_{v,ij} = \left( \frac{E_1}{\ln(p_i/p_j) - \frac{E_j - E_i - E_1}{k_B T_g}} \right) / k_B, \quad (24)$$

where  $E_1$  is the energy of the first level,  $p_i$  and  $p_j$  and  $E_i$  and  $E_j$  are the population and energy of levels  $i$  and  $j$ , respectively,  $T_g$  is the gas temperature and  $k_B$  the Boltzmann constant. We use an average of the temperatures calculated using the first three vibrational levels. Note that for the specific case of the CO<sub>2</sub> bending mode corresponding to  $\nu_2$ , we assume a Boltzmann distribution to obtain the vibrational temperature  $T_2$  (see equation 5 in [99]). Moreover, for simplicity in the presentation of the results, we define a common temperature of the bending and symmetric stretching modes denoted  $T_{1,2}$  [33,89] which is enough for a simple description of the vibrational kinetics even though this is not imposed in the model [38].

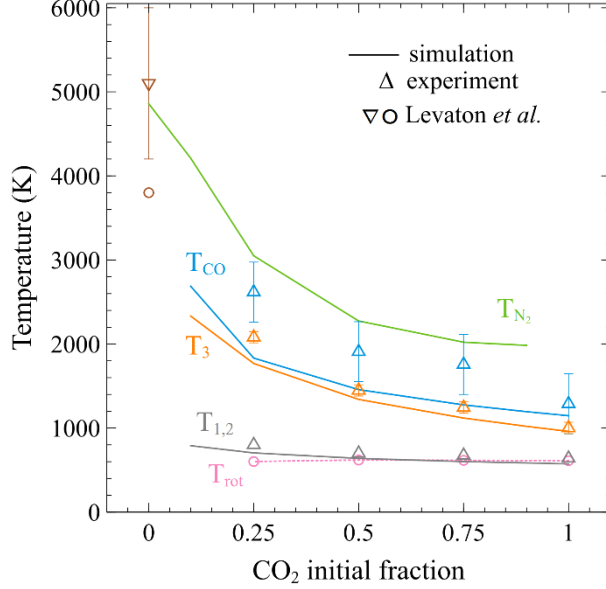


Figure 8: Experimental values ( $\Delta$ ) and calculated values (line) of the common vibrational temperature of the CO<sub>2</sub> bending and symmetric modes  $T_{1,2}$ , the vibrational temperature of the asymmetric stretching mode  $T_3$ , the CO and N<sub>2</sub> vibrational temperatures  $T_{CO}$  and  $T_{N_2}$  and the rotational temperature  $T_{rot}$  ( $\circ$ ) (used as input parameter for the model) when a discharge is ignited in different mixtures of CO<sub>2</sub>-N<sub>2</sub>, at 50mA, and a pressure of 2 Torr.

Figure 8 shows the vibrational temperatures of CO and of the different modes of CO<sub>2</sub> obtained from the model and experiment as well as the experimental rotational temperature  $T_{rot}$  used as input parameter for the model and the calculated vibrational temperature of N<sub>2</sub> as a function of the CO<sub>2</sub> initial fraction. Note that the vibrational temperatures are calculated with expression (24) using the very first points ( $v=0, 1$  and  $2$ ) of the vibrational distributions (see Fig. 11). All the vibrational temperatures increase with the N<sub>2</sub> content. This trend can be partly explained by the reduced quenching of vibrations of CO<sub>2</sub>/CO/N<sub>2</sub> by O atoms as  $[O]/N$  decreases with decreasing the CO<sub>2</sub> initial fraction (cf. Fig. 7). Indeed, O atoms are very efficient quenchers of the CO<sub>2</sub> vibrations as already discussed in section III.2.5. Besides, the vibrational deactivation of N<sub>2</sub> also takes place essentially by V-T deactivation with O atoms and to a lesser extent through the Zel'dovich reaction forming NO, as also shown in [95]. Note that, the CO<sub>2</sub>-N<sub>2</sub> V-V and CO-N<sub>2</sub> V-V transfers play a major role to explain the trends observed and this is discussed in more details at the end of the section (Fig. 12). The rotational temperature  $T_{rot}$  remains almost constant with N<sub>2</sub> addition as already observed in [70]. The temperature  $T_{1,2}$  is very close to  $T_{rot}$ , as expected from the small energy difference between levels of symmetric and bending modes that favours the V-T deexcitation. The V-V up pumping and CO<sub>2</sub>-N<sub>2</sub> V-V mechanism produce important concentrations of vibrationally excited states of CO<sub>2</sub> in the asymmetric stretch mode. The large energy difference between the asymmetric stretch mode levels of CO<sub>2</sub> and the anharmonic V-V up pumping and CO<sub>2</sub>-N<sub>2</sub> V-V transfers are beneficial to reach high concentration of vibrationally excited CO<sub>2</sub>. However, part of the energy stored in  $v_3$  is lost through the intermode V-V transfer ( $CO_2(v_3)+CO_2(v_{1,2}) \rightarrow CO_2(v_3-1)+CO_2(v_{1,2}+1)$ ), and through quenching by O atoms.  $T_{CO}$  systematically showing larger values than  $T_3$  for all the conditions reported can be explained by different rate coefficients for V-T relaxation, the lack of inter-mode V-V relaxation processes for CO, and more efficient vibrational excitation through electron-to-vibrational energy transfers for CO [38,89]. Finally,  $T_{N_2}$  is higher than  $T_{CO}$  and two main reasons can be evoked. First, the quenching of vibrationally excited molecules by O atoms is more efficient for CO than N<sub>2</sub>. Indeed, the rate coefficient included in this work for the N<sub>2</sub>-O V-T, as described in [22, 53], is at least 10 times lower than for CO [38,136] in the temperature range [300 K;1000 K]. Second, the deactivation of vibrationally excited states at the wall is more important in the case of CO than N<sub>2</sub> as the deactivation probability is two orders of magnitude lower for N<sub>2</sub> (cf. section III.2.5).

The calculated and measured vibrational temperatures of N<sub>2</sub> obtained for a flowing DC glow discharge in pure N<sub>2</sub> by Levaton *et al.* [181] are given on Fig. 8 as an indicator since we do not have

access to experimental values for  $T_{N_2}$  with FTIR spectrometry. The experimental conditions are very similar to the ones used in the present work in terms of current, radius of the glass tube, pressure, and type of discharge. The main difference comes from the flow with a rate around 10 times higher in [181]. Since the  $T_{rot}$  obtained by FTIR does not change for the different mixtures studied in this work (cf. Fig. 10), we use the same for the pure  $N_2$  simulation. The  $T_{N_2}$  calculated with our model is in very good agreement with the data point obtained in [181] by Optical Emission Spectroscopy, but higher than the value calculated using the state-to-state kinetic model from the same author [181]. To further validate the vibrational kinetics in  $CO_2$ - $N_2$  plasmas, future measurements (similar to what was done in [75]) require the detection of the vibrational temperature of  $N_2$ .

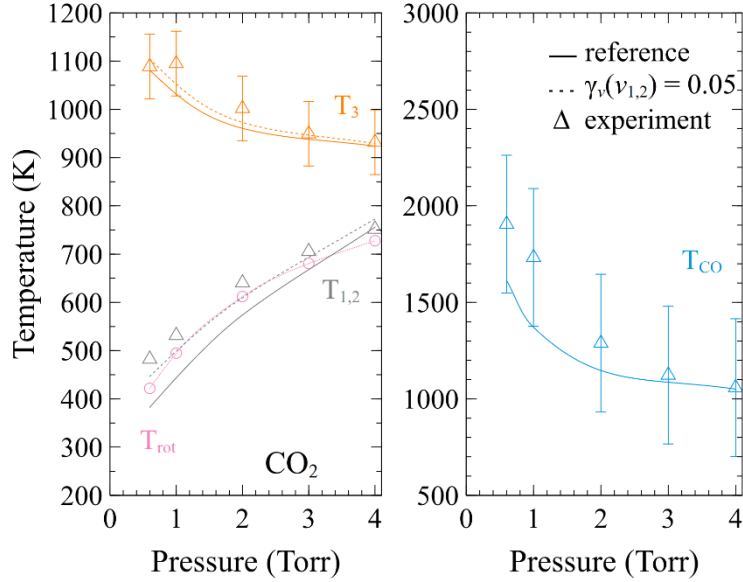


Figure 9: Experimental values ( $\Delta$ ) and calculated values (line) of the common vibrational temperature of the  $CO_2$  bending and symmetric modes  $T_{1,2}$ , the vibrational temperature of the asymmetric stretching mode  $T_3$ , the  $CO$  and  $N_2$  vibrational temperatures  $T_{CO}$  and  $T_{N_2}$  and the rotational temperature  $T_{rot}$  (o) (used as input parameter for the model) when a discharge is ignited in pure  $CO_2$ , at 50mA, as a function of pressure. The model calculations were done including with the default probabilities of deactivation of the vibrationally excited states of  $CO$  and  $N_2$  and the different modes of  $CO_2$ , at the wall from section IV.6. (—) and  $\gamma_v(v_{1,2}) = 0,05$  (···)

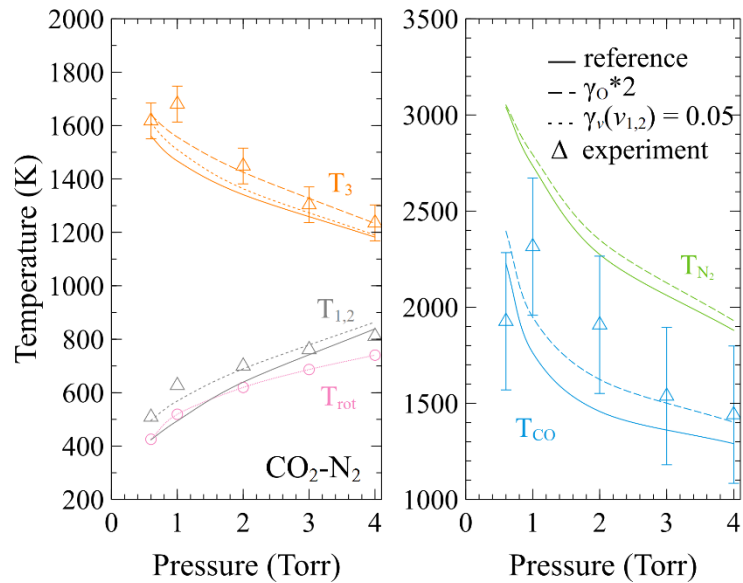


Figure 10: Experimental values ( $\Delta$ ) and calculated values (line) of the common vibrational temperature of the  $CO_2$  bending and symmetric modes  $T_{1,2}$ , the vibrational temperature of the asymmetric stretching mode  $T_3$ , the  $CO$  and  $N_2$  vibrational

temperatures  $T_{CO}$  and  $T_{N_2}$  and the rotational temperature  $T_{rot}(o)$  (used as input parameter for the model) when a discharge is ignited in  $CO_2-N_2$  (50 % of each) at 50mA, as a function of pressure. The model calculations were done including with the default probabilities of deactivation of the vibrationally excited states of CO and  $N_2$  and the different modes of  $CO_2$ , at the wall from section IV.6. (—),  $\gamma_{v(v_{1,2})} = 0,05$  (···) and multiplying the default  $\gamma_o$  values from [89] by two (—).

Figures 9 and 10 show the vibrational temperatures of CO and of the different modes of  $CO_2$  obtained from the model and experiment as well as the experimental rotational temperature  $T_{rot}$  used as input parameter for the model and the calculated vibrational temperature of  $N_2$  as a function of pressure for pure  $CO_2$  and a  $CO_2-N_2$  mixture with 50 %  $CO_2$ , respectively. The increase of  $T_{rot}$  with the pressure can be explained by the higher power dissipated in the plasma because of the higher voltage (and therefore power) required to maintain the current as the pressure is increased. The exact mechanisms responsible for the conversion of electrical energy into gas heating are complex, but include enhanced V-T transfers at higher pressure and possible exothermic reactions [35,70,99]. The influence of deactivation of vibrationally excited  $CO_2$  and CO at the walls, described in section III.2.5., is illustrated in Figure 9 for the case of pure  $CO_2$  and Figure 10 for the  $CO_2-N_2$  mixture. Including the wall deactivation for vibrationally excited  $CO_2$ , CO and  $N_2$  molecules mostly affects the vibrational temperatures of these molecules at lower pressures as observed in [38,172]. The default deactivation probabilities of the different modes of  $CO_2$  are 0.2 (Section III.2.5.) and lead to simulated  $T_{1,2}$  values lower than in the experiment. The results labelled  $\gamma_{v(v_{1,2})} = 0.05$  correspond to simulations with a deactivation probability for the bending, symmetric stretch and mixed modes of  $CO_2$  of 0.05, instead of 0.2, as proposed for pure  $CO_2$  in [38] and lead to a better agreement of the calculated  $T_{1,2}$  with experiment. Since no experimental values for the wall deactivation probability (on Pyrex) of the bending mode of  $CO_2$  was reported in the literature to our knowledge, the present results suggest a value for  $\gamma_{v(v_{1,2})}$  smaller than for  $\gamma_{v(v_3)}$ . Finally, we observe that  $T_{CO}$  and  $T_3$  increase upon multiplying the  $\gamma_o$  by two as a consequence of the reduced deactivation through V-T with O. Note that for readability of the figure we do not represent this case for  $T_{1,2}$  as it changes by a maximum of 3 % only.

The vibrational distribution functions (VDFs) of the asymmetric stretch mode of  $CO_2$ , and bending mode of  $CO_2$ , of  $N_2$  and CO, calculated for a DC glow discharge operating at 2 Torr for different  $CO_2-N_2$  gas mixtures are represented in Figure 11. The simulations evince a remarkable deviation from equilibrium for  $N_2$  and CO, and to a lesser extent for  $CO_2$ , emphasizing the importance of detailed state-to-state models to understand the vibrational energy transfers taking place in the system, as already pointed out in [54]. To maintain this non-equilibrium, the gas temperature must be kept low to suppress the quenching of vibrations. Indeed, V-T relaxation poses an inherent loss mechanism of vibrational energy and increases the gas temperature, which in turn enhances the V-T relaxation creating a positive feedback loop between gas heating and quenching [8]. The VDFs for 90 % and 75% of  $CO_2$  are only represented for the asymmetric stretch of  $CO_2$  for readability of the figure as they almost overlap with each other in the other cases.

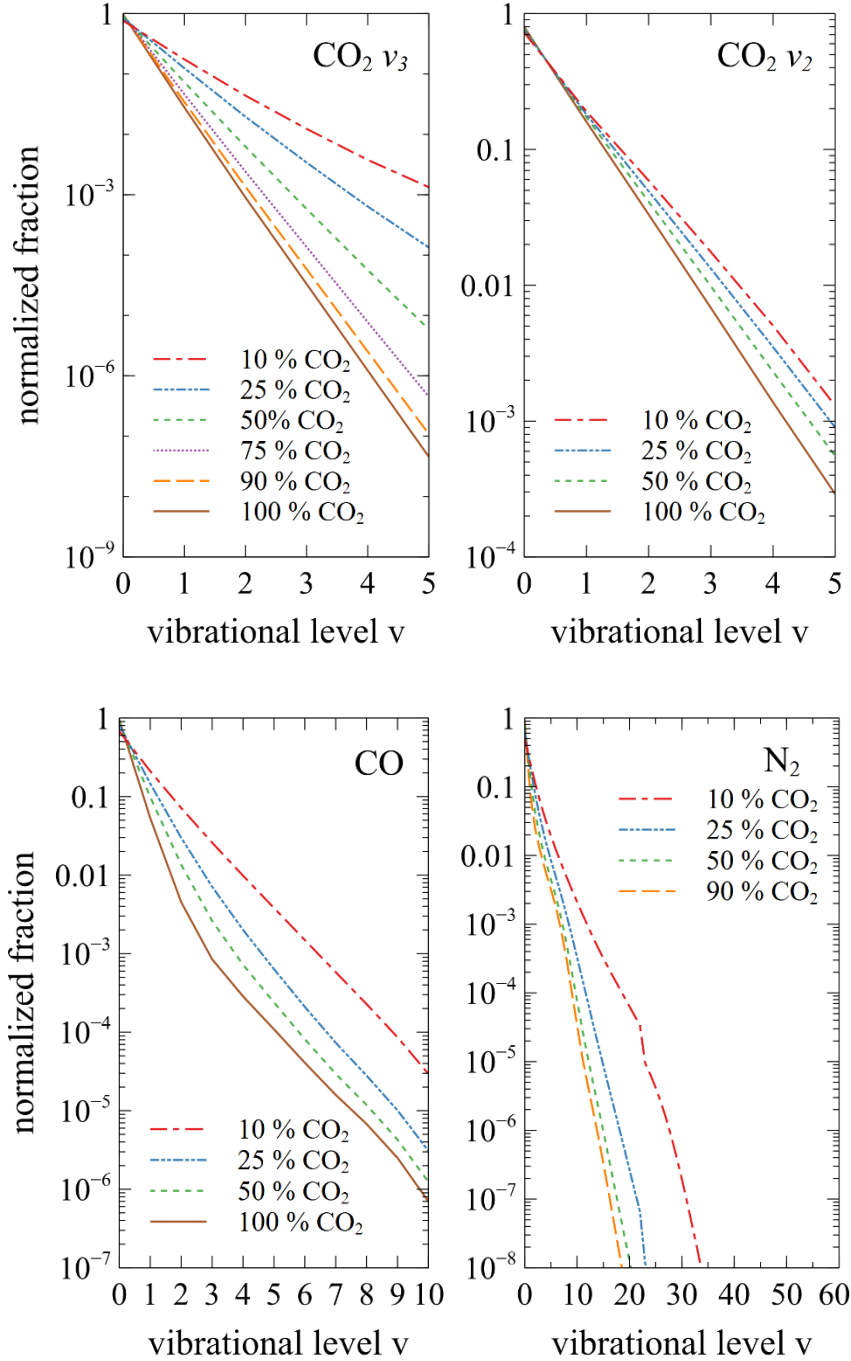


Figure 11: Vibrational distribution functions of the asymmetric stretch mode of  $\text{CO}_2$  ( $v_3$ ), bending mode of  $\text{CO}_2$  ( $v_2$ ), of  $\text{N}_2$  and  $\text{CO}$ , calculated for a DC glow discharge operating at 2 Torr and  $I = 50$  mA for different  $\text{CO}_2$ - $\text{N}_2$  gas mixtures.

It is well-known that an important part of electron energy is transferred into the vibrational excitation of  $\text{CO}_2$ ,  $\text{CO}$  and  $\text{N}_2$ , in the range of  $E/N$  between 1 and 100 Td [172,182]. This emphasizes the necessity of having a correct description of the vibrational energy transfers between these species. In particular, it is expected that near resonant  $\text{CO}_2$ - $\text{N}_2$  and  $\text{CO}$ - $\text{N}_2$  transfers may have an impact shaping the VDFs. To quantify the importance of these transfers, we removed them from the simulations and checked the changes in the vibrational temperatures. The vibrational temperatures  $T_3$ ,  $T_{\text{CO}}$  and  $T_{\text{N}_2}$  are represented as a function of the  $\text{CO}_2$  initial fraction in Figure 12. We can notice that without the  $\text{CO}_2$ - $\text{N}_2$  V-V transfer  $T_3$  is almost constant, and far from experimental values, for all the mixtures considered and the same can be said for  $T_{\text{CO}}$  and the  $\text{CO}$ - $\text{N}_2$  V-V transfer. In the case of  $T_{\text{N}_2}$  both transfers are also playing a significant role but the increase of  $T_{\text{N}_2}$  with decreasing the  $\text{CO}_2$  initial



fraction also comes from the enhancement of the electron-impact excitation of vibrations of  $N_2$  as the fraction of  $N_2$  increases in the mixture.

The scaling of  $CO_2-N_2$  V-V, according to the Sharma Brau theory, explained in detail in section III.2.2., also influences  $T_3$  and  $T_{N_2}$ . Therefore, we represent these vibrational temperatures as a function of the  $CO_2$  initial fraction keeping the rate coefficient for the  $CO_2-N_2$  V-V as represented in Figure 1 regardless of the vibrational levels involved (no SB scaling) and scaling this rate coefficient (reference). From this examination it can be concluded that the increase of  $T_3$  with  $N_2$  is mostly due to the  $CO_2-N_2$  V-V and similarly for  $T_{CO}$  with  $CO-N_2$  V-V. Both processes (and the SB scaling) significantly improve the agreement between the simulations and experiment for  $T_3$  and  $T_{CO}$  further conveying the importance of including these processes in the model.

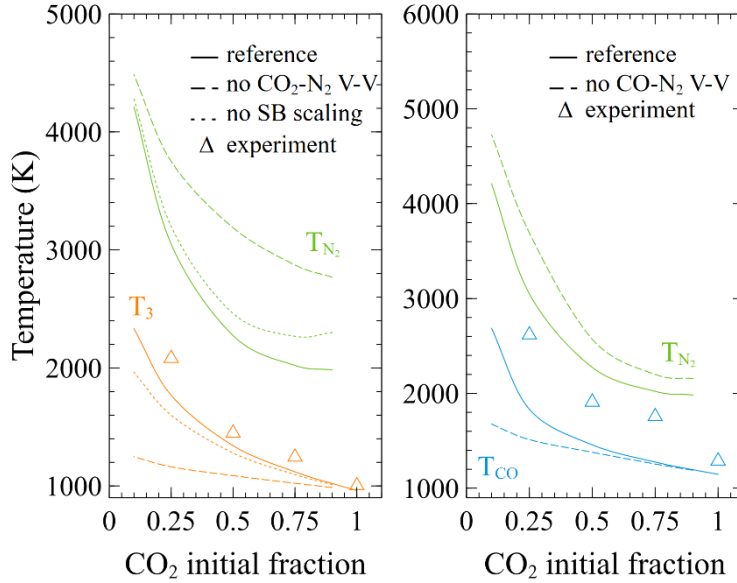


Figure 12: Experimental values ( $\Delta$ ) and calculated values (line) of the common vibrational temperature of the  $CO_2$  of the asymmetric stretching mode  $T_3$ , the  $CO$  and  $N_2$  vibrational temperatures  $T_{CO}$  and  $T_{N_2}$  as a function of the  $CO_2$  initial fraction, at 50mA. The model calculations were done excluding ( $---$ ), including the  $CO_2-N_2$  V-V transfer with ( $---$ ) and without scaling ( $\cdots$ ) (left) and including ( $---$ ) and excluding ( $---$ ) the  $CO-N_2$  V-V transfer (right). The error bars are not represented here but are the same as in Fig. 13.

## IV.2 Effect of $N_2$ on $CO_2$ dissociation

In this section the beneficial effect of admixture of  $N_2$  on the  $CO_2$  dissociation, already observed experimentally and by modeling in [34,68,70,71,183], is investigated. Several reasons can be assigned to this effect. For instance, the enhancement of the reduced electric field, the effect of electronically excited states on the  $CO_2$  dissociation directly or via changes of the EEDF, the vibrational excitation of nitrogen and its transfer to the  $CO_2$  asymmetric stretching mode and the dilution with  $N_2$  limiting the influence of back reaction mechanisms are possibilities often advanced [8,66,172].

Figure 13 shows the absolute ( $\alpha$ ) and effective ( $\alpha_{eff}$ )  $CO_2$  dissociation fraction as a function of the  $CO_2$  initial fraction at 2 Torr. The latter takes into account the initial fraction of  $CO_2$  in the gas mixture (for instance, when only 10 %  $CO_2$  is present in the gas mixture, the absolute conversion needs to be multiplied by a factor 0.1). The increase of the absolute  $CO_2$  dissociation fraction,  $\alpha$ , (cf. equation 1) with  $N_2$ , both in the experimental data and the calculations, indicates that  $N_2$  has a beneficial effect on  $CO_2$  splitting. Dissociation fractions up to 70 % are observed, a very encouraging result considering that the present setup is designed for fundamental studies only. However, it might be more relevant to use the effective dissociation instead as it takes into account the initial fraction of  $CO_2$  in the gas mixture. The effective  $CO_2$  conversion decreasing linearly when adding  $N_2$  can be explained by the lower  $CO_2$  fraction in the mixture, which compensates the enhancement of the absolute conversion of  $CO_2$  in the presence of  $N_2$ . the decrease of  $\alpha_{eff}$  was already observed in the simulations of an unpacked

DBD reactor [183] and of a MW discharge [68]. Note that no significant dissociation of  $N_2$  was observed for all the simulations conducted (below 0.05 %).

Overall, a good agreement is obtained between the experimental and calculated trend for the  $CO_2$  dissociation even when reactions (20)-(23) (cf. section III.1.1) are not included in the simulations (reference case).

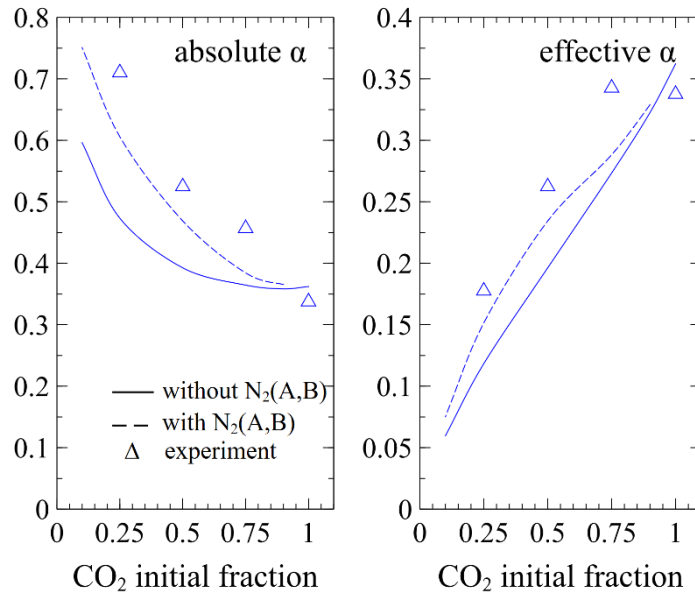


Figure 13: Absolute and effective dissociation fraction for different  $CO_2/N_2$  mixtures for a discharge current of 50 mA and a pressure of 2 Torr. The curve labelled 'with  $N_2(A,B)$ ' corresponds to the reference case to which we added the processes from Tables 2 and 3.

The agreement is further improved when the dissociative quenching processes with the two metastable states,  $N_2(A)$  and  $N_2(B)$ , are included in the model, as described in section III.1.1. Indeed, these states open a new  $CO_2$  dissociation channel and are claimed to be responsible for the increase of  $\alpha$  in the presence of  $N_2$  by several authors [63,66,71,120,121,129,183]. As can be seen in Figure 13, adding these processes noticeably improves the absolute value and trend of the  $CO_2$  dissociation fraction. This shows that the dissociation of  $CO_2$  molecules in collisions with electronically excited states of  $N_2$  gives a substantial contribution to the conversion rate. We have verified that considering the  $CO_2$  dissociation by  $N_2(A)$  does not change appreciably the results, which shows that  $N_2(B)$  is the main contributor. It is worth pointing out that the dissociation fraction is also increasing when these processes are not accounted for, suggesting that other phenomena are also responsible for the beneficial effect of  $N_2$  on the dissociation of  $CO_2$ .

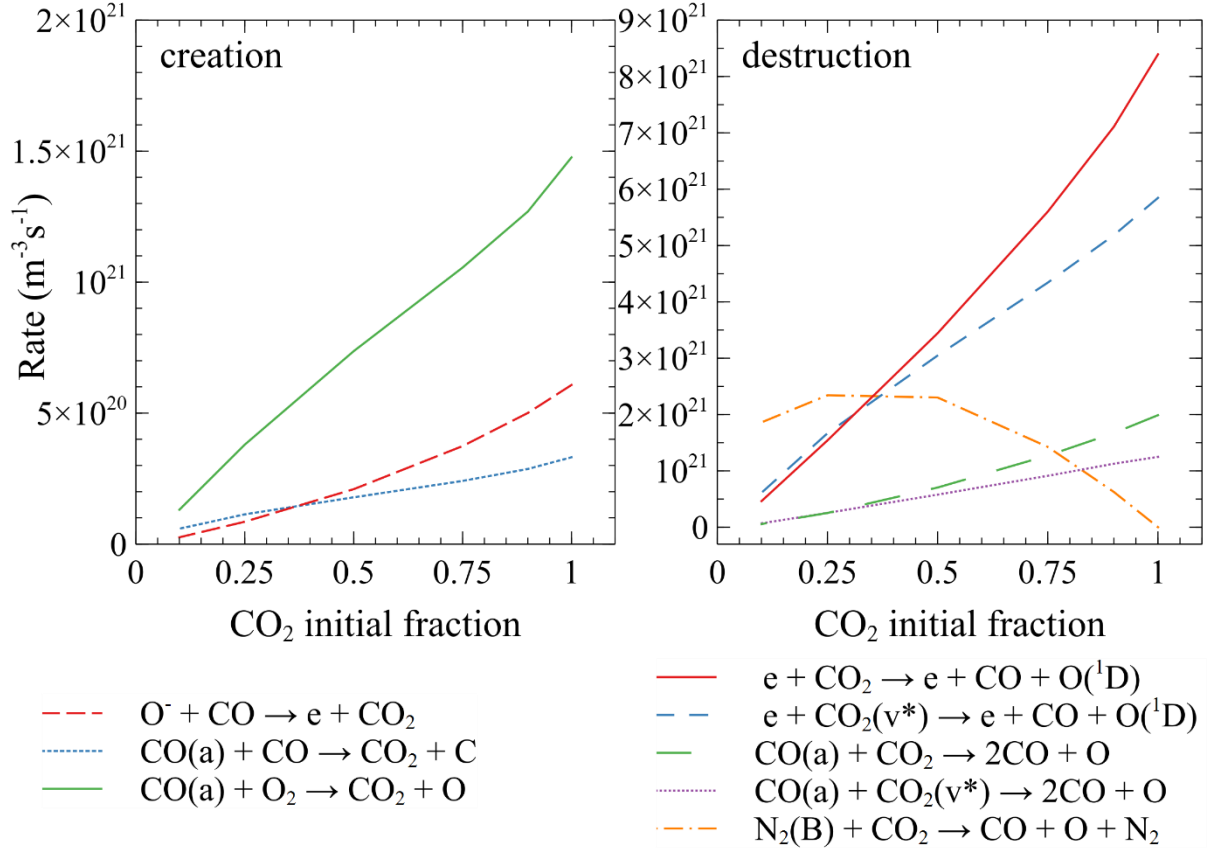


Figure 14: Rate of the most important creation (left) and destruction (right) processes of CO<sub>2</sub>, as a function of CO<sub>2</sub> fraction in the CO<sub>2</sub>-N<sub>2</sub> gas mixture, at 2 Torr.

To explain the trend of the CO<sub>2</sub> dissociation fraction with the addition of N<sub>2</sub>, we plot in Figure 14 the rates of the most important creation and destruction processes of CO<sub>2</sub>, as a function of the CO<sub>2</sub> initial fraction for P = 2 Torr and I = 50 mA. In the system under study, CO<sub>2</sub> can be decomposed by direct electron impact, both on molecules in the vibrational ground-state (GS) and in vibrational excited states (VES), noted CO<sub>2</sub>(v\*), through  $\text{e} + \text{CO}_2 \rightarrow \text{CO} + \text{O}({}^1\text{D})$ . The contribution of the vibrational states comes mainly from the lower-laying levels (01<sup>1</sup>01), (02<sup>2</sup>01), (10<sup>0</sup>02) and (00<sup>0</sup>11). For high N<sub>2</sub> content, corresponding to a higher vibrational temperature of the asymmetric mode of CO<sub>2</sub> (cf. Fig. 10), the electron-impact dissociation on the VES surpasses the one from the GS. However, this does not have any impact on the CO<sub>2</sub> dissociation fraction because overall the rates of electron impact from GS and VES decrease with the N<sub>2</sub> content due to the decrease of CO<sub>2</sub> density and rate coefficient (cf. discussion of figure 15 concerning the EEDF).

At high N<sub>2</sub> fractions, the contribution of CO<sub>2</sub> dissociation in quenching collisions with N<sub>2</sub>(B) via:

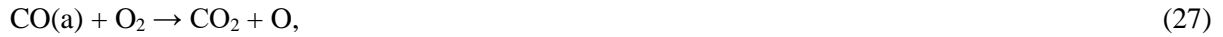


even exceeds that of dissociation of CO<sub>2</sub> molecules by electron impact. However, this is accompanied by a lower CO<sub>2</sub> content in the mixture, leading to a drop in effective CO<sub>2</sub> conversion (Fig. 13). Above 75% N<sub>2</sub>, both the electron-impact dissociation and the dissociation by N<sub>2</sub> metastable molecules rates decrease due to the lower CO<sub>2</sub> concentration, which is not compensated by the higher N<sub>2</sub> concentration (and thus higher dissociation by N<sub>2</sub> metastable molecules). In addition, for small O<sub>2</sub> and CO concentrations, CO<sub>2</sub> dissociation can be stimulated through:



The importance of these two mechanisms shows that despite their low density, electronically excited species can have a large influence on the overall plasma chemistry. The calculated densities of these electronically excited states are given in the Supplementary Information for several conditions. We observe that both the calculated  $N_2(A)$  and  $N_2(B)$  densities increase with the  $N_2$  content, going from  $1.45 \cdot 10^{16} \text{ m}^{-3}$  and  $1.55 \cdot 10^{15} \text{ m}^{-3}$  at 90 %  $CO_2$  to  $1.6 \cdot 10^{18} \text{ m}^{-3}$  and  $6.9 \cdot 10^{16} \text{ m}^{-3}$  at 10 %  $CO_2$ , respectively for  $N_2(A)$  and  $N_2(B)$  while the  $CO(a)$  density remains relatively constant ( $3.85 \pm 0.3 \cdot 10^{16} \text{ m}^{-3}$ ) for the different mixtures, at 2 Torr and 50 mA. Even though the density of  $N_2(A)$  is always, at least, one order of magnitude higher than  $N_2(B)$ , the same process as (25) but involving  $N_2(A)$  contributes to less than 0.2 % of the  $CO_2$  dissociation for all conditions represented in Fig. 14.

Concerning the creation of  $CO_2$ , the electronically excited state  $CO(a^3\Pi_r)$ , noted  $CO(a)$  thereafter, promotes the  $CO$  recombination into  $CO_2$  due to bimolecular reactions with  $O_2$  and  $CO$  as follows:



attesting the complex role that this electronically excited state has on the overall kinetics, as already pointed out in [38,182,184,185]. Finally, another main creation mechanism involving  $O^-$  ions is :



playing a significant role for high  $CO_2$  fractions as already mentioned in [38].

As can be observed in Figure 14, the rates of the back reaction processes (27), (28) and (29) forming  $CO_2$  decrease with increasing  $N_2$  content. Indeed, adding  $N_2$  dilutes the dissociation products which limits the back reaction mechanisms and leads to an increase of the  $CO_2$  dissociation fraction. Some studies of  $CO_2$  dissociation by non-thermal plasma have been performed using not only  $N_2$  but also rare gases like Argon or Helium as a diluent [69,74,186–188]. However, investigating how the dilution affects the  $CO_2$  dissociation fraction is not straightforward as adding a diluent changes the plasma electrical properties.

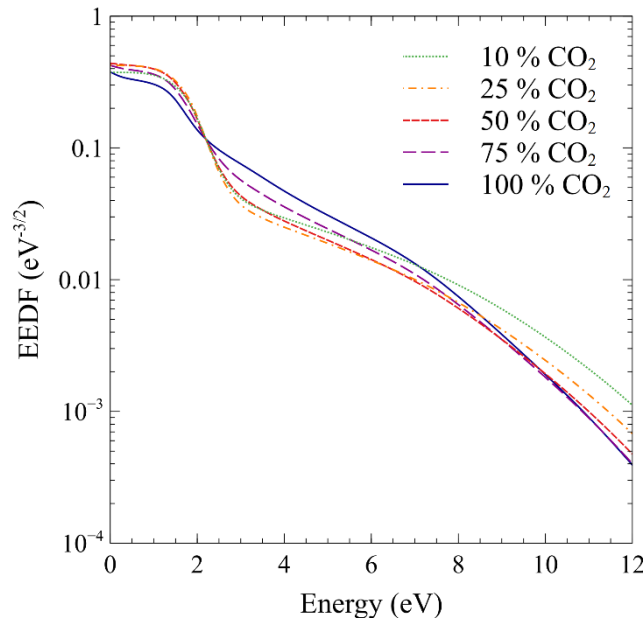


Figure 15: Electron Energy Distribution Function (EEDF) calculated for different  $CO_2/N_2$  mixtures for a discharge current of 50 mA and a pressure of 2 Torr (self-consistent simulations).

Finally, we analyse the changes in the Electron Energy Distribution Function (EEDF) upon addition of  $N_2$ . The self-consistently calculated EEDFs for different  $CO_2/N_2$  mixtures for a discharge current of 50 mA and a pressure of 2 Torr are shown in Figure 15. Note that changes in the EEDF are associated

with several factors, including the modifications in E/N, mixture composition (N<sub>2</sub>, CO, O<sub>2</sub>, O) and/or changes in T<sub>v</sub> and superelastic collisions with vibrationally and electronically excited states.

Two main effects explain the shape and dependence (with the N<sub>2</sub> content) of the EEDFs we observe here. On the one hand, the self-consistently calculated reduced electric field increases (from 79 to 90.5 Td) with the nitrogen fraction (cf. Fig. 7) and on the other hand, as the mixture is changing, the effect of N<sub>2</sub> and of the dissociation products, namely CO, O<sub>2</sub> and O is more pronounced in mixtures with higher N<sub>2</sub> content than in pure CO<sub>2</sub>. The EEDFs derived for the CO<sub>2</sub>-N<sub>2</sub> (above 25% of CO<sub>2</sub>) plasmas have a lower population of electrons around the CO<sub>2</sub> dissociation energies (7.5 and 11.9 eV [180]) than in a pure CO<sub>2</sub> plasma, as already observed in [34] for a CO<sub>2</sub>-N<sub>2</sub> mixture with 50 % CO<sub>2</sub>. Accordingly, the direct electron dissociation rate coefficient for the GS is lower for 50 % CO<sub>2</sub> ( $9.4 \cdot 10^{-17} \text{ m}^3\text{s}^{-1}$ ) and 75 % CO<sub>2</sub> ( $8.9 \cdot 10^{-17} \text{ m}^3\text{s}^{-1}$ ), than for pure CO<sub>2</sub> ( $9.5 \cdot 10^{-17} \text{ m}^3\text{s}^{-1}$ ). Therefore, the enhancement of the reduced electric field is not sufficient to increase the contribution of direct electron-impact dissociation for low N<sub>2</sub> content. We can infer that the increase in the CO<sub>2</sub> dissociation when N<sub>2</sub> is added into the mixture is not due to an enhancement of the direct electron-impact dissociation, but rather to the enhanced contribution of reaction (25) and to the reduction of back reactions as a consequence of dilution with N<sub>2</sub>.

### IV.3 NO<sub>x</sub> formation

Earlier studies in DBD reactors showed that the presence of N<sub>2</sub> during CO<sub>2</sub> splitting, along with the main CO<sub>2</sub> decomposition products (CO and oxygen species), leads to the formation of NO<sub>x</sub> compounds, with concentrations in the range of several hundreds of ppm [71,183]. Furthermore, if NO<sub>x</sub> compounds are produced, it is important to know whether high enough concentrations might be obtained for two reasons. On the one hand, NO<sub>x</sub> can be considered relevant for nitrogen fixation on earth and in the context of ISRU on Mars; on the other hand, these species have a severe negative impact on air quality giving rise to several environmental and health issues [20,21] leading to restriction of their emissions. The mechanisms of NO<sub>x</sub> formation in cold plasmas at reduced pressure are relatively well known and have been described in various modeling works [35,191–194].

In this work, downstream measurements were performed to investigate the composition and concentration of the produced NO<sub>x</sub> species in the effluent of our CO<sub>2</sub>-N<sub>2</sub> DC glow discharge, using FTIR spectroscopy. We could detect NO and nitrogen dioxide (NO<sub>2</sub>) but the amount of NO<sub>2</sub> was too low to be quantified.

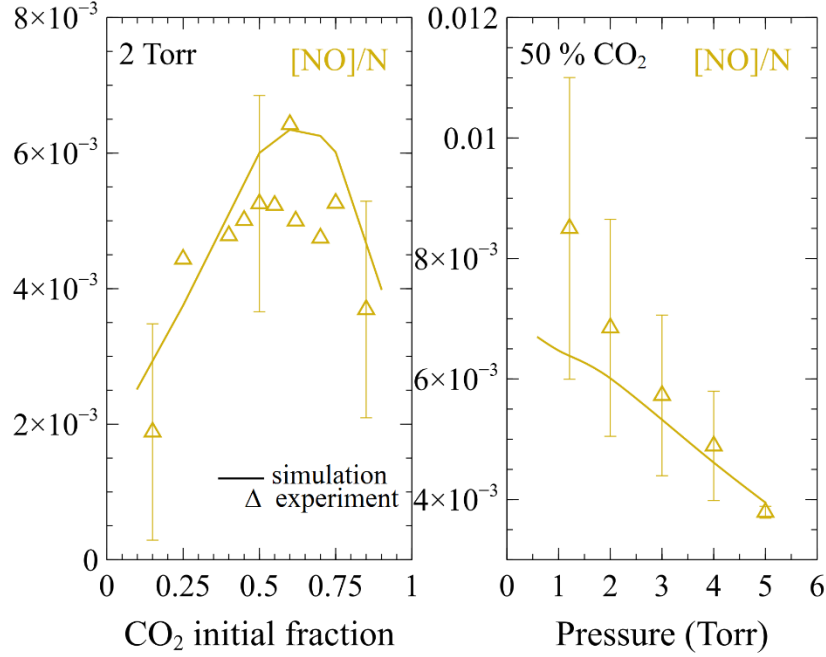


Figure 16: Measured ( $\Delta$ ) and calculated (—) NO fraction,  $[NO]/N$ , of a  $CO_2$ - $N_2$  discharge as a function of the  $CO_2$  initial fraction (left) and as a function of pressure for 50%  $CO_2$  (right).

The measured and calculated NO fractions are plotted as a function of the  $CO_2$  initial fraction in the gas mixture and as a function of pressure at a fixed  $N_2$  content of 50% in Figure 16. Experimentally and in the simulations the NO fraction as a function of the  $CO_2$  initial fraction follows a parabolic trend with a maximum around 50%  $N_2$ . Concerning the pressure dependence, we can observe that both the measured and calculated  $[NO]/N$  decreases with rising pressure. Note that the FTIR measurements were realized in the afterglow while the model results are obtained for the active part of the discharge. However, it was verified that this does not have a significant effect on the NO density measured. Since we find a good agreement between the experiment and simulations (Fig. 16), within the experimental reproducibility error, we believe that our model can be used to explain the observed trends. Therefore, we investigate the contributions of main creation and destruction mechanisms of NO for the different gas mixtures studied at 2 Torr and this is shown in Figure 17. Note that in the simulations the obtained NO fraction is about four orders of magnitude higher than the  $NO_2$  fraction and that the NO density was affected by up to 30% and the maximum was slightly shifted towards 50% when the O recombination probability is multiplied by two in the model (see Section IV.1.).

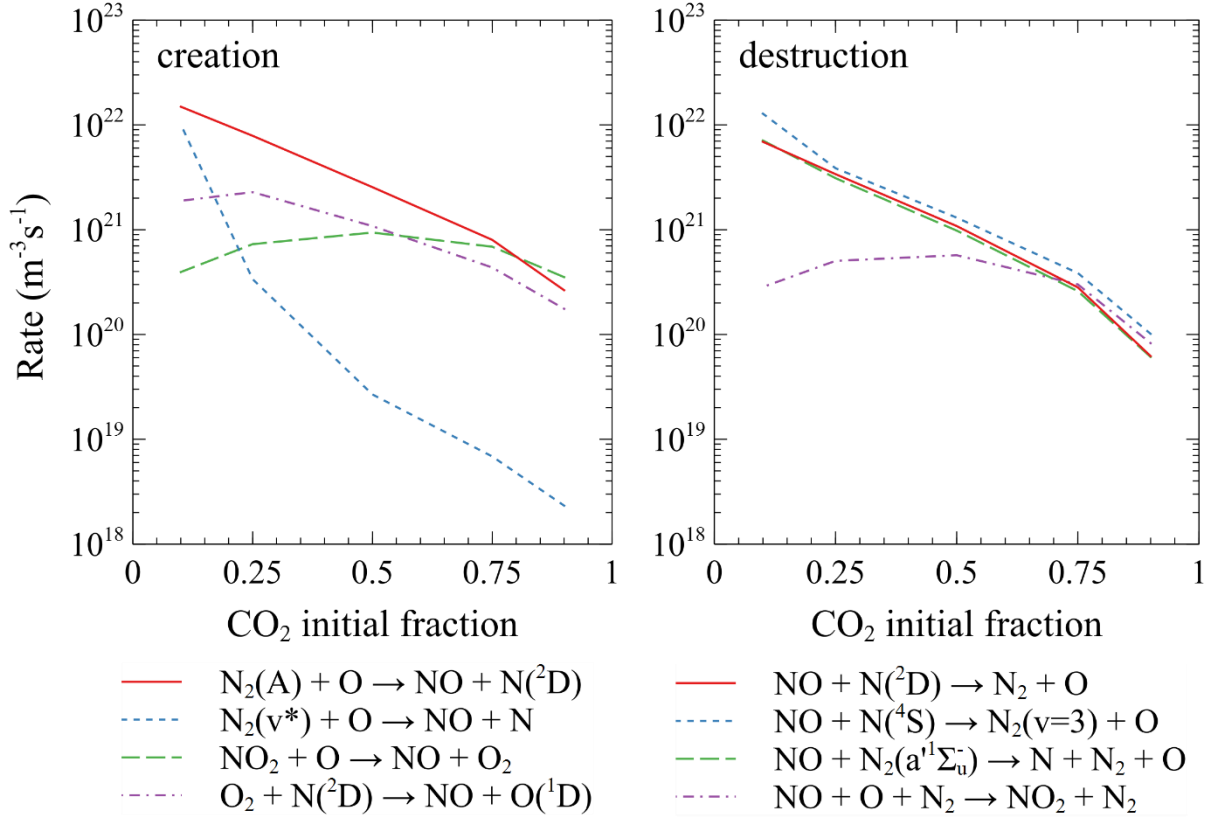


Figure 17: Rate of the most important creation (left) and destruction (right) processes of NO, as a function of CO<sub>2</sub> initial fraction in the CO<sub>2</sub>-N<sub>2</sub> gas mixture, at 2 Torr.

In our CO<sub>2</sub>-N<sub>2</sub> plasma the NO species are formed out of N reacting with O<sub>2</sub> and N<sub>2</sub>(A<sup>3</sup>Σ<sub>u</sub><sup>+</sup>) and N<sub>2</sub>(v≥13) reacting with O atoms, originating from N<sub>2</sub> and CO<sub>2</sub>. Thus, it is not unexpected that the maximum of the NO fraction is achieved when both reactants are present in approximately equal concentrations. The dominant formation mechanism of NO at low N<sub>2</sub> content is the reaction between O radicals and NO<sub>2</sub> molecules, forming NO and O<sub>2</sub> molecules. The NO formation via collisions between N(<sup>2</sup>D) atoms and O<sub>2</sub> is important even if the density of N atoms is much lower than O (typically, by several orders of magnitude in our conditions). On the other hand, nitrogen atoms also play an important role in the destruction of NO. An important NO loss mechanism is the recombination with O atoms into NO<sub>2</sub> through a three-body reaction (see reaction given in (3)). This third body can be either CO<sub>2</sub> (mainly important above 75 % CO<sub>2</sub>), N<sub>2</sub> (especially for N<sub>2</sub> content above 25 %) or O<sub>2</sub>. At higher N<sub>2</sub> fractions, the concentrations of N and N<sub>2</sub>(A) will rise giving increasing importance to their reactions whilst the amount of atomic and molecular oxygen will decrease. This will encourage the loss of NO through processes involving species coming from N<sub>2</sub>. The three-body reaction  $\text{NO} + \text{O} + \text{CO}_2 \rightarrow \text{NO}_2 + \text{CO}_2$  is not represented in Fig. 17 as it only contributes significantly to the NO destruction above 90% of CO<sub>2</sub> (12 % maximum contribution). Regarding charge transfers, it is worth noticing that the process  $\text{O}_2^+ + \text{NO} \rightarrow \text{O}_2 + \text{NO}^+$  does not constitute a real creation process for NO as more than 99% of NO<sup>+</sup> is transformed back to NO at the wall and is thus not represented in Figure 17.

NO<sub>2</sub> is a significant source of NO production and vice versa. The only important process for NO<sub>2</sub> production is the three-body recombination between NO and O, mostly with N<sub>2</sub> (for CO<sub>2</sub> fraction below 75 %) and with CO<sub>2</sub> and O<sub>2</sub> as a third body. The main destruction mechanism accounting for more than 99% of the NO<sub>2</sub> loss is the reaction of NO<sub>2</sub> with O atoms giving NO and O<sub>2</sub> molecules.

The mechanism of the plasma chemistry of CO<sub>2</sub>/N<sub>2</sub> mixtures has been discussed in detail by Snoeckx *et al.* for a DBD reactor [183] and by Heijkers *et al.* for a MW discharge [68]. In both cases the formation of NO was also observed, albeit through a different mechanism. In a microwave plasma, the lower energy of the electrons causes vibrational excitation to become more important than electronic excitation and the vibrationally excited N<sub>2</sub> molecules (with  $v>13$ ) react with O atoms to form N and NO through the Zel'dovich reaction [95,109], instead of the electronically excited N<sub>2</sub> in the DBD. In our conditions, this mechanism is becoming important only for high N<sub>2</sub> content. In Figure 17 we represent the sum of the rates for all the vibrational states of N<sub>2</sub> above  $v=13$  represented as N<sub>2</sub>( $v^*$ ).

## V. Conclusions

This work reports the validation of a 0D self-consistent kinetic model of CO<sub>2</sub>-N<sub>2</sub> plasmas, from the comparison of the model predictions with recent experimental data obtained in a continuous DC glow discharge ignited in different CO<sub>2</sub>-N<sub>2</sub> gas mixtures. A good agreement is obtained between the calculated vibrational temperatures of CO<sub>2</sub> and CO, [O]/N, [NO]/N, E/N and dissociation fractions, and the corresponding experimental data measured by in situ FTIR spectroscopy and actinometry. The reaction mechanism (validated set of reactions and corresponding rate coefficients) we propose predicts the quantities mentioned above for pressures between 0.6 and 4 Torr, discharge current of 50 mA and for different compositions ranging from 100 % to only 25 % of CO<sub>2</sub> in a CO<sub>2</sub>-N<sub>2</sub> mixture.

Our model includes a self-consistent description of the CO<sub>2</sub>, CO and N<sub>2</sub> vibrational kinetics and allows us to evince a remarkable deviation from equilibrium for N<sub>2</sub> and CO vibrational distribution functions, and to a lesser extent for CO<sub>2</sub>. This result emphasizes the importance of detailed state-to-state kinetic models and of an understanding of the vibrational energy transfers taking place. In particular, the transfer of vibrational energy from nitrogen to the asymmetric stretching mode of CO<sub>2</sub>, described by the CO<sub>2</sub>-N<sub>2</sub> V-V transfer in the simulations, greatly influences the vibrational temperature associated to  $v_3$ . However, the dissociation fraction does not depend on it and therefore, we can conclude that the degree of vibrational excitation reached remains insufficient for an effective dissociation via the pure vibrational mechanism in our conditions.

The experimental data show an enhanced dissociation of CO<sub>2</sub> when N<sub>2</sub> is added to the plasma. The effect can be attributed to the presence of the metastable N<sub>2</sub>(B<sup>3</sup>Π<sub>g</sub>) (creating a new channel for CO<sub>2</sub> dissociation) and to the dilution of dissociation products (limiting the back reactions). The electronically excited state CO(a<sup>3</sup>Π<sub>r</sub>) also influences the plasma chemistry even with the addition of a significant amount of N<sub>2</sub>, showing the importance of electronically excited states in the dissociation kinetics. The studies of the self-consistently calculated EEDFs showed that the enhancement of the reduced electric field is not sufficient to increase the contribution of direct electron-impact dissociation for N<sub>2</sub> content below 75 % of the initial mixture. Overall, the admixture of N<sub>2</sub> has a beneficial impact on CO<sub>2</sub> decomposition but it does not compensate for the decrease of the CO<sub>2</sub> initial fraction.

Two main surface processes play a significant role in the plasma kinetics, namely, the recombination of atomic oxygen to form O<sub>2</sub> and the deactivation of the vibrations of CO, N<sub>2</sub> and the different modes of CO<sub>2</sub> at the reactor walls. The O atom densities were shown to strongly depend on the former surface loss process [89]. In turn the vibrational temperatures are greatly affected by the O atoms as they are strong quenchers of vibrations [38,195]. In light of the comparison between the simulations and experimental results in section IV.1., we can infer that the recombination probability of atomic oxygen,  $\gamma_O$ , should increase with the N<sub>2</sub> content. The present results corroborate previous studies that have shown the important role of wall deactivation of vibrationally excited CO<sub>2</sub> and N<sub>2</sub> at pressures around 1 Torr and below, where it changes the vibrational kinetics [34,38] and has a major contribution to gas heating [35]. Similarly, O recombination at the wall and V-T transfers with O atoms greatly contribute to the thermal balance in oxygen discharges [98]. Therefore, an accurate determination of the experimental  $\gamma_O$  and  $\gamma_v$  in realistic gas mixtures, containing CO<sub>2</sub> and N<sub>2</sub> but also



the dissociation products like CO, is therefore needed for further studies of plasmas in CO<sub>2</sub>-N<sub>2</sub> mixtures.

It is important to analyse the formation of NO<sub>x</sub> compounds in CO<sub>2</sub>-N<sub>2</sub> plasmas as NO<sub>x</sub> may have a severe negative impact on air quality giving rise to several environmental and health issues, but high enough concentrations can be considered relevant for nitrogen fixation on earth [49,50] and in the context of In Situ Resource and Utilization on Mars [54]. If necessary, one way to prevent the formation of NO<sub>x</sub> compounds is to use the separation membrane technology where the oxygen species can be transported away from the reaction mixture and therefore prevent oxygen species to react with N<sub>2</sub>. Moreover, an oxygen-permeable membrane placed in the plasma will shift the equilibrium of the CO<sub>2</sub> dissociation reaction towards increased fractions of CO and O [52,196]. However, membranes have only been applied, up to now, to separate O<sub>2</sub> from the gas mixture, and not the O atoms which participate as well in the NO<sub>x</sub> production. One solution would be to modify the surface of the plasma reactor to increase the recombination probability of O atoms at the walls as already done in [195] and modeled in [38]. In contrast, to obtain high concentrations of NO<sub>x</sub> one solution would be exposing the O<sub>2</sub> coming from the membrane to a N<sub>2</sub> plasma leading to the formation of NO<sub>x</sub>, essential for the synthesis of fertilizers and nitrogen fixation [49,50,54].

Overall, the present work adds one more layer to the systematic set-by-step validation strategy of CO<sub>2</sub> non-equilibrium kinetics initiated in [37]. By developing joint experimental, modelling and simulation activities, it has been possible to gather a significant amount of experimental data and simulation results that allow a thorough model validation and can be used to validate or benchmark other models. A similar endeavour is carried out in [98] for pure O<sub>2</sub> plasmas, where the benefits of adopting such paradigm in the development of reaction mechanisms for plasma chemistry is highlighted. Future developments may include a detailed analysis of the surface kinetics, the validation of the kinetics of other species with new measurements performed in the same conditions, such as vibrationally temperatures (or distributions) of N<sub>2</sub> molecules, nitrogen atoms, or molecular nitrogen electronically excited states, or the extension of the domain of validity of the present kinetic scheme to other pressure or excitation conditions.

## VI. Acknowledgments

This work was partially supported by the European Union's Horizon 2020 research and innovation programme under grant agreement MSCA ITN 813393, and by Portuguese FCT-Fundação para a Ciência e a Tecnologia, under projects UIDB/50010/2020, UIDP/50010/2020, PTDC/FIS-PLA/1616/2021, EXPL/FIS-PLA/0076/2021 and PD/BD/150414/2019 (PD-F APPLAuSE).

## VII. References

- [1] J. Rogelj, M. Schaeffer, M. Meinshausen, R. Knutti, J. Alcamo, K. Riahi, W. Hare, Zero emission targets as long-term global goals for climate protection, *Environ. Res. Lett.* 10 (2015) 105007. <https://doi.org/10.1088/1748-9326/10/10/105007>.
- [2] IPCC, 2022: Summary for Policymakers [H.-O. Pörtner, D.C. Roberts, E.S. Poloczanska, K. Mintenbeck, M. Tignor, A. Alegría, M. Craig, S. Langsdorf, S. Löschke, V. Möller, A. Okem (eds.)]. In: *Climate Change 2022: Impacts, Adaptation, and Vulnerability. Contribution of Working Group II to the Sixth Assessment Report of the Intergovernmental Panel on Climate Change* [H.-O. Pörtner, D.C. Roberts, M. Tignor, E.S. Poloczanska, K. Mintenbeck, A. Alegría, M. Craig, S. Langsdorf, S. Löschke, V. Möller, A. Okem, B. Rama (eds.)]. Cambridge University Press. In Press., (n.d.).
- [3] IPCC, 2014: *Climate Change 2014: Synthesis Report. Contribution of Working Groups I, II and III to the Fifth Assessment Report of the Intergovernmental Panel on Climate Change* [Core Writing Team, R.K. Pachauri and L.A. Meyer (eds.)]. IPCC, Geneva, Switzerland, 151 pp., (n.d.).

- [4] Paris Agreement, *Int. Leg. Mater.* 55 (2016) 743.
- [5] C.-H. Huang, C.-S. Tan, A Review: CO<sub>2</sub> Utilization, *Aerosol Air Qual. Res.* 14 (2014) 480–499. <https://doi.org/10.4209/aaqr.2013.10.0326>.
- [6] G.A. Olah, G.K.S. Prakash, A. Goepfert, Anthropogenic Chemical Carbon Cycle for a Sustainable Future, *J. Am. Chem. Soc.* 133 (2011) 12881–12898. <https://doi.org/10.1021/ja202642y>.
- [7] B. Ashford, X. Tu, Non-thermal plasma technology for the conversion of CO<sub>2</sub>, *Curr. Opin. Green Sustain. Chem.* 3 (2017) 45–49. <https://doi.org/10.1016/j.cogsc.2016.12.001>.
- [8] R. Snoeckx, A. Bogaerts, Plasma technology – a novel solution for CO<sub>2</sub> conversion?, *Chem. Soc. Rev.* 46 (2017) 5805–5863. <https://doi.org/10.1039/C6CS00066E>.
- [9] A.D.N. Kamkeng, M. Wang, J. Hu, W. Du, F. Qian, Transformation technologies for CO<sub>2</sub> utilisation: Current status, challenges and future prospects, *Chem. Eng. J.* 409 (2021) 128138. <https://doi.org/10.1016/j.cej.2020.128138>.
- [10] A. Goede, R. van de Sanden, CO<sub>2</sub>-Neutral Fuels, *Europhys. News.* 47 (2016) 22–26. <https://doi.org/10.1051/epn/2016304>.
- [11] A. Bogaerts, G. Centi, Plasma Technology for CO<sub>2</sub> Conversion: A Personal Perspective on Prospects and Gaps, *Front. Energy Res.* 8 (2020). <https://www.frontiersin.org/articles/10.3389/fenrg.2020.00111> (accessed October 22, 2022).
- [12] L.D. Pietanza, O. Guaitella, V. Aquilanti, I. Armenise, A. Bogaerts, M. Capitelli, G. Colonna, V. Guerra, R. Engeln, E. Kustova, A. Lombardi, F. Palazzetti, T. Silva, Advances in non-equilibrium CO<sub>2</sub> plasma kinetics: a theoretical and experimental review, *Eur. Phys. J. D.* 75 (2021) 237. <https://doi.org/10.1140/epjd/s10053-021-00226-0>.
- [13] A. George, B. Shen, M. Craven, Y. Wang, D. Kang, C. Wu, X. Tu, A Review of Non-Thermal Plasma Technology: A novel solution for CO<sub>2</sub> conversion and utilization, *Renew. Sustain. Energy Rev.* 135 (2021) 109702. <https://doi.org/10.1016/j.rser.2020.109702>.
- [14] A. Berthelot, A. Bogaerts, Modeling of CO<sub>2</sub> Splitting in a Microwave Plasma: How to Improve the Conversion and Energy Efficiency, *J. Phys. Chem. C.* 121 (2017) 8236–8251. <https://doi.org/10.1021/acs.jpcc.6b12840>.
- [15] R. Aerts, W. Somers, A. Bogaerts, Carbon Dioxide Splitting in a Dielectric Barrier Discharge Plasma: A Combined Experimental and Computational Study, *ChemSusChem.* 8 (2015) 702–716. <https://doi.org/10.1002/cssc.201402818>.
- [16] T. Kozák, A. Bogaerts, Splitting of CO<sub>2</sub> by vibrational excitation in non-equilibrium plasmas: a reaction kinetics model, *Plasma Sources Sci. Technol.* 23 (2014) 045004. <https://doi.org/10.1088/0963-0252/23/4/045004>.
- [17] W. Wang, R. Snoeckx, X. Zhang, M.S. Cha, A. Bogaerts, Modeling Plasma-based CO<sub>2</sub> and CH<sub>4</sub> Conversion in Mixtures with N<sub>2</sub>, O<sub>2</sub>, and H<sub>2</sub>O: The Bigger Plasma Chemistry Picture, *J. Phys. Chem. C.* 122 (2018) 8704–8723. <https://doi.org/10.1021/acs.jpcc.7b10619>.
- [18] A. Bogaerts, E.C. Neyts, Plasma Technology: An Emerging Technology for Energy Storage, *ACS Energy Lett.* 3 (2018) 1013–1027. <https://doi.org/10.1021/acsenrgylett.8b00184>.
- [19] V.D. Rusanov, A.A. Fridman, G.V. Sholin, The physics of a chemically active plasma with nonequilibrium vibrational excitation of molecules, *Sov. Phys. Uspekhi.* 24 (1981) 447–474. <https://doi.org/10.1070/PU1981v024n06ABEH004884>.
- [20] Y. Itikawa, Cross Sections for Electron Collisions With Carbon Dioxide, *J. Phys. Chem. Ref. Data.* 31 (2002) 749–767. <https://doi.org/10.1063/1.1481879>.
- [21] Fridman A.A., *Plasma chemistry.*, Cambridge University Press, 2012.
- [22] A.S. Morillo-Candas, T. Silva, B.L.M. Klarenaar, M. Grofulović, V. Guerra, O. Guaitella, Electron impact dissociation of CO<sub>2</sub>, *Plasma Sources Sci. Technol.* 29 (2020) 01LT01. <https://doi.org/10.1088/1361-6595/ab6075>.
- [23] N.Y. Babaeva, G.V. Naidis, On the efficiency of CO<sub>2</sub> conversion in corona and dielectric-barrier discharges, *Plasma Sources Sci. Technol.* 30 (2021) 03LT03. <https://doi.org/10.1088/1361-6595/abe6e6>.
- [24] L.D. Pietanza, G. Colonna, M. Capitelli, Self-consistent electron energy distribution functions, vibrational distributions, electronic excited state kinetics in reacting microwave CO<sub>2</sub> plasma: An advanced model, *Phys. Plasmas.* 27 (2020) 023513. <https://doi.org/10.1063/1.5139625>.

- [25] T. Kozák, A. Bogaerts, Evaluation of the energy efficiency of CO<sub>2</sub> conversion in microwave discharges using a reaction kinetics model, *Plasma Sources Sci. Technol.* 24 (2014) 015024. <https://doi.org/10.1088/0963-0252/24/1/015024>.
- [26] M. Capitelli, G. Colonna, G. D'Ammando, L.D. Pietanza, Self-consistent time dependent vibrational and free electron kinetics for CO<sub>2</sub> dissociation and ionization in cold plasmas, *Plasma Sources Sci. Technol.* 26 (2017) 055009. <https://doi.org/10.1088/1361-6595/aa6427>.
- [27] I. Armenise, E. Kustova, Mechanisms of Coupled Vibrational Relaxation and Dissociation in Carbon Dioxide, *J. Phys. Chem. A.* 122 (2018) 5107–5120. <https://doi.org/10.1021/acs.jpca.8b03266>.
- [28] F.A. D'Isa, E.A.D. Carbone, A. Hecimovic, U. Fantz, Performance analysis of a 2.45 GHz microwave plasma torch for CO<sub>2</sub> decomposition in gas swirl configuration, *Plasma Sources Sci. Technol.* 29 (2020) 105009. <https://doi.org/10.1088/1361-6595/abaa84>.
- [29] A.J. Wolf, F.J.J. Peeters, P.W.C. Groen, W.A. Bongers, M.C.M. van de Sanden, CO<sub>2</sub> Conversion in Nonuniform Discharges: Disentangling Dissociation and Recombination Mechanisms, *J. Phys. Chem. C.* 124 (2020) 16806–16819. <https://doi.org/10.1021/acs.jpcc.0c03637>.
- [30] A.J. Wolf, T.W.H. Righart, F.J.J. Peeters, W.A. Bongers, M.C.M. van de Sanden, Implications of thermo-chemical instability on the contracted modes in CO<sub>2</sub> microwave plasmas, *Plasma Sources Sci. Technol.* 29 (2020) 025005. <https://doi.org/10.1088/1361-6595/ab5eca>.
- [31] P. Ogloblina, A.S. Morillo-Candas, A.F. Silva, T. Silva, A. Tejero-del-Caz, L.L. Alves, O. Guaitella, V. Guerra, Mars in situ oxygen and propellant production by non-equilibrium plasmas, *Plasma Sources Sci. Technol.* 30 (2021) 065005. <https://doi.org/10.1088/1361-6595/abec28>.
- [32] T. Silva, M. Grofulović, B.L.M. Klarenaar, A.S. Morillo-Candas, O. Guaitella, R. Engeln, C.D. Pintassilgo, V. Guerra, Kinetic study of low-temperature CO<sub>2</sub> plasmas under non-equilibrium conditions. I. Relaxation of vibrational energy, *Plasma Sources Sci. Technol.* 27 (2018) 015019. <https://doi.org/10.1088/1361-6595/aaa56a>.
- [33] M. Grofulović, T. Silva, B.L.M. Klarenaar, A.S. Morillo-Candas, O. Guaitella, R. Engeln, C.D. Pintassilgo, V. Guerra, Kinetic study of CO<sub>2</sub> plasmas under non-equilibrium conditions. II. Input of vibrational energy, *Plasma Sources Sci. Technol.* 27 (2018) 115009. <https://doi.org/10.1088/1361-6595/aadb60>.
- [34] L. Terraz, T. Silva, A. Morillo-Candas, O. Guaitella, A. Tejero-del-Caz, L.L. Alves, V. Guerra, Influence of N<sub>2</sub> on the CO<sub>2</sub> vibrational distribution function and dissociation yield in non-equilibrium plasmas, *J. Phys. Appl. Phys.* 53 (2019) 094002. <https://doi.org/10.1088/1361-6463/ab55fb>.
- [35] T. Silva, M. Grofulović, L. Terraz, C.D. Pintassilgo, V. Guerra, Dynamics of Gas Heating in the Afterglow of Pulsed CO<sub>2</sub> and CO<sub>2</sub>-N<sub>2</sub> Glow Discharges at Low Pressure, *Plasma Chem. Plasma Process.* 40 (2020) 713–725. <https://doi.org/10.1007/s11090-020-10061-7>.
- [36] B.L.M. Klarenaar, R. Engeln, D.C.M. van den Bekerom, M.C.M. van de Sanden, A.S. Morillo-Candas, O. Guaitella, Time evolution of vibrational temperatures in a CO<sub>2</sub> glow discharge measured with infrared absorption spectroscopy, *Plasma Sources Sci. Technol.* 26 (2017) 115008. <https://doi.org/10.1088/1361-6595/aa902e>.
- [37] T. Silva, M. Grofulović, L. Terraz, C.D. Pintassilgo, V. Guerra, Modelling the input and relaxation of vibrational energy in CO<sub>2</sub> plasmas, *J. Phys. Appl. Phys.* 51 (2018) 464001. <https://doi.org/10.1088/1361-6463/aadb7>.
- [38] C. Fromentin, T. Silva, T.C. Dias, A.S. Morillo-Candas, O. Biondo, O. Guaitella, V. Guerra, Study of vibrational kinetics of CO<sub>2</sub> and CO in CO<sub>2</sub>-O<sub>2</sub> plasmas under non-equilibrium conditions, (2022). <https://doi.org/10.48550/arXiv.2210.07778>.
- [39] Tiago DIAS, Atomic oxygen kinetics in CO<sub>2</sub> plasmas, INSTITUTO SUPERIOR TÉCNICO, 2019. <https://scholar.tecnico.ulisboa.pt/authors/ad9a9348517672649595e209046789e0886527d7d7d96e42ce569f21c5122ad7/records> (accessed October 22, 2022).
- [40] M. Grofulović, L.L. Alves, V. Guerra, Electron-neutral scattering cross sections for CO<sub>2</sub>: a complete and consistent set and an assessment of dissociation, *J. Phys. Appl. Phys.* 49 (2016) 395207. <https://doi.org/10.1088/0022-3727/49/39/395207>.

- [41] P. Ogloblina, A. Tejero-del-Caz, V. Guerra, L.L. Alves, Electron impact cross sections for carbon monoxide and their importance in the electron kinetics of CO<sub>2</sub>–CO mixtures, *Plasma Sources Sci. Technol.* 29 (2019) 015002. <https://doi.org/10.1088/1361-6595/ab4e72>.
- [42] A.F. Silva, A.S. Morillo-Candás, A. Tejero-del-Caz, L.L. Alves, O. Guaitella, V. Guerra, A reaction mechanism for vibrationally-cold low-pressure CO<sub>2</sub> plasmas, *Plasma Sources Sci. Technol.* 29 (2020) 125020. <https://doi.org/10.1088/1361-6595/abc818>.
- [43] Time Evolution of the Dissociation Fraction in rf CO<sub>2</sub> Plasmas: Impact and Nature of Back-Reaction Mechanisms | *The Journal of Physical Chemistry C*, (2020). <https://pubs.acs.org/doi/abs/10.1021/acs.jpcc.0c03354> (accessed October 29, 2020).
- [44] V. Guerra, T. Silva, P. Ogloblina, M. Grofulović, L. Terraz, M.L. da Silva, C.D. Pintassilgo, L.L. Alves, O. Guaitella, The case for in situ resource utilisation for oxygen production on Mars by non-equilibrium plasmas, *Plasma Sources Sci. Technol.* 26 (2017) 11LT01. <https://doi.org/10.1088/1361-6595/aa8dcc>.
- [45] N. Meunier, S. Laribi, L. Dubois, D. Thomas, G. De Weireld, CO<sub>2</sub> Capture in Cement Production and Re-use: First Step for the Optimization of the Overall Process, *Energy Procedia.* 63 (2014) 6492–6503. <https://doi.org/10.1016/j.egypro.2014.11.685>.
- [46] M. Budde, L.M. Martini, M. Ceppelli, S. Quercetti, R. Engeln, Absolute OH density measurements in a CO<sub>2</sub>–H<sub>2</sub>O glow discharge by laser-induced fluorescence spectroscopy, *Plasma Sources Sci. Technol.* 31 (2022) 055002. <https://doi.org/10.1088/1361-6595/ac5ecc>.
- [47] C. Verheyen, T. Silva, V. Guerra, A. Bogaerts, The effect of H<sub>2</sub>O on the vibrational populations of CO<sub>2</sub> in a CO<sub>2</sub>/H<sub>2</sub>O microwave plasma: a kinetic modelling investigation, *Plasma Sources Sci. Technol.* 29 (2020) 095009. <https://doi.org/10.1088/1361-6595/aba1c8>.
- [48] World Health Organization. Regional Office for Europe, Air quality guidelines: global update 2005: particulate matter, ozone, nitrogen dioxide and sulfur dioxide, World Health Organization. Regional Office for Europe, 2006. <https://apps.who.int/iris/handle/10665/107823> (accessed October 28, 2022).
- [49] H. Chen, D. Yuan, A. Wu, X. Lin, X. Li, Review of low-temperature plasma nitrogen fixation technology, *Waste Dispos. Sustain. Energy.* 3 (2021) 201–217. <https://doi.org/10.1007/s42768-021-00074-z>.
- [50] L. Lin, H. Xu, H. Gao, X. Zhu, V. Hessel, Plasma-assisted nitrogen fixation in nanomaterials: fabrication, characterization, and application, *J. Phys. Appl. Phys.* 53 (2020) 133001. <https://doi.org/10.1088/1361-6463/ab5f1f>.
- [51] M.Y. Ong, S. Nomanbhay, F. Kusumo, P.L. Show, Application of microwave plasma technology to convert carbon dioxide (CO<sub>2</sub>) into high value products: A review, *J. Clean. Prod.* 336 (2022) 130447. <https://doi.org/10.1016/j.jclepro.2022.130447>.
- [52] D. Premathilake, R.A. Outlaw, R.A. Quinlan, C.E. Byvik, Oxygen Generation by Carbon Dioxide Glow Discharge and Separation by Permeation Through Ultrathin Silver Membranes, *Earth Space Sci.* 6 (2019) 557–564. <https://doi.org/10.1029/2018EA000521>.
- [53] V. Guerra, T. Silva, O. Guaitella, Living on mars: how to produce oxygen and fuel to get home, *Europhys. News.* 49 (2018) 15–18. <https://doi.org/10.1051/epn/2018302>.
- [54] V. Guerra, T. Silva, N. Pinhão, O. Guaitella, C. Guerra-Garcia, F.J.J. Peeters, M.N. Tsampas, M.C.M. van de Sanden, Plasmas for in situ resource utilization on Mars: Fuels, life support, and agriculture, *J. Appl. Phys.* 132 (2022) 070902. <https://doi.org/10.1063/5.0098011>.
- [55] D. Fitz, H. Reiner, B.M. Rode, Chemical evolution toward the origin of life, *Pure Appl. Chem.* 79 (2007) 2101–2117. <https://doi.org/10.1351/pac200779122101>.
- [56] M. Janda, V. Martišovič, M. Morvová, Z. Machala, K. Hensel, Monte Carlo simulations of electron dynamics in N<sub>2</sub>/CO<sub>2</sub> mixtures, *Eur. Phys. J. D.* 45 (2007) 309–315. <https://doi.org/10.1140/epjd/e2007-00254-x>.
- [57] M. Janda, M. Morvova, Z. Machala, I. Morva, Study of Plasma Induced Chemistry by DC Discharges in CO<sub>2</sub>/N<sub>2</sub>/H<sub>2</sub>O Mixtures Above a Water Surface, *Orig. Life Evol. Biospheres.* 38 (2008) 23–35. <https://doi.org/10.1007/s11084-007-9115-0>.
- [58] J. Annaloro, A. Bultel, Vibrational and electronic collisional-radiative model in CO<sub>2</sub>-N<sub>2</sub>-Ar mixtures for Mars entry problems, *Phys. Plasmas.* 26 (2019) 103505. <https://doi.org/10.1063/1.5114792>.

- [59] V. Joly, A. Roblin, Vibrational relaxation of CO<sub>2</sub> (m, nl, p) in a CO<sub>2</sub>-N<sub>2</sub> mixture. Part 1: Survey of available data, *Aerosp. Sci. Technol.* 3 (1999) 229–238. [https://doi.org/10.1016/S1270-9638\(99\)80045-5](https://doi.org/10.1016/S1270-9638(99)80045-5).
- [60] V. Joly, C. Marmignon, P. Jacquet, Vibrational relaxation of CO<sub>2</sub>(m, nl, p) in a CO<sub>2</sub>□N<sub>2</sub> mixture. Part 2: Application to a one-dimensional problem, *Aerosp. Sci. Technol.* 3 (1999) 313–322. [https://doi.org/10.1016/S1270-9638\(00\)86967-9](https://doi.org/10.1016/S1270-9638(00)86967-9).
- [61] Z. Bouyahiaoui, R. Haoui, A. Zidane, Numerical investigation of a hypersonic flow around a capsule in CO<sub>2</sub>–N<sub>2</sub> environment, *Eur. J. Mech. - BFluids.* 80 (2020) 146–156. <https://doi.org/10.1016/j.euromechflu.2019.12.009>.
- [62] G.N. Zalogin, P.V. Kozlov, L.A. Kuznetsova, S.A. Losev, V.N. Makarov, Yu.V. Romanenko, S.T. Surzhikov, Radiation excited by shock waves in a CO<sub>2</sub>-N<sub>2</sub>-Ar mixture: Experiment and theory, *Tech. Phys.* 46 (2001) 654–661. <https://doi.org/10.1134/1.1379629>.
- [63] H. Zhang, L. Li, X. Li, W. Wang, J. Yan, X. Tu, Warm plasma activation of CO<sub>2</sub> in a rotating gliding arc discharge reactor, *J. CO<sub>2</sub> Util.* 27 (2018) 472–479. <https://doi.org/10.1016/j.jcou.2018.08.020>.
- [64] H.L.K. Manning, I.L. ten Kate, S.J. Battel, P.R. Mahaffy, Electric discharge in the Martian atmosphere, Paschen curves and implications for future missions, *Adv. Space Res.* 46 (2010) 1334–1340. <https://doi.org/10.1016/j.asr.2010.07.006>.
- [65] G. Garcia-Cosio, H. Martinez, M. Calixto-Rodriguez, A. Gomez, DC discharge experiment in an Ar/N<sub>2</sub>/CO<sub>2</sub> ternary mixture: A laboratory simulation of the Martian ionosphere’s plasma environment, *J. Quant. Spectrosc. Radiat. Transf.* 112 (2011) 2787–2793. <https://doi.org/10.1016/j.jqsrt.2011.09.008>.
- [66] G.V. Naidis, N.Y. Babaeva, Modeling of CO<sub>2</sub> conversion in low-pressure glow discharges in CO<sub>2</sub>-N<sub>2</sub> mixtures, *J. Phys. Appl. Phys.* 55 (2022) 335202. <https://doi.org/10.1088/1361-6463/ac7266>.
- [67] R. Snoeckx, S. Heijkers, K.V. Wesenbeeck, S. Lenaerts, A. Bogaerts, CO<sub>2</sub> conversion in a dielectric barrier discharge plasma: N<sub>2</sub> in the mix as a helping hand or problematic impurity?, *Energy Environ. Sci.* 9 (2016) 999–1011. <https://doi.org/10.1039/C5EE03304G>.
- [68] S. Heijkers, R. Snoeckx, T. Kozák, T. Silva, T. Godfroid, N. Britun, R. Snyders, A. Bogaerts, CO<sub>2</sub> Conversion in a Microwave Plasma Reactor in the Presence of N<sub>2</sub>: Elucidating the Role of Vibrational Levels, *J. Phys. Chem. C.* 119 (2015) 12815–12828. <https://doi.org/10.1021/acs.jpcc.5b01466>.
- [69] M. Schiorlin, R. Klink, R. Brandenburg, Carbon dioxide conversion by means of coplanar dielectric barrier discharges, *Eur. Phys. J. Appl. Phys.* 75 (2016) 24704. <https://doi.org/10.1051/epjap/2016160073>.
- [70] M. Grofulović, B.L.M. Klarenaar, O. Guaitella, V. Guerra, R. Engeln, A rotational Raman study under non-thermal conditions in pulsed CO<sub>2</sub>–N<sub>2</sub> and CO<sub>2</sub>–O<sub>2</sub> glow discharges, *Plasma Sources Sci. Technol.* 28 (2019) 045014. <https://doi.org/10.1088/1361-6595/ab1240>.
- [71] W. Wang, R. Snoeckx, X. Zhang, M.S. Cha, A. Bogaerts, Modeling Plasma-based CO<sub>2</sub> and CH<sub>4</sub> Conversion in Mixtures with N<sub>2</sub>, O<sub>2</sub>, and H<sub>2</sub>O: The Bigger Plasma Chemistry Picture, *J. Phys. Chem. C.* 122 (2018) 8704–8723. <https://doi.org/10.1021/acs.jpcc.7b10619>.
- [72] M.I. Khan, N.U. Rehman, S. Khan, N. Ullah, A. Masood, A. Ullah, Spectroscopic study of CO<sub>2</sub> and CO<sub>2</sub>–N<sub>2</sub> mixture plasma using dielectric barrier discharge, *AIP Adv.* 9 (2019) 085015. <https://doi.org/10.1063/1.5096399>.
- [73] R. Brandenburg, A. Sarani, About the development of single microdischarges in dielectric barrier discharges in CO<sub>2</sub> and CO<sub>2</sub>/N<sub>2</sub> gas mixtures: DBD-MDs in CO<sub>2</sub> and CO<sub>2</sub>/N<sub>2</sub>, *Eur. Phys. J. Spec. Top.* 226 (2017) 2911–2922. <https://doi.org/10.1140/epjst/e2016-60339-8>.
- [74] S. Mohsenian, D. Nagassou, R. Elahi, P. Yu, M. Nallar, H.-W. Wong, J.P. Trelles, Carbon dioxide conversion by solar-enhanced microwave plasma: Effect of specific power and argon/nitrogen carrier gases, *J. CO<sub>2</sub> Util.* 34 (2019) 725–732. <https://doi.org/10.1016/j.jcou.2019.09.002>.
- [75] C. Richards, E. Jans, D. Mignogna, I.V. Adamovich, Time-resolved CO<sub>2</sub>, CO, and N<sub>2</sub> vibrational population measurements in Ns pulse discharge plasmas, *Plasma Sources Sci. Technol.* 31 (2022) 094011. <https://doi.org/10.1088/1361-6595/ac8f6d>.

- [76] I. Gulko, E.R. Jans, C. Richards, S. Raskar, X. Yang, D.C.M. van den Bekerom, I.V. Adamovich, Selective generation of excited species in ns pulse/RF hybrid plasmas for plasma chemistry applications, *Plasma Sources Sci. Technol.* 29 (2020) 104002. <https://doi.org/10.1088/1361-6595/abb3a1>.
- [77] G.V. Pokrovskiy, N.A. Popov, S.M. Starikovskaia, Fast gas heating and kinetics of electronically excited states in a nanosecond capillary discharge in CO<sub>2</sub>, *Plasma Sources Sci. Technol.* 31 (2022) 035010. <https://doi.org/10.1088/1361-6595/ac5102>.
- [78] M. Grofulović, B.L.M. Klarenaar, O. Guaitella, V. Guerra, R. Engeln, A rotational Raman study under non-thermal conditions in pulsed CO<sub>2</sub>-N<sub>2</sub> and CO<sub>2</sub>-O<sub>2</sub> glow discharges, *Plasma Sources Sci. Technol.* 28 (2019) 045014. <https://doi.org/10.1088/1361-6595/ab1240>.
- [79] M.A. Damen, L.M. Martini, R. Engeln, Temperature evolution in a pulsed CO<sub>2</sub>-N<sub>2</sub> glow discharge measured using quantum cascade laser absorption spectroscopy, *Plasma Sources Sci. Technol.* 29 (2020) 065016. <https://doi.org/10.1088/1361-6595/ab8e50>.
- [80] D. Mignogna, E.R. Jans, S. Raskar, I.V. Adamovich, Generation and decay of N<sub>2</sub>(A<sup>3</sup>Σ<sup>+</sup>) molecules in reacting CO<sub>2</sub> and CH<sub>4</sub> plasmas, *Plasma Sources Sci. Technol.* (2022). <https://doi.org/10.1088/1361-6595/ac99fc>.
- [81] R.L. TAYLOR, S. BITTERMAN, Survey of Vibrational Relaxation Data for Processes Important in the CO<sub>2</sub>-N<sub>2</sub> Laser System, *Rev. Mod. Phys.* 41 (1969) 26–47. <https://doi.org/10.1103/RevModPhys.41.26>.
- [82] N.N. Sobolev, V.V. Sokovikov, CO<sub>2</sub> LASERS, *Sov. Phys. Uspekhi.* 10 (1967) 153. <https://doi.org/10.1070/PU1967v010n02ABEH005861>.
- [83] C.K.N. Patel, Selective Excitation Through Vibrational Energy Transfer and Optical Maser Action in N<sub>2</sub>-CO<sub>2</sub>, *Phys. Rev. Lett.* 13 (1964) 617–619. <https://doi.org/10.1103/PhysRevLett.13.617>.
- [84] W.J. Witteman, G.V.D. Goot, High-Power Infrared Laser with Adjustable Coupling-Out, *J. Appl. Phys.* 37 (1966) 2919–2919. <https://doi.org/10.1063/1.1782158>.
- [85] W.J. Witteman, *The CO<sub>2</sub> Laser*, Springer, 2013.
- [86] A.W. van de Steeg, T. Butterworth, D.C.M. van den Bekerom, A.F. Silva, M.C.M. van de Sanden, G.J. van Rooij, Plasma activation of N<sub>2</sub>, CH<sub>4</sub> and CO<sub>2</sub>: an assessment of the vibrational non-equilibrium time window, *Plasma Sources Sci. Technol.* 29 (2020) 115001. <https://doi.org/10.1088/1361-6595/abbae4>.
- [87] P. Diomede, M.C.M. van de Sanden, S. Longo, Vibrational Kinetics in Plasma as a Functional Problem: A Flux-Matching Approach, *J. Phys. Chem. A.* 122 (2018) 7918–7923. <https://doi.org/10.1021/acs.jpca.8b05623>.
- [88] B.L.M. Klarenaar, A.S. Morillo-Candas, M. Grofulović, M.C.M. van de Sanden, R. Engeln, O. Guaitella, Excitation and relaxation of the asymmetric stretch mode of CO<sub>2</sub> in a pulsed glow discharge, *Plasma Sources Sci. Technol.* 28 (2019) 035011. <https://doi.org/10.1088/1361-6595/aada5e>.
- [89] A.S. Morillo-Candas, C. Drag, J.-P. Booth, T.C. Dias, V. Guerra, O. Guaitella, Oxygen atom kinetics in CO<sub>2</sub> plasmas ignited in a DC glow discharge, *Plasma Sources Sci. Technol.* 28 (2019) 075010. <https://doi.org/10.1088/1361-6595/ab2b84>.
- [90] C.E. Treanor, J.W. Rich, R.G. Rehm, Vibrational Relaxation of Anharmonic Oscillators with Exchange-Dominated Collisions, *J. Chem. Phys.* 48 (1968) 1798–1807. <https://doi.org/10.1063/1.1668914>.
- [91] A. Morillo candas, Investigation of fundamental mechanisms of CO<sub>2</sub> plasmas, doctoral thesis, Université Paris-Saclay (ComUE), 2019. <https://www.theses.fr/2019SACLX091> (accessed October 22, 2022).
- [92] A. Tejero-del-Caz, V. Guerra, D. Gonçalves, M.L. da Silva, L. Marques, N. Pinhão, C.D. Pintassilgo, L.L. Alves, The LisbOn KInetics Boltzmann solver, *Plasma Sources Sci. Technol.* 28 (2019) 043001. <https://doi.org/10.1088/1361-6595/ab0537>.
- [93] LoKI - IPFN, (n.d.). <https://nprime.tecnico.ulisboa.pt/loki/> (accessed January 20, 2023).
- [94] A. Tejero-del-Caz, V. Guerra, N. Pinhão, C.D. Pintassilgo, L.L. Alves, On the quasi-stationary approach to solve the electron Boltzmann equation in pulsed plasmas, *Plasma Sources Sci. Technol.* 30 (2021) 065008. <https://doi.org/10.1088/1361-6595/abf858>.

- [95] V. Guerra, A. Tejero-del-Caz, C.D. Pintassilgo, L.L. Alves, Modelling N<sub>2</sub>-O<sub>2</sub> plasmas: volume and surface kinetics, *Plasma Sources Sci. Technol.* 28 (2019) 073001. <https://doi.org/10.1088/1361-6595/ab252c>.
- [96] P.J. Chantry, A simple formula for diffusion calculations involving wall reflection and low density, *J. Appl. Phys.* 62 (1987) 1141–1148. <https://doi.org/10.1063/1.339662>.
- [97] V. Guerra, J. Loureiro, Kinetic model of a low-pressure microwave discharge in O<sub>2</sub>-H<sub>2</sub> including the effects of O<sup>-</sup> ions on the characteristics for plasma maintenance, *Plasma Sources Sci. Technol.* 8 (1999) 110. <https://doi.org/10.1088/0963-0252/8/1/014>.
- [98] T. C. Dias, C. Fromentin, L. L. Alves, A. T. del Caz, T. Silva, and V. Guerra, Reaction mechanisms for O<sub>2</sub> plasmas, In preparation to submit to the Special Issue on Verification, Validation and Benchmarking of Low-temperature Plasma Models of *Plasma Sources Sci. Technol.* (2022).
- [99] O. Biondo, C. Fromentin, T. Silva, V. Guerra, G. van Rooij, A. Bogaerts, Insights into the limitations to vibrational excitation of CO<sub>2</sub>: validation of a kinetic model with pulsed glow discharge experiments, *Plasma Sources Sci. Technol.* 31 (2022) 074003. <https://doi.org/10.1088/1361-6595/ac8019>.
- [100] L.L. Alves, The IST-LISBON database on LXCat, *J. Phys. Conf. Ser.* 565 (2014) 012007. <https://doi.org/10.1088/1742-6596/565/1/012007>.
- [101] IST-Lisbon database, (n.d.). [www.lxcat.net](http://www.lxcat.net) (accessed November 22, 2022).
- [102] J. Loureiro, C.M. Ferreira, Coupled electron energy and vibrational distribution functions in stationary N<sub>2</sub> discharges, *J. Phys. Appl. Phys.* 19 (1986) 17. <https://doi.org/10.1088/0022-3727/19/1/007>.
- [103] P. Coche, V. Guerra, L.L. Alves, Microwave air plasmas in capillaries at low pressure I. Self-consistent modeling, *J. Phys. Appl. Phys.* 49 (2016) 235207. <https://doi.org/10.1088/0022-3727/49/23/235207>.
- [104] Y. Wang, O. Zatsarinny, K. Bartschat, B-spline R-matrix-with-pseudostates calculations for electron-impact excitation and ionization of nitrogen, *Phys. Rev. A.* 89 (2014) 062714. <https://doi.org/10.1103/PhysRevA.89.062714>.
- [105] G. Gousset, C.M. Ferreira, M. Pinheiro, P.A. Sa, M. Touzeau, M. Vialle, J. Loureiro, Electron and heavy-particle kinetics in the low pressure oxygen positive column, *J. Phys. Appl. Phys.* 24 (1991) 290. <https://doi.org/10.1088/0022-3727/24/3/010>.
- [106] L.L. Alves, P. Coche, M.A. Ridenti, V. Guerra, Electron scattering cross sections for the modelling of oxygen-containing plasmas\*, *Eur. Phys. J. D.* 70 (2016) 124. <https://doi.org/10.1140/epjd/e2016-70102-1>.
- [107] V.O. Klein, S. Rosseland, Uber Zusammenstöße zwischen Atomen und freien Elektronen., (n.d.).
- [108] M. Foucher, D. Marinov, E. Carbone, P. Chabert, J.-P. Booth, Highly vibrationally excited O<sub>2</sub> molecules in low-pressure inductively-coupled plasmas detected by high sensitivity ultra-broad-band optical absorption spectroscopy, *Plasma Sources Sci. Technol.* 24 (2015) 042001. <https://doi.org/10.1088/0963-0252/24/4/042001>.
- [109] V. Guerra, J. Loureiro, Non-equilibrium coupled kinetics in stationary N<sub>2</sub>-O<sub>2</sub> discharges, *J. Phys. Appl. Phys.* 28 (1995) 1903. <https://doi.org/10.1088/0022-3727/28/9/018>.
- [110] V. Guerra, J. Loureiro, Self-consistent electron and heavy-particle kinetics in a low-pressure - glow discharge, *Plasma Sources Sci. Technol.* 6 (1997) 373. <https://doi.org/10.1088/0963-0252/6/3/014>.
- [111] A. Anušová, D. Marinov, J.-P. Booth, N. Sirse, M.L. da Silva, B. Lopez, V. Guerra, Kinetics of highly vibrationally excited O<sub>2</sub>(X) molecules in inductively-coupled oxygen plasmas, *Plasma Sources Sci. Technol.* 27 (2018) 045006. <https://doi.org/10.1088/1361-6595/aab47d>.
- [112] M.A. Ridenti, L.L. Alves, V. Guerra, J. Amorim, The role of rotational mechanisms in electron swarm parameters at low reduced electric field in N<sub>2</sub>, O<sub>2</sub> and H<sub>2</sub>, *Plasma Sources Sci. Technol.* 24 (2015) 035002. <https://doi.org/10.1088/0963-0252/24/3/035002>.
- [113] D. Marinov, V. Guerra, O. Guaitella, J.-P. Booth, A. Rousseau, Ozone kinetics in low-pressure discharges: vibrationally excited ozone and molecule formation on surfaces, *Plasma Sources Sci. Technol.* 22 (2013) 055018. <https://doi.org/10.1088/0963-0252/22/5/055018>.

- [114] V. Guerra, P.A. Sá, J. Loureiro, Kinetic modeling of low-pressure nitrogen discharges and post-discharges, *Eur. Phys. J. Appl. Phys.* 28 (2004) 125–152. <https://doi.org/10.1051/epjap:2004188>.
- [115] V. Guerra, J. Loureiro, Electron and heavy particle kinetics in a low-pressure nitrogen glow discharge, *Plasma Sources Sci. Technol.* 6 (1997) 361. <https://doi.org/10.1088/0963-0252/6/3/013>.
- [116] O.V. Braginskiy, A.N. Vasilieva, K.S. Klopovskiy, A.S. Kovalev, D.V. Lopaev, O.V. Proshina, T.V. Rakhimova, A.T. Rakhimov, Singlet oxygen generation in O<sub>2</sub> flow excited by RF discharge: I. Homogeneous discharge mode:  $\Sigma^{\alpha}$ -mode, *J. Phys. Appl. Phys.* 38 (2005) 3609–3625. <https://doi.org/10.1088/0022-3727/38/19/010>.
- [117] J.P. Booth, A. Chatterjee, O. Guaitella, D. Lopaev, S. Zyryanov, A. Volynets, T. Rakhimova, D. Voloshin, A. Chukalovsky, Y. Mankelevich, V. Guerra, Quenching of O<sub>2</sub>(b<sup>1</sup>Σ<sub>g</sub><sup>+</sup>) by O(3P) atoms. Effect of gas temperature, *Plasma Sources Sci. Technol.* 31 (2022) 065012. <https://doi.org/10.1088/1361-6595/ac7749>.
- [118] C.D. Pintassilgo, J. Loureiro, Kinetic study of a N<sub>2</sub>-CH<sub>4</sub> afterglow plasma for production of N-containing hydrocarbon species of Titan's atmosphere, *Adv. Space Res.* 46 (2010) 657–671. <https://doi.org/10.1016/j.asr.2010.04.027>.
- [119] N.A. Popov, Investigation of the mechanism for rapid heating of nitrogen and air in gas discharges, *Plasma Phys. Rep.* 27 (2001) 886–896. <https://doi.org/10.1134/1.1409722>.
- [120] R.A. Young, G. Black, T.G. Slanger, Vacuum-Ultraviolet Photolysis of N<sub>2</sub>O. II. Deactivation of N<sub>2</sub>(A <sup>3</sup>Σ<sub>u</sub><sup>+</sup>; and N<sub>2</sub>(B <sup>3</sup>Π<sub>g</sub>), *J. Chem. Phys.* 50 (1969) 303–308. <https://doi.org/10.1063/1.1670792>.
- [121] I. M. Campbell, B. A. Thrush, Behaviour of carbon dioxide and nitrous oxide in active nitrogen, *Trans. Faraday Soc.* 62 (1966) 3366–3374. <https://doi.org/10.1039/TF9666203366>.
- [122] L.G. Piper, Energy transfer studies on N<sub>2</sub>(X <sup>1</sup>Σ<sub>g</sub><sup>+</sup>, v) and N<sub>2</sub>(B <sup>3</sup>Π<sub>g</sub>), *J. Chem. Phys.* 97 (1992) 270–275. <https://doi.org/10.1063/1.463625>.
- [123] J.T. Herron, Evaluated Chemical Kinetics Data for Reactions of N(2D), N(2P), and N<sub>2</sub>(A <sup>3</sup>Σ<sub>u</sub><sup>+</sup>) in the Gas Phase, *J. Phys. Chem. Ref. Data.* 28 (1999) 1453–1483. <https://doi.org/10.1063/1.556043>.
- [124] W. j. Wiegand, W.L. Nighan, Plasma chemistry of CO<sub>2</sub>–N<sub>2</sub>–He discharges, *Appl. Phys. Lett.* 22 (1973) 583–586. <https://doi.org/10.1063/1.1654516>.
- [125] J.A. Meyer, D.W. Setser, W.G. Clark, Rate constants for quenching of molecular nitrogen (A<sup>3</sup>Σ<sub>u</sub><sup>+</sup>) in active nitrogen, *J. Phys. Chem.* 76 (1972) 1–9. <https://doi.org/10.1021/j100645a001>.
- [126] D.W. Setser, G.W. Taylor, Comparison of the reactivities of the lowest excited states of nitrogen (A<sup>3</sup>Σ<sub>u</sub><sup>+</sup>) and of carbon monoxide (a<sup>3</sup>Π<sub>1</sub>), *J. Am. Chem. Soc.* 93 (1971) 4930–4932. <https://doi.org/10.1021/ja00748a058>.
- [127] A.B. Callear, I.W.M. Smith, Fluorescence of nitric oxide. Part 4.—Mechanism of deactivation of NO C<sup>2</sup>Π(v= 0) in nitrogen, *Trans. Faraday Soc.* 61 (1965) 2383–2394. <https://doi.org/10.1039/TF9656102383>.
- [128] N.A. Popov, Vibrational kinetics of electronically-excited molecules in nitrogen discharge plasma, *J. Phys. Appl. Phys.* 46 (2013) 355204. <https://doi.org/10.1088/0022-3727/46/35/355204>.
- [129] F. Albugues, A. Birot, D. Blanc, H. Brunet, J. Galy, P. Millet, J.L. Teyssier, Destruction of the levels C<sup>3</sup>Π<sub>u</sub> (v'=0, v'=1) of nitrogen by O<sub>2</sub>, CO<sub>2</sub>, CH<sub>4</sub>, and H<sub>2</sub>O, *J. Chem. Phys.* 61 (1974) 2695–2699. <https://doi.org/10.1063/1.1682401>.
- [130] L.L. Alves, L. Marques, C.D. Pintassilgo, G. Wattieaux, E. Es-sebbar, J. Berndt, E. Kovacević, N. Carrasco, L. Boufendi, G. Cernogora, Capacitively coupled radio-frequency discharges in nitrogen at low pressures, *Plasma Sources Sci. Technol.* 21 (2012) 045008. <https://doi.org/10.1088/0963-0252/21/4/045008>.
- [131] M. Capitelli, C. Gorse, G.D. Billing, V—V pumping up in non-equilibrium nitrogen: Effects on the dissociation rate, *Chem. Phys.* 52 (1980) 299–304. [https://doi.org/10.1016/0301-0104\(80\)85233-5](https://doi.org/10.1016/0301-0104(80)85233-5).
- [132] G.D. Billing, E.R. Fisher, VV and VT rate coefficients in N<sub>2</sub> by a quantum-classical model, *Chem. Phys.* 43 (1979) 395–401. [https://doi.org/10.1016/0301-0104\(79\)85207-6](https://doi.org/10.1016/0301-0104(79)85207-6).



- [133] R.N. Schwartz, Z.I. Slawsky, K.F. Herzfeld, Calculation of Vibrational Relaxation Times in Gases, *J. Chem. Phys.* 20 (1952) 1591–1599. <https://doi.org/10.1063/1.1700221>.
- [134] R.D. Sharma, C.A. Brau, Near-Resonant Vibrational Energy Transfer in N<sub>2</sub>-CO<sub>2</sub> Mixtures, *Phys. Rev. Lett.* 19 (1967) 1273–1275. <https://doi.org/10.1103/PhysRevLett.19.1273>.
- [135] R.D. Sharma, C.A. Brau, Energy Transfer in Near-Resonant Molecular Collisions due to Long-Range Forces with Application to Transfer of Vibrational Energy from  $\nu_3$  Mode of CO<sub>2</sub> to N<sub>2</sub>, *J. Chem. Phys.* 50 (1969) 924–930. <https://doi.org/10.1063/1.1671145>.
- [136] M. Capitelli, C.M. Ferreira, B.F. Gordiets, A.I. Osipov, *Plasma Kinetics in Atmospheric Gases*, Springer Science & Business Media, 2013.
- [137] M. Lino da Silva, V. Guerra, J. Loureiro, P.A. Sá, Vibrational distributions in N<sub>2</sub> with an improved calculation of energy levels using the RKR method, *Chem. Phys.* 348 (2008) 187–194. <https://doi.org/10.1016/j.chemphys.2008.02.048>.
- [138] A. Chedin, The carbon dioxide molecule, *J. Mol. Spectrosc.* 76 (1979) 430–491. [https://doi.org/10.1016/0022-2852\(79\)90236-4](https://doi.org/10.1016/0022-2852(79)90236-4).
- [139] P. Ogloblina, A. Tejero-del-Caz, V. Guerra, L.L. Alves, Electron impact cross sections for carbon monoxide and their importance in the electron kinetics of CO<sub>2</sub>-CO mixtures, *Plasma Sources Sci. Technol.* 29 (2020) 015002. <https://doi.org/10.1088/1361-6595/ab4e72>.
- [140] V. Laporta, C.M. Cassidy, J. Tennyson, R. Celiberto, Electron-impact resonant vibration excitation cross sections and rate coefficients for carbon monoxide, *Plasma Sources Sci. Technol.* 21 (2012) 045005. <https://doi.org/10.1088/0963-0252/21/4/045005>.
- [141] A.V. Phelps, Rotational and Vibrational Excitation of Molecules by Low-Energy Electrons, *Rev. Mod. Phys.* 40 (1968) 399–410. <https://doi.org/10.1103/RevModPhys.40.399>.
- [142] G. Colonna, V. Laporta, R. Celiberto, M. Capitelli, J. Tennyson, Non-equilibrium vibrational and electron energy distributions functions in atmospheric nitrogen ns pulsed discharges and  $\mu$ s post-discharges: the role of electron molecule vibrational excitation scaling-laws, *Plasma Sources Sci. Technol.* 24 (2015) 035004. <https://doi.org/10.1088/0963-0252/24/3/035004>.
- [143] A. Bourdon, P. Vervisch, Analytical Models for Electron-Vibration Coupling in Nitrogen Plasma Flows, *J. Thermophys. Heat Transf.* (2012). <https://doi.org/10.2514/2.6571>.
- [144] G.J. Schulz, Vibrational Excitation of N<sub>2</sub>, CO and H<sub>2</sub> by Electron Impact, *Phys. Rev.* 135 (1964) A988–A994. <https://doi.org/10.1103/PhysRev.135.A988>.
- [145] H. Ehrhardt, L. Langhans, F. Linder, H.S. Taylor, Resonance Scattering of Slow Electrons from H<sub>2</sub> and CO Angular Distributions, *Phys. Rev.* 173 (1968) 222–230. <https://doi.org/10.1103/PhysRev.173.222>.
- [146] J.C. Stephenson, R.E. Wood, C.B. Moore, Near-Resonant Energy Transfer between Infrared-Active Vibrations, *J. Chem. Phys.* 48 (1968) 4790–4791. <https://doi.org/10.1063/1.1668068>.
- [147] E.V. Kustova, E.A. Nagnibeda, I. Armenise, Vibrational-Chemical Kinetics in Mars Entry Problems, *Open Plasma Phys. J.* 7 (2014) 76–87. <https://doi.org/10.2174/1876534301407010076>.
- [148] J. Blauer, G. Nickerson, A survey of vibrational relaxation rate data for processes important to CO<sub>2</sub>-N<sub>2</sub>-H<sub>2</sub>O infrared plume radiation, in: 7th Fluid Plasma Dynamics Conf., American Institute of Aeronautics and Astronautics, Palo Alto, CA, U.S.A., 1974. <https://doi.org/10.2514/6.1974-536>.
- [149] R.L. Taylor, M. Camac, R.M. Feinberg, Measurements of vibration-vibration coupling in gas mixtures, *Symp. Int. Combust.* 11 (1967) 49–65. [https://doi.org/10.1016/S0082-0784\(67\)80133-4](https://doi.org/10.1016/S0082-0784(67)80133-4).
- [150] W.A. Rosser, A.D. Wood, E.T. Gerry, Deactivation of Vibrationally Excited Carbon Dioxide ( $\nu_3$ ) by Collisions with Carbon Dioxide or with Nitrogen, *J. Chem. Phys.* 50 (1969) 4996–5008. <https://doi.org/10.1063/1.1670996>.
- [151] R.L. Taylor, S. Bitterman, Experimental Measurements of the Resonant Vibrational Energy Transfer between Mode  $\nu_3$  of CO<sub>2</sub> and N<sub>2</sub>, *J. Chem. Phys.* 50 (1969) 1720–1726. <https://doi.org/10.1063/1.1671265>.
- [152] C.B. Moore, R.E. Wood, B. Hu, J.T. Yardley, Vibrational Energy Transfer in CO<sub>2</sub> Lasers, *J. Chem. Phys.* 46 (1967) 4222–4231. <https://doi.org/10.1063/1.1840527>.

- [153] D.F. Starr, J.K. Hancock, Vibrational energy transfer in CO<sub>2</sub>-CO mixtures from 163 to 406 °K, *J. Chem. Phys.* 63 (1975) 4730–4734. <https://doi.org/10.1063/1.431259>.
- [154] W.A. Rosser, R.D. Sharma, E.T. Gerry, Deactivation of Vibrationally Excited Carbon Dioxide (001) by Collisions with Carbon Monoxide, *J. Chem. Phys.* 54 (1971) 1196–1205. <https://doi.org/10.1063/1.1674955>.
- [155] R.D. Sharma, Near-resonant vibration-to-vibration energy transfer in the NO+-N<sub>2</sub> collisions, *J. Chem. Phys.* 125 (2006) 114306. <https://doi.org/10.1063/1.2348874>.
- [156] Losev, S. A., Kozlov, P. V., Kuznetsova, L. A., Makarov, V. N., Romanenko, Y. V., Romanenko, Y. V. Surzhikov, S. T., Radiation of a Mixture CO<sub>2</sub>-N<sub>2</sub>-Ar in Shock Waves: Experiment & Modelling, *Aerothermodynamics for space vehicles, Proceedings of the 3rd European Symposium on Aerothermodynamics for space vehicles held at ESTEC, Noordwijk, The Netherlands. (1998) 437.*
- [157] K.F. Herzfeld, Deactivation of Vibrations by Collision in the Presence of Fermi Resonance, *J. Chem. Phys.* 47 (1967) 743–752. <https://doi.org/10.1063/1.1711947>.
- [158] A.K. Kurnosov, A.P. Napartovich, S.L. Shnyrev, M. Cacciatore, A database for V-V state-to-state rate constants in N<sub>2</sub>-N<sub>2</sub> and N<sub>2</sub>-CO collisions in a wide temperature range: dynamical calculations and analytical approximations, *Plasma Sources Sci. Technol.* 19 (2010) 045015. <https://doi.org/10.1088/0963-0252/19/4/045015>.
- [159] D.C. Allen, C.J.S.M. Simpson, Vibrational energy exchange between CO and the isotopes of N<sub>2</sub> between 300 K and 80 K, *Chem. Phys.* 45 (1980) 203–211. [https://doi.org/10.1016/0301-0104\(80\)85068-3](https://doi.org/10.1016/0301-0104(80)85068-3).
- [160] G. Mastrocinque, A. Chakroun, L. Doyennette, H. Gueguen, M. Margottin-Maclou, L. Henry, Vibrational energy transfer from the  $\nu = 1$  level of carbon monoxide to the  $\nu = 1$  level of the two isotopic species of nitrogen: <sup>14</sup>N<sub>2</sub> and <sup>15</sup>N<sub>2</sub>, *Chem. Phys. Lett.* 39 (1976) 347–349. [https://doi.org/10.1016/0009-2614\(76\)80092-9](https://doi.org/10.1016/0009-2614(76)80092-9).
- [161] Q. Hong, M. Bartolomei, C. Coletti, A. Lombardi, Q. Sun, F. Pirani, Vibrational Energy Transfer in CO+N<sub>2</sub> Collisions: A Database for V-V and V-T/R Quantum-Classical Rate Coefficients, *Molecules.* 26 (2021) 7152. <https://doi.org/10.3390/molecules26237152>.
- [162] Y. Sato, S. Tsuchiya, K. Kuratani, Shock-Wave Study of Vibrational Energy Exchange between Diatomic Molecules, *J. Chem. Phys.* 50 (1969) 1911–1919. <https://doi.org/10.1063/1.1671306>.
- [163] H.K. Shin, Vibration-to-vibration energy transfer in near-resonant collisions, *J. Chem. Phys.* 60 (1974) 1064–1070. <https://doi.org/10.1063/1.1681114>.
- [164] P.F. Zittel, C.B. Moore, Vibration-to-vibration energy transfer in N<sub>2</sub>-CO, *Appl. Phys. Lett.* 21 (1972) 81–83. <https://doi.org/10.1063/1.1654298>.
- [165] J.C. Stephenson, E.R. Mosburg, Vibrational energy transfer in CO from 100 to 300 °K, *J. Chem. Phys.* 60 (1974) 3562–3566. <https://doi.org/10.1063/1.1681574>.
- [166] D.F. Starr, J.K. Hancock, W.H. Green, Vibrational deactivation of carbon monoxide by hydrogen and nitrogen from 100 to 650 °K, *J. Chem. Phys.* 61 (1974) 5421–5425. <https://doi.org/10.1063/1.1681897>.
- [167] W.H. Green, J.K. Hancock, Measurement of CO( $\nu = 1$ ) vibrational energy transfer rates using a frequency-doubled CO<sub>2</sub> laser, *J. Chem. Phys.* 59 (1973) 4326–4335. <https://doi.org/10.1063/1.1680629>.
- [168] E. Plönjes, P. Palm, W. Lee, M. D. Chidley, I.V. Adamovich, W. R. Lempert, J.W. Rich, Vibrational energy storage in high pressure mixtures of diatomic molecules, *Chem. Phys.* 260 (2000) 353–366. [https://doi.org/10.1016/S0301-0104\(00\)00257-3](https://doi.org/10.1016/S0301-0104(00)00257-3).
- [169] M. Capitelli, M. Dilonardo, E. Molinari, A theoretical calculation of dissociation rates of molecular hydrogen in electrical discharges, *Chem. Phys.* 20 (1977) 417–429. [https://doi.org/10.1016/0301-0104\(77\)87030-4](https://doi.org/10.1016/0301-0104(77)87030-4).
- [170] M. Capitelli, *Nonequilibrium Vibrational Kinetics*, Springer-Verlag, Berlin, New York, 1986.
- [171] R. J. Kee, F. M. Rupley, J. A. Miller, M. E. Coltrin, J. F. Grcar, E. Meeks, H. K. Moffat, A. E. Lutz, G. DixonLewis, M. D. Smooke, J. Warnatz, G. H. Evans, R. S. Larson, R. E. Mitchell, L. R. Petzold, W. C. Reynolds, M. Caracotsios, W. E. Stewart, P. Glarborg, C. Wang, and O. Adigun, *CHEMKIN Collection, Release 3.6*, San Diego, CA, 2000.
- [172] L. Terraz, T. Silva, A. Morillo-Candas, O. Guaitella, A. Tejero-del-Caz, L.L. Alves, V. Guerra, Influence of N<sub>2</sub> on the CO<sub>2</sub> vibrational distribution function and dissociation yield in non-

- equilibrium plasmas, *J. Phys. Appl. Phys.* 53 (2019) 094002. <https://doi.org/10.1088/1361-6463/ab55fb>.
- [173] G. Black, H. Wise, S. Schechter, R.L. Sharpless, Measurements of vibrationally excited molecules by Raman scattering. II. Surface deactivation of vibrationally excited N<sub>2</sub>, *J. Chem. Phys.* 60 (1974) 3526–3536. <https://doi.org/10.1063/1.1681570>.
- [174] D. Marinov, D. Lopatik, O. Guaitella, M. Hübner, Y. Ionikh, J. Röpcke, A. Rousseau, Surface vibrational relaxation of N<sub>2</sub> studied by CO<sub>2</sub> titration with time-resolved quantum cascade laser absorption spectroscopy, *J. Phys. Appl. Phys.* 45 (2012) 175201. <https://doi.org/10.1088/0022-3727/45/17/175201>.
- [175] P. Ogloblina, In situ resource utilization on Mars using non-equilibrium plasmas, (2020) 139.
- [176] J.P. Booth, O. Guaitella, A. Chatterjee, C. Drag, V. Guerra, D. Lopaev, S. Zyryanov, T. Rakhimova, D. Voloshin, Y. Mankelevich, Oxygen (3P) atom recombination on a Pyrex surface in an O<sub>2</sub> plasma, *Plasma Sources Sci. Technol.* 28 (2019) 055005. <https://doi.org/10.1088/1361-6595/ab13e8>.
- [177] A. Cenian, A. Chernukho, V. Borodin, G. Śliwiński, Modeling of Plasma-Chemical Reactions in Gas Mixture of CO<sub>2</sub> Lasers I. Gas Decomposition in Pure CO<sub>2</sub> Glow Discharge, *Contrib. Plasma Phys.* 34 (1994) 25–37. <https://doi.org/10.1002/ctpp.2150340105>.
- [178] A.S. Kovalev, D.V. Lopaev, Y.A. Mankelevich, N.A. Popov, T.V. Rakhimova, A.Y. Poroykov, D.L. Carroll, Kinetics of in oxygen RF discharges, *J. Phys. Appl. Phys.* 38 (2005) 2360–2370. <https://doi.org/10.1088/0022-3727/38/14/010>.
- [179] V.V. Ivanov, K.S. Klopovskii, D.V. Lopaev, A.T. Rakhimov, T.V. Rakhimova, Nonlocal nature of the electron energy spectrum in a glow discharge in pure O<sub>2</sub>: I. Nonlocal character of the electron distribution function, *Plasma Phys. Rep.* 26 (2000) 972–979. <https://doi.org/10.1134/1.1323562>.
- [180] L.S. Polak, D.I. Slovetsky, Electron impact induced electronic excitation and molecular dissociation, *Int. J. Radiat. Phys. Chem.* 8 (1976) 257–282. [https://doi.org/10.1016/0020-7055\(76\)90070-X](https://doi.org/10.1016/0020-7055(76)90070-X).
- [181] J. Levaton, A.N. Klein, J. Amorim, Kinetic investigation of N<sub>2</sub> flowing DC discharges, *Phys. Plasmas*. 27 (2020) 063503. <https://doi.org/10.1063/1.5144467>.
- [182] A.F. Silva, A.S. Morillo-Candás, A. Tejero-del-Caz, L.L. Alves, O. Guaitella, V. Guerra, A reaction mechanism for vibrationally-cold low-pressure CO<sub>2</sub> plasmas, *Plasma Sources Sci. Technol.* 29 (2020) 125020. <https://doi.org/10.1088/1361-6595/abc818>.
- [183] R. Snoeckx, S. Heijckers, K.V. Wesenbeeck, S. Lenaerts, A. Bogaerts, CO<sub>2</sub> conversion in a dielectric barrier discharge plasma: N<sub>2</sub> in the mix as a helping hand or problematic impurity?, *Energy Environ. Sci.* 9 (2016) 999–1011. <https://doi.org/10.1039/C5EE03304G>.
- [184] A.S. Morillo-Candas, V. Guerra, O. Guaitella, Time Evolution of the Dissociation Fraction in rf CO<sub>2</sub> Plasmas: Impact and Nature of Back-Reaction Mechanisms, *J. Phys. Chem. C*. 124 (2020) 17459–17475. <https://doi.org/10.1021/acs.jpcc.0c03354>.
- [185] T. Silva, A.S. Morillo-Candas, O. Guaitella, V. Guerra, Modeling the time evolution of the dissociation fraction in low-pressure CO<sub>2</sub> plasmas, *J. CO<sub>2</sub> Util.* 53 (2021) 101719. <https://doi.org/10.1016/j.jcou.2021.101719>.
- [186] S. Xu, J.C. Whitehead, P.A. Martin, CO<sub>2</sub> conversion in a non-thermal, barium titanate packed bed plasma reactor: The effect of dilution by Ar and N<sub>2</sub>, *Chem. Eng. J.* 327 (2017) 764–773. <https://doi.org/10.1016/j.cej.2017.06.090>.
- [187] M. Ramakers, I. Michielsen, R. Aerts, V. Meynen, A. Bogaerts, Effect of Argon or Helium on the CO<sub>2</sub> Conversion in a Dielectric Barrier Discharge, *Plasma Process. Polym.* 12 (2015) 755–763. <https://doi.org/10.1002/ppap.201400213>.
- [188] A. Ozkan, T. Dufour, G. Arnoult, P. De Keyzer, A. Bogaerts, F. Reniers, CO<sub>2</sub>–CH<sub>4</sub> conversion and syngas formation at atmospheric pressure using a multi-electrode dielectric barrier discharge, *J. CO<sub>2</sub> Util.* 9 (2015) 74–81. <https://doi.org/10.1016/j.jcou.2015.01.002>.
- [189] World Health Organization, WHO global air quality guidelines: particulate matter (PM<sub>2.5</sub> and PM<sub>10</sub>), ozone, nitrogen dioxide, sulfur dioxide and carbon monoxide, World Health Organization, 2021. <https://apps.who.int/iris/handle/10665/345329> (accessed November 28, 2022).

- [190] Directive 2008/50/EC of the European Parliament and of the Council on ambient air quality and cleaner air for Europe., (2008). <https://www.ecolex.org/details/legislation/directive-200850ec-of-the-european-parliament-and-of-the-council-on-ambient-air-quality-and-cleaner-air-for-europe-lex-faoc080016/> (accessed November 28, 2022).
- [191] B.F. Gordiets, C.M. Ferreira, V.L. Guerra, J.M.A.H. Loureiro, J. Nahorny, D. Pagnon, M. Touzeau, M. Vialle, Kinetic model of a low-pressure N<sub>2</sub>-O<sub>2</sub> flowing glow discharge, *IEEE Trans. Plasma Sci.* 23 (1995) 750–768. <https://doi.org/10.1109/27.467998>.
- [192] P. Coche, V. Guerra, L.L. Alves, Microwave air plasmas in capillaries at low pressure I. Self-consistent modeling, *J. Phys. Appl. Phys.* 49 (2016) 235207. <https://doi.org/10.1088/0022-3727/49/23/235207>.
- [193] C.D. Pintassilgo, J. Loureiro, V. Guerra, Modelling of a N<sub>2</sub>-O<sub>2</sub> flowing afterglow for plasma sterilization, *J. Phys. Appl. Phys.* 38 (2005) 417. <https://doi.org/10.1088/0022-3727/38/3/011>.
- [194] B.F. Gordiets, C.M. Ferreira, Self-Consistent Modeling of Volume and Surface Processes in Air Plasma, *AIAA J.* 36 (1998) 1643–1651. <https://doi.org/10.2514/2.566>.
- [195] A.S. Morillo-Candas, B.L.M. Klarenaar, C. Amoedo, V. Guerra, O. Guaitella, Effect of oxygen atoms on the vibrational kinetics of CO<sub>2</sub> and CO revealed by the use of a large surface area material, *J. Phys. Appl. Phys.* 54 (2021) 095208. <https://doi.org/10.1088/1361-6463/abc992>.
- [196] R. Vertongen, G. Trenchev, R. Van Loenhout, A. Bogaerts, Enhancing CO<sub>2</sub> conversion with plasma reactors in series and O<sub>2</sub> removal, *J. CO<sub>2</sub> Util.* 66 (2022) 102252. <https://doi.org/10.1016/j.jcou.2022.102252>.

# Supporting Information

## Validation of non-equilibrium kinetics in CO<sub>2</sub>-N<sub>2</sub> plasmas

C. Fromentin<sup>1</sup>, T. Silva<sup>1</sup>, T. C. Dias<sup>1</sup>, E. Baratte<sup>2</sup>, O. Guaitella<sup>2</sup> and V. Guerra<sup>1</sup>

<sup>1</sup> Instituto de Plasmas e Fusão Nuclear, Instituto Superior Técnico, Universidade de Lisboa, Portugal

<sup>2</sup> Laboratoire de Physique des Plasmas (UMR 7648), CNRS, Univ. Paris Saclay, Sorbonne Université, École Polytechnique, France

### A. Rate coefficients of some V-V processes included in the model

#### i. N<sub>2</sub>-CO V-V:

The process:



has a rate coefficient of  $k = 1,66 \cdot 10^{-30} \cdot \exp(a + b \cdot T^{-1/3} + c \cdot T^{-2/3})$  in m<sup>3</sup>s<sup>-1</sup>, with T the gas temperature.

N2(X,v=1) + CO(X,v=0) ↔ N2(X,v=0) + CO(X,v=1)	nitrogenCO2VV   26.3332, -28.231, 36.2268
N2(X,v=2) + CO(X,v=0) ↔ N2(X,v=1) + CO(X,v=1)	nitrogenCO2VV   20.3092, 68.1801, -287.656
N2(X,v=3) + CO(X,v=0) ↔ N2(X,v=2) + CO(X,v=1)	nitrogenCO2VV   22.0824, 44.2821, -175.498
N2(X,v=4) + CO(X,v=0) ↔ N2(X,v=3) + CO(X,v=1)	nitrogenCO2VV   24.0239, 18.1109, -65.108
N2(X,v=5) + CO(X,v=0) ↔ N2(X,v=4) + CO(X,v=1)	nitrogenCO2VV   25.8676, -6.42702, 32.3927
N2(X,v=6) + CO(X,v=0) ↔ N2(X,v=5) + CO(X,v=1)	nitrogenCO2VV   27.7473, -31.3048, 125.122
N2(X,v=7) + CO(X,v=0) ↔ N2(X,v=6) + CO(X,v=1)	nitrogenCO2VV   29.5121, -54.0773, 203.928
N2(X,v=8) + CO(X,v=0) ↔ N2(X,v=7) + CO(X,v=1)	nitrogenCO2VV   30.0891, -58.7989, 212.465
N2(X,v=9) + CO(X,v=0) ↔ N2(X,v=8) + CO(X,v=1)	nitrogenCO2VV   30.881, -69.8849, 256.471
N2(X,v=10) + CO(X,v=0) ↔ N2(X,v=9) + CO(X,v=1)	nitrogenCO2VV   29.5312, -45.2338, 149.915
N2(X,v=11) + CO(X,v=0) ↔ N2(X,v=10) + CO(X,v=1)	nitrogenCO2VV   29.5352, -42.901, 129.101
N2(X,v=12) + CO(X,v=0) ↔ N2(X,v=11) + CO(X,v=1)	nitrogenCO2VV   29.8874, -45.2534, 120.008
N2(X,v=13) + CO(X,v=0) ↔ N2(X,v=12) + CO(X,v=1)	nitrogenCO2VV   29.9643, -42.9403, 89.0297
N2(X,v=14) + CO(X,v=0) ↔ N2(X,v=13) + CO(X,v=1)	nitrogenCO2VV   29.3396, -29.103, 9.7148
N2(X,v=15) + CO(X,v=0) ↔ N2(X,v=14) + CO(X,v=1)	nitrogenCO2VV   27.8155, -0.646867, -129.407
N2(X,v=16) + CO(X,v=0) ↔ N2(X,v=15) + CO(X,v=1)	nitrogenCO2VV   27.1068, 12.9426, -203.402
N2(X,v=17) + CO(X,v=0) ↔ N2(X,v=16) + CO(X,v=1)	nitrogenCO2VV   28.6016, -12.1581, -111.344
N2(X,v=18) + CO(X,v=0) ↔ N2(X,v=17) + CO(X,v=1)	nitrogenCO2VV   29.7772, -30.2926, -58.3128
N2(X,v=19) + CO(X,v=0) ↔ N2(X,v=18) + CO(X,v=1)	nitrogenCO2VV   29.17, -17.065, -143.787
N2(X,v=20) + CO(X,v=0) ↔ N2(X,v=19) + CO(X,v=1)	nitrogenCO2VV   34.6908, -104.556, 179.69
N2(X,v=21) + CO(X,v=0) ↔ N2(X,v=20) + CO(X,v=1)	nitrogenCO2VV   32.109, -54.5671, -74.0396

$N_2(X,v=22) + CO(X,v=0) \leftrightarrow N_2(X,v=21) + CO(X,v=1)$	nitrogenCO2VV  24.7211, 79.8345, -695.697
$N_2(X,v=23) + CO(X,v=0) \leftrightarrow N_2(X,v=22) + CO(X,v=1)$	nitrogenCO2VV  24.9209, 73.9707, -674.065
$N_2(X,v=24) + CO(X,v=0) \leftrightarrow N_2(X,v=23) + CO(X,v=1)$	nitrogenCO2VV  28.5622, 5.81752, -373.63
$N_2(X,v=25) + CO(X,v=0) \leftrightarrow N_2(X,v=24) + CO(X,v=1)$	nitrogenCO2VV  31.154, -41.5012, -176.977
$N_2(X,v=26) + CO(X,v=0) \leftrightarrow N_2(X,v=25) + CO(X,v=1)$	nitrogenCO2VV  32.2306, -60.632, -111.204
$N_2(X,v=27) + CO(X,v=0) \leftrightarrow N_2(X,v=26) + CO(X,v=1)$	nitrogenCO2VV  33.0182, -74.8529, -65.8755
$N_2(X,v=28) + CO(X,v=0) \leftrightarrow N_2(X,v=27) + CO(X,v=1)$	nitrogenCO2VV  33.9564, -91.9747, -6.32267
$N_2(X,v=29) + CO(X,v=0) \leftrightarrow N_2(X,v=28) + CO(X,v=1)$	nitrogenCO2VV  43.4796, -254.273, 663.788
$N_2(X,v=30) + CO(X,v=0) \leftrightarrow N_2(X,v=29) + CO(X,v=1)$	nitrogenCO2VV  30.564, -17.9899, -424.744
$N_2(X,v=31) + CO(X,v=0) \leftrightarrow N_2(X,v=30) + CO(X,v=1)$	nitrogenCO2VV  27.7379, 28.5226, -625.886
$N_2(X,v=32) + CO(X,v=0) \leftrightarrow N_2(X,v=31) + CO(X,v=1)$	nitrogenCO2VV  30.829, -33.3464, -334.196
$N_2(X,v=33) + CO(X,v=0) \leftrightarrow N_2(X,v=32) + CO(X,v=1)$	nitrogenCO2VV  33.6843, -88.9491, -81.1479
$N_2(X,v=34) + CO(X,v=0) \leftrightarrow N_2(X,v=33) + CO(X,v=1)$	nitrogenCO2VV  34.7668, -110.18, 5.64985
$N_2(X,v=35) + CO(X,v=0) \leftrightarrow N_2(X,v=34) + CO(X,v=1)$	nitrogenCO2VV  34.8102, -111.565, -1.97593
$N_2(X,v=36) + CO(X,v=0) \leftrightarrow N_2(X,v=35) + CO(X,v=1)$	nitrogenCO2VV  34.7416, -110.751, -20.2669
$N_2(X,v=37) + CO(X,v=0) \leftrightarrow N_2(X,v=36) + CO(X,v=1)$	nitrogenCO2VV  34.4341, -105.579, -58.3648
$N_2(X,v=38) + CO(X,v=0) \leftrightarrow N_2(X,v=37) + CO(X,v=1)$	nitrogenCO2VV  45.5932, -299.167, 761.766
$N_2(X,v=39) + CO(X,v=0) \leftrightarrow N_2(X,v=38) + CO(X,v=1)$	nitrogenCO2VV  26.2462, 59.0595, -902.365
$N_2(X,v=40) + CO(X,v=0) \leftrightarrow N_2(X,v=39) + CO(X,v=1)$	nitrogenCO2VV  27.0993, 36.8597, -782.868
$N_2(X,v=41) + CO(X,v=0) \leftrightarrow N_2(X,v=40) + CO(X,v=1)$	nitrogenCO2VV  31.73, -54.0204, -354.017
$N_2(X,v=42) + CO(X,v=0) \leftrightarrow N_2(X,v=41) + CO(X,v=1)$	nitrogenCO2VV  34.2438, -102.633, -136.098
$N_2(X,v=43) + CO(X,v=0) \leftrightarrow N_2(X,v=42) + CO(X,v=1)$	nitrogenCO2VV  34.5945, -109.5, -119.431
$N_2(X,v=44) + CO(X,v=0) \leftrightarrow N_2(X,v=43) + CO(X,v=1)$	nitrogenCO2VV  34.6051, -109.844, -134.055
$N_2(X,v=45) + CO(X,v=0) \leftrightarrow N_2(X,v=44) + CO(X,v=1)$	nitrogenCO2VV  34.6302, -110.461, -147.463
$N_2(X,v=46) + CO(X,v=0) \leftrightarrow N_2(X,v=45) + CO(X,v=1)$	nitrogenCO2VV  34.4717, -107.741, -176.064
$N_2(X,v=47) + CO(X,v=0) \leftrightarrow N_2(X,v=46) + CO(X,v=1)$	nitrogenCO2VV  48.1873, -349.272, 867.79
$N_2(X,v=48) + CO(X,v=0) \leftrightarrow N_2(X,v=47) + CO(X,v=1)$	nitrogenCO2VV  22.0091, 138.858, -1412.78
$N_2(X,v=49) + CO(X,v=0) \leftrightarrow N_2(X,v=48) + CO(X,v=1)$	nitrogenCO2VV  27.3199, 31.3902, -886.6
$N_2(X,v=50) + CO(X,v=0) \leftrightarrow N_2(X,v=49) + CO(X,v=1)$	nitrogenCO2VV  33.2078, -83.5415, -343.361
$N_2(X,v=51) + CO(X,v=0) \leftrightarrow N_2(X,v=50) + CO(X,v=1)$	nitrogenCO2VV  34.7509, -113.508, -215.362
$N_2(X,v=52) + CO(X,v=0) \leftrightarrow N_2(X,v=51) + CO(X,v=1)$	nitrogenCO2VV  34.8601, -115.775, -221.044
$N_2(X,v=53) + CO(X,v=0) \leftrightarrow N_2(X,v=52) + CO(X,v=1)$	nitrogenCO2VV  34.8929, -116.58, -233.768
$N_2(X,v=54) + CO(X,v=0) \leftrightarrow N_2(X,v=53) + CO(X,v=1)$	nitrogenCO2VV  34.9307, -117.489, -245.996
$N_2(X,v=55) + CO(X,v=0) \leftrightarrow N_2(X,v=54) + CO(X,v=1)$	nitrogenCO2VV  34.7726, -114.8, -274.767
$N_2(X,v=56) + CO(X,v=0) \leftrightarrow N_2(X,v=55) + CO(X,v=1)$	nitrogenCO2VV  50.7052, -398.104, 965.111
$N_2(X,v=57) + CO(X,v=0) \leftrightarrow N_2(X,v=56) + CO(X,v=1)$	nitrogenCO2VV  19.6094, 183.904, -1763.

$N_2(X,v=58) + CO(X,v=0) \leftrightarrow N_2(X,v=57) + CO(X,v=1)$	nitrogenCO2VV  28.7204, 2.91625, -881.976
$N_2(X,v=59) + CO(X,v=0) \leftrightarrow N_2(X,v=58) + CO(X,v=1)$	nitrogenCO2VV  34.3987, -107.96, -358.729
$N_2(X,v=1) + CO(X,v=1) \leftrightarrow N_2(X,v=0) + CO(X,v=2)$	nitrogenCO2VV  26.981, -26.0999, 7.89671
$N_2(X,v=2) + CO(X,v=1) \leftrightarrow N_2(X,v=1) + CO(X,v=2)$	nitrogenCO2VV  19.4259, 95.0473, -412.61
$N_2(X,v=3) + CO(X,v=1) \leftrightarrow N_2(X,v=2) + CO(X,v=2)$	nitrogenCO2VV  21.9281, 58.5236, -244.966
$N_2(X,v=4) + CO(X,v=1) \leftrightarrow N_2(X,v=3) + CO(X,v=2)$	nitrogenCO2VV  24.1953, 26.5833, -107.814
$N_2(X,v=5) + CO(X,v=1) \leftrightarrow N_2(X,v=4) + CO(X,v=2)$	nitrogenCO2VV  26.2081, -1.14478, 6.12999
$N_2(X,v=6) + CO(X,v=1) \leftrightarrow N_2(X,v=5) + CO(X,v=2)$	nitrogenCO2VV  28.2131, -28.4666, 112.38
$N_2(X,v=7) + CO(X,v=1) \leftrightarrow N_2(X,v=6) + CO(X,v=2)$	nitrogenCO2VV  30.1963, -55.0413, 209.764
$N_2(X,v=8) + CO(X,v=1) \leftrightarrow N_2(X,v=7) + CO(X,v=2)$	nitrogenCO2VV  31.1801, -65.8525, 243.291
$N_2(X,v=9) + CO(X,v=1) \leftrightarrow N_2(X,v=8) + CO(X,v=2)$	nitrogenCO2VV  31.6112, -70.6277, 262.664
$N_2(X,v=10) + CO(X,v=1) \leftrightarrow N_2(X,v=9) + CO(X,v=2)$	nitrogenCO2VV  30.3535, -47.7734, 166.84
$N_2(X,v=11) + CO(X,v=1) \leftrightarrow N_2(X,v=10) + CO(X,v=2)$	nitrogenCO2VV  30.0098, -40.4913, 132.572
$N_2(X,v=12) + CO(X,v=1) \leftrightarrow N_2(X,v=11) + CO(X,v=2)$	nitrogenCO2VV  30.4767, -44.8218, 134.47
$N_2(X,v=13) + CO(X,v=1) \leftrightarrow N_2(X,v=12) + CO(X,v=2)$	nitrogenCO2VV  30.6932, -45.0098, 116.586
$N_2(X,v=14) + CO(X,v=1) \leftrightarrow N_2(X,v=13) + CO(X,v=2)$	nitrogenCO2VV  30.3889, -36.6968, 62.4105
$N_2(X,v=15) + CO(X,v=1) \leftrightarrow N_2(X,v=14) + CO(X,v=2)$	nitrogenCO2VV  29.2469, -14.809, -47.3793
$N_2(X,v=16) + CO(X,v=1) \leftrightarrow N_2(X,v=15) + CO(X,v=2)$	nitrogenCO2VV  28.1446, 5.66111, -149.719
$N_2(X,v=17) + CO(X,v=1) \leftrightarrow N_2(X,v=16) + CO(X,v=2)$	nitrogenCO2VV  28.9285, -6.99532, -110.216
$N_2(X,v=18) + CO(X,v=1) \leftrightarrow N_2(X,v=17) + CO(X,v=2)$	nitrogenCO2VV  30.6683, -35.2702, -10.7146
$N_2(X,v=19) + CO(X,v=1) \leftrightarrow N_2(X,v=18) + CO(X,v=2)$	nitrogenCO2VV  29.8027, -17.6694, -113.42
$N_2(X,v=20) + CO(X,v=1) \leftrightarrow N_2(X,v=19) + CO(X,v=2)$	nitrogenCO2VV  34.4967, -90.5394, 146.727
$N_2(X,v=21) + CO(X,v=1) \leftrightarrow N_2(X,v=20) + CO(X,v=2)$	nitrogenCO2VV  32.998, -59.8838, -20.9005
$N_2(X,v=22) + CO(X,v=1) \leftrightarrow N_2(X,v=21) + CO(X,v=2)$	nitrogenCO2VV  26.3412, 61.4596, -584.133
$N_2(X,v=23) + CO(X,v=1) \leftrightarrow N_2(X,v=22) + CO(X,v=2)$	nitrogenCO2VV  25.2668, 79.482, -673.535
$N_2(X,v=24) + CO(X,v=1) \leftrightarrow N_2(X,v=23) + CO(X,v=2)$	nitrogenCO2VV  28.4635, 19.8308, -413.254
$N_2(X,v=25) + CO(X,v=1) \leftrightarrow N_2(X,v=24) + CO(X,v=2)$	nitrogenCO2VV  31.2705, -31.1343, -201.283
$N_2(X,v=26) + CO(X,v=1) \leftrightarrow N_2(X,v=25) + CO(X,v=2)$	nitrogenCO2VV  32.3347, -49.5656, -141.075
$N_2(X,v=27) + CO(X,v=1) \leftrightarrow N_2(X,v=26) + CO(X,v=2)$	nitrogenCO2VV  33.133, -63.5476, -99.1671
$N_2(X,v=28) + CO(X,v=1) \leftrightarrow N_2(X,v=27) + CO(X,v=2)$	nitrogenCO2VV  34.1563, -81.8531, -36.3461
$N_2(X,v=29) + CO(X,v=1) \leftrightarrow N_2(X,v=28) + CO(X,v=2)$	nitrogenCO2VV  43.6842, -243.848, 630.203
$N_2(X,v=30) + CO(X,v=1) \leftrightarrow N_2(X,v=29) + CO(X,v=2)$	nitrogenCO2VV  31.3319, -17.9028, -411.373
$N_2(X,v=31) + CO(X,v=1) \leftrightarrow N_2(X,v=30) + CO(X,v=2)$	nitrogenCO2VV  28.0961, 36.2131, -647.92
$N_2(X,v=32) + CO(X,v=1) \leftrightarrow N_2(X,v=31) + CO(X,v=2)$	nitrogenCO2VV  31.2603, -26.9969, -350.44

$N_2(X,v=33) + CO(X,v=1) \leftrightarrow N_2(X,v=32) + CO(X,v=2)$	nitrogenCO2VV  34.1982, -84.1272, -90.6923
$N_2(X,v=34) + CO(X,v=1) \leftrightarrow N_2(X,v=33) + CO(X,v=2)$	nitrogenCO2VV  35.4413, -108.427, 10.453
$N_2(X,v=35) + CO(X,v=1) \leftrightarrow N_2(X,v=34) + CO(X,v=2)$	nitrogenCO2VV  35.5695, -111.486, 10.8357
$N_2(X,v=36) + CO(X,v=1) \leftrightarrow N_2(X,v=35) + CO(X,v=2)$	nitrogenCO2VV  35.5216, -111.153, -4.9239
$N_2(X,v=37) + CO(X,v=1) \leftrightarrow N_2(X,v=36) + CO(X,v=2)$	nitrogenCO2VV  35.231, -106.389, -40.79
$N_2(X,v=38) + CO(X,v=1) \leftrightarrow N_2(X,v=37) + CO(X,v=2)$	nitrogenCO2VV  46.1449, -295.323, 757.31
$N_2(X,v=39) + CO(X,v=1) \leftrightarrow N_2(X,v=38) + CO(X,v=2)$	nitrogenCO2VV  27.5905, 47.765, -834.771
$N_2(X,v=40) + CO(X,v=1) \leftrightarrow N_2(X,v=39) + CO(X,v=2)$	nitrogenCO2VV  27.916, 35.5083, -762.061
$N_2(X,v=41) + CO(X,v=1) \leftrightarrow N_2(X,v=40) + CO(X,v=2)$	nitrogenCO2VV  32.3243, -51.1791, -352.959
$N_2(X,v=42) + CO(X,v=1) \leftrightarrow N_2(X,v=41) + CO(X,v=2)$	nitrogenCO2VV  34.9206, -101.417, -127.061
$N_2(X,v=43) + CO(X,v=1) \leftrightarrow N_2(X,v=42) + CO(X,v=2)$	nitrogenCO2VV  35.3166, -109.18, -105.987
$N_2(X,v=44) + CO(X,v=1) \leftrightarrow N_2(X,v=43) + CO(X,v=2)$	nitrogenCO2VV  35.3177, -109.364, -121.263
$N_2(X,v=45) + CO(X,v=1) \leftrightarrow N_2(X,v=44) + CO(X,v=2)$	nitrogenCO2VV  35.3346, -109.84, -135.264
$N_2(X,v=46) + CO(X,v=1) \leftrightarrow N_2(X,v=45) + CO(X,v=2)$	nitrogenCO2VV  35.1675, -106.973, -164.474
$N_2(X,v=47) + CO(X,v=1) \leftrightarrow N_2(X,v=46) + CO(X,v=2)$	nitrogenCO2VV  48.6326, -343.759, 856.996
$N_2(X,v=48) + CO(X,v=1) \leftrightarrow N_2(X,v=47) + CO(X,v=2)$	nitrogenCO2VV  23.0774, 132.474, -1366.88
$N_2(X,v=49) + CO(X,v=1) \leftrightarrow N_2(X,v=48) + CO(X,v=2)$	nitrogenCO2VV  27.9304, 33.803, -882.896
$N_2(X,v=50) + CO(X,v=1) \leftrightarrow N_2(X,v=49) + CO(X,v=2)$	nitrogenCO2VV  33.7625, -80.0616, -344.732
$N_2(X,v=51) + CO(X,v=1) \leftrightarrow N_2(X,v=50) + CO(X,v=2)$	nitrogenCO2VV  35.4266, -112.355, -205.541
$N_2(X,v=52) + CO(X,v=1) \leftrightarrow N_2(X,v=51) + CO(X,v=2)$	nitrogenCO2VV  35.5522, -114.938, -209.702
$N_2(X,v=53) + CO(X,v=1) \leftrightarrow N_2(X,v=52) + CO(X,v=2)$	nitrogenCO2VV  35.5844, -115.731, -222.468
$N_2(X,v=54) + CO(X,v=1) \leftrightarrow N_2(X,v=53) + CO(X,v=2)$	nitrogenCO2VV  35.6222, -116.641, -234.682
$N_2(X,v=55) + CO(X,v=1) \leftrightarrow N_2(X,v=54) + CO(X,v=2)$	nitrogenCO2VV  35.4659, -113.988, -263.261
$N_2(X,v=56) + CO(X,v=1) \leftrightarrow N_2(X,v=55) + CO(X,v=2)$	nitrogenCO2VV  51.1906, -393.34, 957.882
$N_2(X,v=57) + CO(X,v=1) \leftrightarrow N_2(X,v=56) + CO(X,v=2)$	nitrogenCO2VV  20.5333, 180.254, -1729.91
$N_2(X,v=58) + CO(X,v=1) \leftrightarrow N_2(X,v=57) + CO(X,v=2)$	nitrogenCO2VV  29.2418, 7.06244, -886.597
$N_2(X,v=59) + CO(X,v=1) \leftrightarrow N_2(X,v=58) + CO(X,v=2)$	nitrogenCO2VV  35.0137, -105.633, -354.509

$N_2(X,v=1) + CO(X,v=2) \leftrightarrow N_2(X,v=0) + CO(X,v=3)$	nitrogenCO2VV  27.4833, -26.3038, -12.1825
$N_2(X,v=2) + CO(X,v=2) \leftrightarrow N_2(X,v=1) + CO(X,v=3)$	nitrogenCO2VV  17.3403, 137.944, -608.467
$N_2(X,v=3) + CO(X,v=2) \leftrightarrow N_2(X,v=2) + CO(X,v=3)$	nitrogenCO2VV  21.2886, 76.4103, -332.498
$N_2(X,v=4) + CO(X,v=2) \leftrightarrow N_2(X,v=3) + CO(X,v=3)$	nitrogenCO2VV  24.0462, 35.9698, -157.594
$N_2(X,v=5) + CO(X,v=2) \leftrightarrow N_2(X,v=4) + CO(X,v=3)$	nitrogenCO2VV  26.2951, 4.01149, -23.4525
$N_2(X,v=6) + CO(X,v=2) \leftrightarrow N_2(X,v=5) + CO(X,v=3)$	nitrogenCO2VV  28.4639, -26.3416, 98.2404
$N_2(X,v=7) + CO(X,v=2) \leftrightarrow N_2(X,v=6) + CO(X,v=3)$	nitrogenCO2VV  30.624, -56.0838, 211.466



$N_2(X,v=8) + CO(X,v=2) \leftrightarrow N_2(X,v=7) + CO(X,v=3)$	nitrogenCO2VV  31.9653, -72.7365, 270.594
$N_2(X,v=9) + CO(X,v=2) \leftrightarrow N_2(X,v=8) + CO(X,v=3)$	nitrogenCO2VV  31.9634, -69.7467, 259.35
$N_2(X,v=10) + CO(X,v=2) \leftrightarrow N_2(X,v=9) + CO(X,v=3)$	nitrogenCO2VV  30.8039, -48.7856, 174.562
$N_2(X,v=11) + CO(X,v=2) \leftrightarrow N_2(X,v=10) + CO(X,v=3)$	nitrogenCO2VV  30.3042, -39.6059, 137.909
$N_2(X,v=12) + CO(X,v=2) \leftrightarrow N_2(X,v=11) + CO(X,v=3)$	nitrogenCO2VV  30.5861, -41.4426, 135.187
$N_2(X,v=13) + CO(X,v=2) \leftrightarrow N_2(X,v=12) + CO(X,v=3)$	nitrogenCO2VV  31.0533, -45.6196, 135.52
$N_2(X,v=14) + CO(X,v=2) \leftrightarrow N_2(X,v=13) + CO(X,v=3)$	nitrogenCO2VV  31.0201, -41.895, 102.467
$N_2(X,v=15) + CO(X,v=2) \leftrightarrow N_2(X,v=14) + CO(X,v=3)$	nitrogenCO2VV  30.2641, -26.5553, 21.6727
$N_2(X,v=16) + CO(X,v=2) \leftrightarrow N_2(X,v=15) + CO(X,v=3)$	nitrogenCO2VV  29.0803, -4.68498, -85.0465
$N_2(X,v=17) + CO(X,v=2) \leftrightarrow N_2(X,v=16) + CO(X,v=3)$	nitrogenCO2VV  29.1216, -4.43065, -99.578
$N_2(X,v=18) + CO(X,v=2) \leftrightarrow N_2(X,v=17) + CO(X,v=3)$	nitrogenCO2VV  31.3302, -41.1274, 38.8394
$N_2(X,v=19) + CO(X,v=2) \leftrightarrow N_2(X,v=18) + CO(X,v=3)$	nitrogenCO2VV  30.217, -19.4877, -78.8056
$N_2(X,v=20) + CO(X,v=2) \leftrightarrow N_2(X,v=19) + CO(X,v=3)$	nitrogenCO2VV  34.1178, -78.5852, 123.126
$N_2(X,v=21) + CO(X,v=2) \leftrightarrow N_2(X,v=20) + CO(X,v=3)$	nitrogenCO2VV  33.4137, -62.0127, 18.0351
$N_2(X,v=22) + CO(X,v=2) \leftrightarrow N_2(X,v=21) + CO(X,v=3)$	nitrogenCO2VV  27.9888, 37.15, -445.385
$N_2(X,v=23) + CO(X,v=2) \leftrightarrow N_2(X,v=22) + CO(X,v=3)$	nitrogenCO2VV  25.6785, 78.1875, -640.839
$N_2(X,v=24) + CO(X,v=2) \leftrightarrow N_2(X,v=23) + CO(X,v=3)$	nitrogenCO2VV  28.1667, 31.8651, -442.514
$N_2(X,v=25) + CO(X,v=2) \leftrightarrow N_2(X,v=24) + CO(X,v=3)$	nitrogenCO2VV  31.136, -21.8395, -218.864
$N_2(X,v=26) + CO(X,v=2) \leftrightarrow N_2(X,v=25) + CO(X,v=3)$	nitrogenCO2VV  32.2214, -40.2223, -160.912
$N_2(X,v=27) + CO(X,v=2) \leftrightarrow N_2(X,v=26) + CO(X,v=3)$	nitrogenCO2VV  32.9528, -52.5048, -129.149
$N_2(X,v=28) + CO(X,v=2) \leftrightarrow N_2(X,v=27) + CO(X,v=3)$	nitrogenCO2VV  33.9497, -69.923, -72.576
$N_2(X,v=29) + CO(X,v=2) \leftrightarrow N_2(X,v=28) + CO(X,v=3)$	nitrogenCO2VV  43.4483, -230.927, 587.018
$N_2(X,v=30) + CO(X,v=2) \leftrightarrow N_2(X,v=29) + CO(X,v=3)$	nitrogenCO2VV  31.7653, -17.1373, -399.931
$N_2(X,v=31) + CO(X,v=2) \leftrightarrow N_2(X,v=30) + CO(X,v=3)$	nitrogenCO2VV  28.0068, 46.7731, -682.424
$N_2(X,v=32) + CO(X,v=2) \leftrightarrow N_2(X,v=31) + CO(X,v=3)$	nitrogenCO2VV  31.2746, -18.3129, -376.844
$N_2(X,v=33) + CO(X,v=2) \leftrightarrow N_2(X,v=32) + CO(X,v=3)$	nitrogenCO2VV  34.335, -77.6478, -107.59
$N_2(X,v=34) + CO(X,v=2) \leftrightarrow N_2(X,v=33) + CO(X,v=3)$	nitrogenCO2VV  35.7497, -105.163, 8.2543
$N_2(X,v=35) + CO(X,v=2) \leftrightarrow N_2(X,v=34) + CO(X,v=3)$	nitrogenCO2VV  35.9973, -110.513, 19.3345
$N_2(X,v=36) + CO(X,v=2) \leftrightarrow N_2(X,v=35) + CO(X,v=3)$	nitrogenCO2VV  35.994, -111.097, 8.02783
$N_2(X,v=37) + CO(X,v=2) \leftrightarrow N_2(X,v=36) + CO(X,v=3)$	nitrogenCO2VV  35.7519, -107.318, -23.0184
$N_2(X,v=38) + CO(X,v=2) \leftrightarrow N_2(X,v=37) + CO(X,v=3)$	nitrogenCO2VV  46.4312, -291.792, 753.901
$N_2(X,v=39) + CO(X,v=2) \leftrightarrow N_2(X,v=38) + CO(X,v=3)$	nitrogenCO2VV  28.6614, 36.2975, -766.758
$N_2(X,v=40) + CO(X,v=2) \leftrightarrow N_2(X,v=39) + CO(X,v=3)$	nitrogenCO2VV  28.4726, 33.6972, -739.334
$N_2(X,v=41) + CO(X,v=2) \leftrightarrow N_2(X,v=40) + CO(X,v=3)$	nitrogenCO2VV  32.6487, -48.6264, -350.742
$N_2(X,v=42) + CO(X,v=2) \leftrightarrow N_2(X,v=41) + CO(X,v=3)$	nitrogenCO2VV  35.3147, -100.26, -117.921
$N_2(X,v=43) + CO(X,v=2) \leftrightarrow N_2(X,v=42) + CO(X,v=3)$	nitrogenCO2VV  35.762, -109.041, -91.8179

$N_2(X,v=44) + CO(X,v=2) \leftrightarrow N_2(X,v=43) + CO(X,v=3)$	nitrogenCO2VV  35.7518, -109.04, -107.828
$N_2(X,v=45) + CO(X,v=2) \leftrightarrow N_2(X,v=44) + CO(X,v=3)$	nitrogenCO2VV  35.7581, -109.334, -122.586
$N_2(X,v=46) + CO(X,v=2) \leftrightarrow N_2(X,v=45) + CO(X,v=3)$	nitrogenCO2VV  35.5787, -106.254, -152.683
$N_2(X,v=47) + CO(X,v=2) \leftrightarrow N_2(X,v=46) + CO(X,v=3)$	nitrogenCO2VV  48.7883, -338.208, 845.993
$N_2(X,v=48) + CO(X,v=2) \leftrightarrow N_2(X,v=47) + CO(X,v=3)$	nitrogenCO2VV  23.884, 125.604, -1318.74
$N_2(X,v=49) + CO(X,v=2) \leftrightarrow N_2(X,v=48) + CO(X,v=3)$	nitrogenCO2VV  28.2683, 35.9281, -877.83
$N_2(X,v=50) + CO(X,v=2) \leftrightarrow N_2(X,v=49) + CO(X,v=3)$	nitrogenCO2VV  34.0246, -76.4881, -346.563
$N_2(X,v=51) + CO(X,v=2) \leftrightarrow N_2(X,v=50) + CO(X,v=3)$	nitrogenCO2VV  35.8121, -111.155, -195.96
$N_2(X,v=52) + CO(X,v=2) \leftrightarrow N_2(X,v=51) + CO(X,v=3)$	nitrogenCO2VV  35.9568, -114.104, -198.354
$N_2(X,v=53) + CO(X,v=2) \leftrightarrow N_2(X,v=52) + CO(X,v=3)$	nitrogenCO2VV  35.9882, -114.882, -211.178
$N_2(X,v=54) + CO(X,v=2) \leftrightarrow N_2(X,v=53) + CO(X,v=3)$	nitrogenCO2VV  36.026, -115.791, -223.388
$N_2(X,v=55) + CO(X,v=2) \leftrightarrow N_2(X,v=54) + CO(X,v=3)$	nitrogenCO2VV  35.8714, -113.171, -251.782
$N_2(X,v=56) + CO(X,v=2) \leftrightarrow N_2(X,v=55) + CO(X,v=3)$	nitrogenCO2VV  51.3828, -388.47, 950.152
$N_2(X,v=57) + CO(X,v=2) \leftrightarrow N_2(X,v=56) + CO(X,v=3)$	nitrogenCO2VV  21.1819, 176.366, -1695.69
$N_2(X,v=58) + CO(X,v=2) \leftrightarrow N_2(X,v=57) + CO(X,v=3)$	nitrogenCO2VV  29.4826, 11.0718, -890.557
$N_2(X,v=59) + CO(X,v=2) \leftrightarrow N_2(X,v=58) + CO(X,v=3)$	nitrogenCO2VV  35.3341, -103.171, -350.943
$N_2(X,v=1) + CO(X,v=3) \leftrightarrow N_2(X,v=0) + CO(X,v=4)$	nitrogenCO2VV  28.0399, -29.5167, -20.2133
$N_2(X,v=2) + CO(X,v=3) \leftrightarrow N_2(X,v=1) + CO(X,v=4)$	nitrogenCO2VV  13.8918, 203.073, -904.017
$N_2(X,v=3) + CO(X,v=3) \leftrightarrow N_2(X,v=2) + CO(X,v=4)$	nitrogenCO2VV  20.2934, 98.6659, -441.184
$N_2(X,v=4) + CO(X,v=3) \leftrightarrow N_2(X,v=3) + CO(X,v=4)$	nitrogenCO2VV  23.7898, 45.528, -211.175
$N_2(X,v=5) + CO(X,v=3) \leftrightarrow N_2(X,v=4) + CO(X,v=4)$	nitrogenCO2VV  26.3439, 8.28304, -53.105
$N_2(X,v=6) + CO(X,v=3) \leftrightarrow N_2(X,v=5) + CO(X,v=4)$	nitrogenCO2VV  28.7007, -25.4209, 84.7976
$N_2(X,v=7) + CO(X,v=3) \leftrightarrow N_2(X,v=6) + CO(X,v=4)$	nitrogenCO2VV  30.9861, -57.514, 210.531
$N_2(X,v=8) + CO(X,v=3) \leftrightarrow N_2(X,v=7) + CO(X,v=4)$	nitrogenCO2VV  32.5146, -77.4178, 285.439
$N_2(X,v=9) + CO(X,v=3) \leftrightarrow N_2(X,v=8) + CO(X,v=4)$	nitrogenCO2VV  32.1491, -68.2122, 250.454
$N_2(X,v=10) + CO(X,v=3) \leftrightarrow N_2(X,v=9) + CO(X,v=4)$	nitrogenCO2VV  31.0571, -48.1596, 172.47
$N_2(X,v=11) + CO(X,v=3) \leftrightarrow N_2(X,v=10) + CO(X,v=4)$	nitrogenCO2VV  30.5592, -39.6642, 142.824
$N_2(X,v=12) + CO(X,v=3) \leftrightarrow N_2(X,v=11) + CO(X,v=4)$	nitrogenCO2VV  30.5894, -38.1716, 132.761
$N_2(X,v=13) + CO(X,v=3) \leftrightarrow N_2(X,v=12) + CO(X,v=4)$	nitrogenCO2VV  31.0996, -43.231, 140.519
$N_2(X,v=14) + CO(X,v=3) \leftrightarrow N_2(X,v=13) + CO(X,v=4)$	nitrogenCO2VV  31.4071, -44.8769, 130.811
$N_2(X,v=15) + CO(X,v=3) \leftrightarrow N_2(X,v=14) + CO(X,v=4)$	nitrogenCO2VV  31.019, -35.6442, 76.8818
$N_2(X,v=16) + CO(X,v=3) \leftrightarrow N_2(X,v=15) + CO(X,v=4)$	nitrogenCO2VV  29.9767, -16.1616, -18.1923
$N_2(X,v=17) + CO(X,v=3) \leftrightarrow N_2(X,v=16) + CO(X,v=4)$	nitrogenCO2VV  29.4407, -5.96878, -73.3649
$N_2(X,v=18) + CO(X,v=3) \leftrightarrow N_2(X,v=17) + CO(X,v=4)$	nitrogenCO2VV  31.9056, -47.3071, 87.4179

$N_2(X,v=19) + CO(X,v=3) \leftrightarrow N_2(X,v=18) + CO(X,v=4)$	nitrogenCO2VV  30.5841, -22.437, -40.94
$N_2(X,v=20) + CO(X,v=3) \leftrightarrow N_2(X,v=19) + CO(X,v=4)$	nitrogenCO2VV  33.7437, -68.9434, 109.336
$N_2(X,v=21) + CO(X,v=3) \leftrightarrow N_2(X,v=20) + CO(X,v=4)$	nitrogenCO2VV  33.5605, -61.5366, 45.0187
$N_2(X,v=22) + CO(X,v=3) \leftrightarrow N_2(X,v=21) + CO(X,v=4)$	nitrogenCO2VV  29.6205, 10.961, -298.823
$N_2(X,v=23) + CO(X,v=3) \leftrightarrow N_2(X,v=22) + CO(X,v=4)$	nitrogenCO2VV  26.3567, 69.6395, -574.67
$N_2(X,v=24) + CO(X,v=3) \leftrightarrow N_2(X,v=23) + CO(X,v=4)$	nitrogenCO2VV  27.9109, 40.7174, -456.41
$N_2(X,v=25) + CO(X,v=3) \leftrightarrow N_2(X,v=24) + CO(X,v=4)$	nitrogenCO2VV  30.9008, -13.1942, -232.125
$N_2(X,v=26) + CO(X,v=3) \leftrightarrow N_2(X,v=25) + CO(X,v=4)$	nitrogenCO2VV  32.1043, -33.3844, -167.386
$N_2(X,v=27) + CO(X,v=3) \leftrightarrow N_2(X,v=26) + CO(X,v=4)$	nitrogenCO2VV  32.7013, -42.7386, -151.171
$N_2(X,v=28) + CO(X,v=3) \leftrightarrow N_2(X,v=27) + CO(X,v=4)$	nitrogenCO2VV  33.5599, -57.2306, -109.976
$N_2(X,v=29) + CO(X,v=3) \leftrightarrow N_2(X,v=28) + CO(X,v=4)$	nitrogenCO2VV  42.9428, -215.624, 535.166
$N_2(X,v=30) + CO(X,v=3) \leftrightarrow N_2(X,v=29) + CO(X,v=4)$	nitrogenCO2VV  32.1047, -17.1061, -383.413
$N_2(X,v=31) + CO(X,v=3) \leftrightarrow N_2(X,v=30) + CO(X,v=4)$	nitrogenCO2VV  27.6726, 59.5068, -725.782
$N_2(X,v=32) + CO(X,v=3) \leftrightarrow N_2(X,v=31) + CO(X,v=4)$	nitrogenCO2VV  31.0242, -7.03326, -414.264
$N_2(X,v=33) + CO(X,v=3) \leftrightarrow N_2(X,v=32) + CO(X,v=4)$	nitrogenCO2VV  34.2496, -69.2999, -132.463
$N_2(X,v=34) + CO(X,v=3) \leftrightarrow N_2(X,v=33) + CO(X,v=4)$	nitrogenCO2VV  35.8407, -100.041, -2.28859
$N_2(X,v=35) + CO(X,v=3) \leftrightarrow N_2(X,v=34) + CO(X,v=4)$	nitrogenCO2VV  36.2392, -108.222, 21.7098
$N_2(X,v=36) + CO(X,v=3) \leftrightarrow N_2(X,v=35) + CO(X,v=4)$	nitrogenCO2VV  36.3094, -110.233, 17.0567
$N_2(X,v=37) + CO(X,v=3) \leftrightarrow N_2(X,v=36) + CO(X,v=4)$	nitrogenCO2VV  36.1555, -108.154, -6.02542
$N_2(X,v=38) + CO(X,v=3) \leftrightarrow N_2(X,v=37) + CO(X,v=4)$	nitrogenCO2VV  46.6161, -288.454, 750.973
$N_2(X,v=39) + CO(X,v=3) \leftrightarrow N_2(X,v=38) + CO(X,v=4)$	nitrogenCO2VV  29.6106, 25.0124, -700.032
$N_2(X,v=40) + CO(X,v=3) \leftrightarrow N_2(X,v=39) + CO(X,v=4)$	nitrogenCO2VV  28.9312, 31.5849, -715.466
$N_2(X,v=41) + CO(X,v=3) \leftrightarrow N_2(X,v=40) + CO(X,v=4)$	nitrogenCO2VV  32.8731, -46.3516, -347.456
$N_2(X,v=42) + CO(X,v=3) \leftrightarrow N_2(X,v=41) + CO(X,v=4)$	nitrogenCO2VV  35.5957, -99.1396, -108.816
$N_2(X,v=43) + CO(X,v=3) \leftrightarrow N_2(X,v=42) + CO(X,v=4)$	nitrogenCO2VV  36.102, -109.098, -76.8904
$N_2(X,v=44) + CO(X,v=3) \leftrightarrow N_2(X,v=43) + CO(X,v=4)$	nitrogenCO2VV  36.0795, -108.904, -93.6271
$N_2(X,v=45) + CO(X,v=3) \leftrightarrow N_2(X,v=44) + CO(X,v=4)$	nitrogenCO2VV  36.0726, -108.976, -109.297
$N_2(X,v=46) + CO(X,v=3) \leftrightarrow N_2(X,v=45) + CO(X,v=4)$	nitrogenCO2VV  35.8766, -105.614, -140.58
$N_2(X,v=47) + CO(X,v=3) \leftrightarrow N_2(X,v=46) + CO(X,v=4)$	nitrogenCO2VV  48.8266, -332.654, 834.931
$N_2(X,v=48) + CO(X,v=3) \leftrightarrow N_2(X,v=47) + CO(X,v=4)$	nitrogenCO2VV  24.6019, 118.195, -1268.11
$N_2(X,v=49) + CO(X,v=3) \leftrightarrow N_2(X,v=48) + CO(X,v=4)$	nitrogenCO2VV  28.5052, 37.735, -871.265
$N_2(X,v=50) + CO(X,v=3) \leftrightarrow N_2(X,v=49) + CO(X,v=4)$	nitrogenCO2VV  34.1655, -72.8472, -348.735
$N_2(X,v=51) + CO(X,v=3) \leftrightarrow N_2(X,v=50) + CO(X,v=4)$	nitrogenCO2VV  36.0776, -109.909, -186.621
$N_2(X,v=52) + CO(X,v=3) \leftrightarrow N_2(X,v=51) + CO(X,v=4)$	nitrogenCO2VV  36.2442, -113.279, -186.977
$N_2(X,v=53) + CO(X,v=3) \leftrightarrow N_2(X,v=52) + CO(X,v=4)$	nitrogenCO2VV  36.2745, -114.036, -199.883
$N_2(X,v=54) + CO(X,v=3) \leftrightarrow N_2(X,v=53) + CO(X,v=4)$	nitrogenCO2VV  36.312, -114.94, -212.107

$N_2(X,v=55) + CO(X,v=3) \leftrightarrow N_2(X,v=54) + CO(X,v=4)$	nitrogenCO2VV  36.1588, -112.35, -240.332
$N_2(X,v=56) + CO(X,v=3) \leftrightarrow N_2(X,v=55) + CO(X,v=4)$	nitrogenCO2VV  51.4514, -383.492, 941.914
$N_2(X,v=57) + CO(X,v=3) \leftrightarrow N_2(X,v=56) + CO(X,v=4)$	nitrogenCO2VV  21.7262, 172.225, -1660.27
$N_2(X,v=58) + CO(X,v=3) \leftrightarrow N_2(X,v=57) + CO(X,v=4)$	nitrogenCO2VV  29.6133, 14.9291, -893.783
$N_2(X,v=59) + CO(X,v=3) \leftrightarrow N_2(X,v=58) + CO(X,v=4)$	nitrogenCO2VV  35.5294, -100.57, -348.055
$N_2(X,v=1) + CO(X,v=4) \leftrightarrow N_2(X,v=0) + CO(X,v=5)$	nitrogenCO2VV  28.7124, -36.0457, -13.9044
$N_2(X,v=2) + CO(X,v=4) \leftrightarrow N_2(X,v=1) + CO(X,v=5)$	nitrogenCO2VV  9.96555, 276.42, -1240.94
$N_2(X,v=3) + CO(X,v=4) \leftrightarrow N_2(X,v=2) + CO(X,v=5)$	nitrogenCO2VV  19.0126, 125.06, -570.169
$N_2(X,v=4) + CO(X,v=4) \leftrightarrow N_2(X,v=3) + CO(X,v=5)$	nitrogenCO2VV  23.5601, 53.8472, -262.334
$N_2(X,v=5) + CO(X,v=4) \leftrightarrow N_2(X,v=4) + CO(X,v=5)$	nitrogenCO2VV  26.4837, 10.3646, -77.186
$N_2(X,v=6) + CO(X,v=4) \leftrightarrow N_2(X,v=5) + CO(X,v=5)$	nitrogenCO2VV  29.0255, -26.5243, 75.5598
$N_2(X,v=7) + CO(X,v=4) \leftrightarrow N_2(X,v=6) + CO(X,v=5)$	nitrogenCO2VV  31.3554, -59.646, 208.363
$N_2(X,v=8) + CO(X,v=4) \leftrightarrow N_2(X,v=7) + CO(X,v=5)$	nitrogenCO2VV  32.9103, -80.3156, 289.647
$N_2(X,v=9) + CO(X,v=4) \leftrightarrow N_2(X,v=8) + CO(X,v=5)$	nitrogenCO2VV  32.2215, -65.6863, 234.278
$N_2(X,v=10) + CO(X,v=4) \leftrightarrow N_2(X,v=9) + CO(X,v=5)$	nitrogenCO2VV  31.1683, -46.4548, 163.069
$N_2(X,v=11) + CO(X,v=4) \leftrightarrow N_2(X,v=10) + CO(X,v=5)$	nitrogenCO2VV  30.3445, -33.2697, 120.98
$N_2(X,v=12) + CO(X,v=4) \leftrightarrow N_2(X,v=11) + CO(X,v=5)$	nitrogenCO2VV  30.8673, -39.6111, 142.913
$N_2(X,v=13) + CO(X,v=4) \leftrightarrow N_2(X,v=12) + CO(X,v=5)$	nitrogenCO2VV  30.9429, -38.807, 134.935
$N_2(X,v=14) + CO(X,v=4) \leftrightarrow N_2(X,v=13) + CO(X,v=5)$	nitrogenCO2VV  31.536, -44.8697, 145.124
$N_2(X,v=15) + CO(X,v=4) \leftrightarrow N_2(X,v=14) + CO(X,v=5)$	nitrogenCO2VV  31.5625, -42.1543, 118.813
$N_2(X,v=16) + CO(X,v=4) \leftrightarrow N_2(X,v=15) + CO(X,v=5)$	nitrogenCO2VV  30.7966, -27.205, 43.9881
$N_2(X,v=17) + CO(X,v=4) \leftrightarrow N_2(X,v=16) + CO(X,v=5)$	nitrogenCO2VV  29.9453, -11.6386, -31.9725
$N_2(X,v=18) + CO(X,v=4) \leftrightarrow N_2(X,v=17) + CO(X,v=5)$	nitrogenCO2VV  32.4229, -53.3216, 132.543
$N_2(X,v=19) + CO(X,v=4) \leftrightarrow N_2(X,v=18) + CO(X,v=5)$	nitrogenCO2VV  30.9588, -26.4456, -0.733776
$N_2(X,v=20) + CO(X,v=4) \leftrightarrow N_2(X,v=19) + CO(X,v=5)$	nitrogenCO2VV  33.4465, -61.8396, 105.668
$N_2(X,v=21) + CO(X,v=4) \leftrightarrow N_2(X,v=20) + CO(X,v=5)$	nitrogenCO2VV  33.5614, -59.6581, 65.0434
$N_2(X,v=22) + CO(X,v=4) \leftrightarrow N_2(X,v=21) + CO(X,v=5)$	nitrogenCO2VV  31.0166, -12.0466, -167.913
$N_2(X,v=23) + CO(X,v=4) \leftrightarrow N_2(X,v=22) + CO(X,v=5)$	nitrogenCO2VV  27.3369, 54.3095, -478.07
$N_2(X,v=24) + CO(X,v=4) \leftrightarrow N_2(X,v=23) + CO(X,v=5)$	nitrogenCO2VV  27.8215, 45.1497, -449.872
$N_2(X,v=25) + CO(X,v=4) \leftrightarrow N_2(X,v=24) + CO(X,v=5)$	nitrogenCO2VV  30.601, -4.80598, -243.414
$N_2(X,v=26) + CO(X,v=4) \leftrightarrow N_2(X,v=25) + CO(X,v=5)$	nitrogenCO2VV  32.0497, -29.2349, -160.124
$N_2(X,v=27) + CO(X,v=4) \leftrightarrow N_2(X,v=26) + CO(X,v=5)$	nitrogenCO2VV  32.4764, -35.0556, -161.759
$N_2(X,v=28) + CO(X,v=4) \leftrightarrow N_2(X,v=27) + CO(X,v=5)$	nitrogenCO2VV  33.1095, -45.0786, -142.571
$N_2(X,v=29) + CO(X,v=4) \leftrightarrow N_2(X,v=28) + CO(X,v=5)$	nitrogenCO2VV  42.2409, -198.377, 476.918

$N_2(X,v=30) + CO(X,v=4) \leftrightarrow N_2(X,v=29) + CO(X,v=5)$	nitrogenCO2VV  32.4783, -19.2927, -354.594
$N_2(X,v=31) + CO(X,v=4) \leftrightarrow N_2(X,v=30) + CO(X,v=5)$	nitrogenCO2VV  27.2177, 73.0085, -771.099
$N_2(X,v=32) + CO(X,v=4) \leftrightarrow N_2(X,v=31) + CO(X,v=5)$	nitrogenCO2VV  30.5627, 6.75581, -461.952
$N_2(X,v=33) + CO(X,v=4) \leftrightarrow N_2(X,v=32) + CO(X,v=5)$	nitrogenCO2VV  33.9878, -59.0261, -165.177
$N_2(X,v=34) + CO(X,v=4) \leftrightarrow N_2(X,v=33) + CO(X,v=5)$	nitrogenCO2VV  35.7541, -92.8773, -21.6812
$N_2(X,v=35) + CO(X,v=4) \leftrightarrow N_2(X,v=34) + CO(X,v=5)$	nitrogenCO2VV  36.3242, -104.205, 16.3304
$N_2(X,v=36) + CO(X,v=4) \leftrightarrow N_2(X,v=35) + CO(X,v=5)$	nitrogenCO2VV  36.4985, -108.17, 20.504
$N_2(X,v=37) + CO(X,v=4) \leftrightarrow N_2(X,v=36) + CO(X,v=5)$	nitrogenCO2VV  36.4777, -108.577, 8.76549
$N_2(X,v=38) + CO(X,v=4) \leftrightarrow N_2(X,v=37) + CO(X,v=5)$	nitrogenCO2VV  46.7419, -285.105, 747.615
$N_2(X,v=39) + CO(X,v=4) \leftrightarrow N_2(X,v=38) + CO(X,v=5)$	nitrogenCO2VV  30.4683, 14.3525, -636.677
$N_2(X,v=40) + CO(X,v=4) \leftrightarrow N_2(X,v=39) + CO(X,v=5)$	nitrogenCO2VV  29.3312, 29.4419, -691.741
$N_2(X,v=41) + CO(X,v=4) \leftrightarrow N_2(X,v=40) + CO(X,v=5)$	nitrogenCO2VV  33.0479, -44.2884, -343.437
$N_2(X,v=42) + CO(X,v=4) \leftrightarrow N_2(X,v=41) + CO(X,v=5)$	nitrogenCO2VV  35.8143, -97.9997, -100.055
$N_2(X,v=43) + CO(X,v=4) \leftrightarrow N_2(X,v=42) + CO(X,v=5)$	nitrogenCO2VV  36.3897, -109.339, -61.2993
$N_2(X,v=44) + CO(X,v=4) \leftrightarrow N_2(X,v=43) + CO(X,v=5)$	nitrogenCO2VV  36.3557, -108.98, -78.5912
$N_2(X,v=45) + CO(X,v=4) \leftrightarrow N_2(X,v=44) + CO(X,v=5)$	nitrogenCO2VV  36.3334, -108.799, -95.2798
$N_2(X,v=46) + CO(X,v=4) \leftrightarrow N_2(X,v=45) + CO(X,v=5)$	nitrogenCO2VV  36.1168, -105.086, -128.024
$N_2(X,v=47) + CO(X,v=4) \leftrightarrow N_2(X,v=46) + CO(X,v=5)$	nitrogenCO2VV  48.8035, -327.144, 824.006
$N_2(X,v=48) + CO(X,v=4) \leftrightarrow N_2(X,v=47) + CO(X,v=5)$	nitrogenCO2VV  25.2874, 110.195, -1214.76
$N_2(X,v=49) + CO(X,v=4) \leftrightarrow N_2(X,v=48) + CO(X,v=5)$	nitrogenCO2VV  28.6964, 39.1873, -863.042
$N_2(X,v=50) + CO(X,v=4) \leftrightarrow N_2(X,v=49) + CO(X,v=5)$	nitrogenCO2VV  34.2404, -69.1724, -351.095
$N_2(X,v=51) + CO(X,v=4) \leftrightarrow N_2(X,v=50) + CO(X,v=5)$	nitrogenCO2VV  36.2763, -108.619, -177.511
$N_2(X,v=52) + CO(X,v=4) \leftrightarrow N_2(X,v=51) + CO(X,v=5)$	nitrogenCO2VV  36.468, -112.471, -175.537
$N_2(X,v=53) + CO(X,v=4) \leftrightarrow N_2(X,v=52) + CO(X,v=5)$	nitrogenCO2VV  36.4968, -113.2, -188.558
$N_2(X,v=54) + CO(X,v=4) \leftrightarrow N_2(X,v=53) + CO(X,v=5)$	nitrogenCO2VV  36.5336, -114.091, -200.825
$N_2(X,v=55) + CO(X,v=4) \leftrightarrow N_2(X,v=54) + CO(X,v=5)$	nitrogenCO2VV  36.3815, -111.526, -228.909
$N_2(X,v=56) + CO(X,v=4) \leftrightarrow N_2(X,v=55) + CO(X,v=5)$	nitrogenCO2VV  51.4497, -378.406, 933.164
$N_2(X,v=57) + CO(X,v=4) \leftrightarrow N_2(X,v=56) + CO(X,v=5)$	nitrogenCO2VV  22.2202, 167.809, -1623.57
$N_2(X,v=58) + CO(X,v=4) \leftrightarrow N_2(X,v=57) + CO(X,v=5)$	nitrogenCO2VV  29.6881, 18.6193, -896.203
$N_2(X,v=59) + CO(X,v=4) \leftrightarrow N_2(X,v=58) + CO(X,v=5)$	nitrogenCO2VV  35.6527, -97.8252, -345.861
$N_2(X,v=1) + CO(X,v=5) \leftrightarrow N_2(X,v=0) + CO(X,v=6)$	nitrogenCO2VV  29.5142, -45.8604, 7.53336
$N_2(X,v=2) + CO(X,v=5) \leftrightarrow N_2(X,v=1) + CO(X,v=6)$	nitrogenCO2VV  6.01693, 350.254, -1584.71
$N_2(X,v=3) + CO(X,v=5) \leftrightarrow N_2(X,v=2) + CO(X,v=6)$	nitrogenCO2VV  17.6738, 152.078, -704.339
$N_2(X,v=4) + CO(X,v=5) \leftrightarrow N_2(X,v=3) + CO(X,v=6)$	nitrogenCO2VV  23.4978, 58.8402, -301.726

$N_2(X,v=5) + CO(X,v=5) \leftrightarrow N_2(X,v=4) + CO(X,v=6)$	nitrogenCO2VV  26.8328, 8.57754, -88.2173
$N_2(X,v=6) + CO(X,v=5) \leftrightarrow N_2(X,v=5) + CO(X,v=6)$	nitrogenCO2VV  29.5105, -30.5336, 74.581
$N_2(X,v=7) + CO(X,v=5) \leftrightarrow N_2(X,v=6) + CO(X,v=6)$	nitrogenCO2VV  31.7628, -62.6401, 205.957
$N_2(X,v=8) + CO(X,v=5) \leftrightarrow N_2(X,v=7) + CO(X,v=6)$	nitrogenCO2VV  33.1834, -81.5264, 283.71
$N_2(X,v=9) + CO(X,v=5) \leftrightarrow N_2(X,v=8) + CO(X,v=6)$	nitrogenCO2VV  32.2106, -62.1688, 210.767
$N_2(X,v=10) + CO(X,v=5) \leftrightarrow N_2(X,v=9) + CO(X,v=6)$	nitrogenCO2VV  31.1889, -43.7306, 146.179
$N_2(X,v=11) + CO(X,v=5) \leftrightarrow N_2(X,v=10) + CO(X,v=6)$	nitrogenCO2VV  30.1934, -28.4173, 100.894
$N_2(X,v=12) + CO(X,v=5) \leftrightarrow N_2(X,v=11) + CO(X,v=6)$	nitrogenCO2VV  30.4178, -30.5468, 112.43
$N_2(X,v=13) + CO(X,v=5) \leftrightarrow N_2(X,v=12) + CO(X,v=6)$	nitrogenCO2VV  31.3229, -42.3498, 152.611
$N_2(X,v=14) + CO(X,v=5) \leftrightarrow N_2(X,v=13) + CO(X,v=6)$	nitrogenCO2VV  31.349, -40.9694, 142.642
$N_2(X,v=15) + CO(X,v=5) \leftrightarrow N_2(X,v=14) + CO(X,v=6)$	nitrogenCO2VV  31.8887, -45.8982, 147.361
$N_2(X,v=16) + CO(X,v=5) \leftrightarrow N_2(X,v=15) + CO(X,v=6)$	nitrogenCO2VV  31.508, -36.9472, 97.9109
$N_2(X,v=17) + CO(X,v=5) \leftrightarrow N_2(X,v=16) + CO(X,v=6)$	nitrogenCO2VV  30.5881, -20.1511, 18.6202
$N_2(X,v=18) + CO(X,v=5) \leftrightarrow N_2(X,v=17) + CO(X,v=6)$	nitrogenCO2VV  32.8848, -58.7855, 172.331
$N_2(X,v=19) + CO(X,v=5) \leftrightarrow N_2(X,v=18) + CO(X,v=6)$	nitrogenCO2VV  31.3515, -31.1981, 39.9442
$N_2(X,v=20) + CO(X,v=5) \leftrightarrow N_2(X,v=19) + CO(X,v=6)$	nitrogenCO2VV  33.2572, -57.285, 111.454
$N_2(X,v=21) + CO(X,v=5) \leftrightarrow N_2(X,v=20) + CO(X,v=6)$	nitrogenCO2VV  33.5127, -57.6153, 83.1573
$N_2(X,v=22) + CO(X,v=5) \leftrightarrow N_2(X,v=21) + CO(X,v=6)$	nitrogenCO2VV  32.0087, -28.4057, -68.2942
$N_2(X,v=23) + CO(X,v=5) \leftrightarrow N_2(X,v=22) + CO(X,v=6)$	nitrogenCO2VV  28.5656, 33.7739, -359.147
$N_2(X,v=24) + CO(X,v=5) \leftrightarrow N_2(X,v=23) + CO(X,v=6)$	nitrogenCO2VV  27.9806, 44.1908, -419.117
$N_2(X,v=25) + CO(X,v=5) \leftrightarrow N_2(X,v=24) + CO(X,v=6)$	nitrogenCO2VV  30.2715, 3.2029, -252.75
$N_2(X,v=26) + CO(X,v=5) \leftrightarrow N_2(X,v=25) + CO(X,v=6)$	nitrogenCO2VV  32.0498, -27.1048, -142.78
$N_2(X,v=27) + CO(X,v=5) \leftrightarrow N_2(X,v=26) + CO(X,v=6)$	nitrogenCO2VV  32.33, -29.924, -159.196
$N_2(X,v=28) + CO(X,v=5) \leftrightarrow N_2(X,v=27) + CO(X,v=6)$	nitrogenCO2VV  32.6899, -34.6917, -165.003
$N_2(X,v=29) + CO(X,v=5) \leftrightarrow N_2(X,v=28) + CO(X,v=6)$	nitrogenCO2VV  41.4027, -179.9, 415.623
$N_2(X,v=30) + CO(X,v=5) \leftrightarrow N_2(X,v=29) + CO(X,v=6)$	nitrogenCO2VV  32.9607, -24.6947, -308.695
$N_2(X,v=31) + CO(X,v=5) \leftrightarrow N_2(X,v=30) + CO(X,v=6)$	nitrogenCO2VV  26.7718, 85.2295, -808.576
$N_2(X,v=32) + CO(X,v=5) \leftrightarrow N_2(X,v=31) + CO(X,v=6)$	nitrogenCO2VV  29.9399, 22.4977, -517.029
$N_2(X,v=33) + CO(X,v=5) \leftrightarrow N_2(X,v=32) + CO(X,v=6)$	nitrogenCO2VV  33.5765, -46.9662, -204.696
$N_2(X,v=34) + CO(X,v=5) \leftrightarrow N_2(X,v=33) + CO(X,v=6)$	nitrogenCO2VV  35.5135, -83.7479, -49.1636
$N_2(X,v=35) + CO(X,v=5) \leftrightarrow N_2(X,v=34) + CO(X,v=6)$	nitrogenCO2VV  36.2572, -98.173, 2.18915
$N_2(X,v=36) + CO(X,v=5) \leftrightarrow N_2(X,v=35) + CO(X,v=6)$	nitrogenCO2VV  36.5624, -104.525, 16.8451
$N_2(X,v=37) + CO(X,v=5) \leftrightarrow N_2(X,v=36) + CO(X,v=6)$	nitrogenCO2VV  36.7179, -108.158, 19.524
$N_2(X,v=38) + CO(X,v=5) \leftrightarrow N_2(X,v=37) + CO(X,v=6)$	nitrogenCO2VV  46.8157, -281.452, 742.575
$N_2(X,v=39) + CO(X,v=5) \leftrightarrow N_2(X,v=38) + CO(X,v=6)$	nitrogenCO2VV  31.2319, 4.81176, -578.966
$N_2(X,v=40) + CO(X,v=5) \leftrightarrow N_2(X,v=39) + CO(X,v=6)$	nitrogenCO2VV  29.6753, 27.667, -670.008

$N_2(X,v=41) + CO(X,v=5) \leftrightarrow N_2(X,v=40) + CO(X,v=6)$	nitrogenCO2VV  33.1897, -42.2954, -339.355
$N_2(X,v=42) + CO(X,v=5) \leftrightarrow N_2(X,v=41) + CO(X,v=6)$	nitrogenCO2VV  35.9893, -96.735, -92.1615
$N_2(X,v=43) + CO(X,v=5) \leftrightarrow N_2(X,v=42) + CO(X,v=6)$	nitrogenCO2VV  36.6468, -109.711, -45.3402
$N_2(X,v=44) + CO(X,v=5) \leftrightarrow N_2(X,v=43) + CO(X,v=6)$	nitrogenCO2VV  36.6049, -109.269, -62.7512
$N_2(X,v=45) + CO(X,v=5) \leftrightarrow N_2(X,v=44) + CO(X,v=6)$	nitrogenCO2VV  36.566, -108.824, -80.4649
$N_2(X,v=46) + CO(X,v=5) \leftrightarrow N_2(X,v=45) + CO(X,v=6)$	nitrogenCO2VV  36.3256, -104.713, -114.849
$N_2(X,v=47) + CO(X,v=5) \leftrightarrow N_2(X,v=46) + CO(X,v=6)$	nitrogenCO2VV  48.7461, -321.736, 813.453
$N_2(X,v=48) + CO(X,v=5) \leftrightarrow N_2(X,v=47) + CO(X,v=6)$	nitrogenCO2VV  25.9671, 101.551, -1158.5
$N_2(X,v=49) + CO(X,v=5) \leftrightarrow N_2(X,v=48) + CO(X,v=6)$	nitrogenCO2VV  28.868, 40.2428, -852.982
$N_2(X,v=50) + CO(X,v=5) \leftrightarrow N_2(X,v=49) + CO(X,v=6)$	nitrogenCO2VV  34.2751, -65.5053, -353.456
$N_2(X,v=51) + CO(X,v=5) \leftrightarrow N_2(X,v=50) + CO(X,v=6)$	nitrogenCO2VV  36.4327, -107.294, -168.597
$N_2(X,v=52) + CO(X,v=5) \leftrightarrow N_2(X,v=51) + CO(X,v=6)$	nitrogenCO2VV  36.6527, -111.693, -163.981
$N_2(X,v=53) + CO(X,v=5) \leftrightarrow N_2(X,v=52) + CO(X,v=6)$	nitrogenCO2VV  36.6792, -112.382, -177.168
$N_2(X,v=54) + CO(X,v=5) \leftrightarrow N_2(X,v=53) + CO(X,v=6)$	nitrogenCO2VV  36.7149, -113.251, -189.519
$N_2(X,v=55) + CO(X,v=5) \leftrightarrow N_2(X,v=54) + CO(X,v=6)$	nitrogenCO2VV  36.5633, -110.7, -217.507
$N_2(X,v=56) + CO(X,v=5) \leftrightarrow N_2(X,v=55) + CO(X,v=6)$	nitrogenCO2VV  51.4013, -373.211, 923.903
$N_2(X,v=57) + CO(X,v=5) \leftrightarrow N_2(X,v=56) + CO(X,v=6)$	nitrogenCO2VV  22.6891, 163.1, -1585.49
$N_2(X,v=58) + CO(X,v=5) \leftrightarrow N_2(X,v=57) + CO(X,v=6)$	nitrogenCO2VV  29.7315, 22.1274, -897.746
$N_2(X,v=59) + CO(X,v=5) \leftrightarrow N_2(X,v=58) + CO(X,v=6)$	nitrogenCO2VV  35.7277, -94.9358, -344.367

$N_2(X,v=1) + CO(X,v=6) \leftrightarrow N_2(X,v=0) + CO(X,v=7)$	nitrogenCO2VV  30.4277, -58.554, 43.123
$N_2(X,v=2) + CO(X,v=6) \leftrightarrow N_2(X,v=1) + CO(X,v=7)$	nitrogenCO2VV  2.225, 421.313, -1919.33
$N_2(X,v=3) + CO(X,v=6) \leftrightarrow N_2(X,v=2) + CO(X,v=7)$	nitrogenCO2VV  16.604, 174.121, -818.798
$N_2(X,v=4) + CO(X,v=6) \leftrightarrow N_2(X,v=3) + CO(X,v=7)$	nitrogenCO2VV  23.7337, 58.3391, -319.318
$N_2(X,v=5) + CO(X,v=6) \leftrightarrow N_2(X,v=4) + CO(X,v=7)$	nitrogenCO2VV  27.4781, 1.50919, -79.4283
$N_2(X,v=6) + CO(X,v=6) \leftrightarrow N_2(X,v=5) + CO(X,v=7)$	nitrogenCO2VV  30.1914, -37.9909, 84.9749
$N_2(X,v=7) + CO(X,v=6) \leftrightarrow N_2(X,v=6) + CO(X,v=7)$	nitrogenCO2VV  32.2119, -66.4584, 203.827
$N_2(X,v=8) + CO(X,v=6) \leftrightarrow N_2(X,v=7) + CO(X,v=7)$	nitrogenCO2VV  33.3528, -81.1625, 268.278
$N_2(X,v=9) + CO(X,v=6) \leftrightarrow N_2(X,v=8) + CO(X,v=7)$	nitrogenCO2VV  32.1412, -57.8323, 180.698
$N_2(X,v=10) + CO(X,v=6) \leftrightarrow N_2(X,v=9) + CO(X,v=7)$	nitrogenCO2VV  31.1498, -40.177, 122.496
$N_2(X,v=11) + CO(X,v=6) \leftrightarrow N_2(X,v=10) + CO(X,v=7)$	nitrogenCO2VV  29.9809, -22.7362, 73.7917
$N_2(X,v=12) + CO(X,v=6) \leftrightarrow N_2(X,v=11) + CO(X,v=7)$	nitrogenCO2VV  30.1567, -24.6314, 89.1957
$N_2(X,v=13) + CO(X,v=6) \leftrightarrow N_2(X,v=12) + CO(X,v=7)$	nitrogenCO2VV  30.7599, -32.2445, 119.402
$N_2(X,v=14) + CO(X,v=6) \leftrightarrow N_2(X,v=13) + CO(X,v=7)$	nitrogenCO2VV  31.8423, -46.4704, 166.942
$N_2(X,v=15) + CO(X,v=6) \leftrightarrow N_2(X,v=14) + CO(X,v=7)$	nitrogenCO2VV  31.8545, -45.2031, 157.911

$N_2(X,v=16) + CO(X,v=6) \leftrightarrow N_2(X,v=15) + CO(X,v=7)$	nitrogenCO2VV  32.0918, -45.0987, 142.771
$N_2(X,v=17) + CO(X,v=6) \leftrightarrow N_2(X,v=16) + CO(X,v=7)$	nitrogenCO2VV  31.2948, -30.0207, 71.8323
$N_2(X,v=18) + CO(X,v=6) \leftrightarrow N_2(X,v=17) + CO(X,v=7)$	nitrogenCO2VV  33.2876, -63.4307, 205.534
$N_2(X,v=19) + CO(X,v=6) \leftrightarrow N_2(X,v=18) + CO(X,v=7)$	nitrogenCO2VV  31.7481, -36.1841, 78.553
$N_2(X,v=20) + CO(X,v=6) \leftrightarrow N_2(X,v=19) + CO(X,v=7)$	nitrogenCO2VV  33.1728, -54.891, 124.322
$N_2(X,v=21) + CO(X,v=6) \leftrightarrow N_2(X,v=20) + CO(X,v=7)$	nitrogenCO2VV  33.4772, -56.2233, 102.442
$N_2(X,v=22) + CO(X,v=6) \leftrightarrow N_2(X,v=21) + CO(X,v=7)$	nitrogenCO2VV  32.6263, -38.4704, 1.79401
$N_2(X,v=23) + CO(X,v=6) \leftrightarrow N_2(X,v=22) + CO(X,v=7)$	nitrogenCO2VV  29.8937, 11.108, -232.591
$N_2(X,v=24) + CO(X,v=6) \leftrightarrow N_2(X,v=23) + CO(X,v=7)$	nitrogenCO2VV  28.4263, 37.4974, -363.3
$N_2(X,v=25) + CO(X,v=6) \leftrightarrow N_2(X,v=24) + CO(X,v=7)$	nitrogenCO2VV  29.9746, 10.0087, -256.959
$N_2(X,v=26) + CO(X,v=6) \leftrightarrow N_2(X,v=25) + CO(X,v=7)$	nitrogenCO2VV  32.0364, -25.4241, -123.112
$N_2(X,v=27) + CO(X,v=6) \leftrightarrow N_2(X,v=26) + CO(X,v=7)$	nitrogenCO2VV  32.2862, -27.4687, -143.492
$N_2(X,v=28) + CO(X,v=6) \leftrightarrow N_2(X,v=27) + CO(X,v=7)$	nitrogenCO2VV  32.3621, -26.8957, -173.96
$N_2(X,v=29) + CO(X,v=6) \leftrightarrow N_2(X,v=28) + CO(X,v=7)$	nitrogenCO2VV  40.4871, -161.043, 355.045
$N_2(X,v=30) + CO(X,v=6) \leftrightarrow N_2(X,v=29) + CO(X,v=7)$	nitrogenCO2VV  33.5615, -33.2699, -245.985
$N_2(X,v=31) + CO(X,v=6) \leftrightarrow N_2(X,v=30) + CO(X,v=7)$	nitrogenCO2VV  26.4747, 93.7493, -826.846
$N_2(X,v=32) + CO(X,v=6) \leftrightarrow N_2(X,v=31) + CO(X,v=7)$	nitrogenCO2VV  29.2236, 39.1121, -574.291
$N_2(X,v=33) + CO(X,v=6) \leftrightarrow N_2(X,v=32) + CO(X,v=7)$	nitrogenCO2VV  33.0423, -33.4572, -249.135
$N_2(X,v=34) + CO(X,v=6) \leftrightarrow N_2(X,v=33) + CO(X,v=7)$	nitrogenCO2VV  35.1482, -73.0539, -82.4635
$N_2(X,v=35) + CO(X,v=6) \leftrightarrow N_2(X,v=34) + CO(X,v=7)$	nitrogenCO2VV  36.0438, -90.0706, -20.5866
$N_2(X,v=36) + CO(X,v=6) \leftrightarrow N_2(X,v=35) + CO(X,v=7)$	nitrogenCO2VV  36.495, -99.0088, 5.06243
$N_2(X,v=37) + CO(X,v=6) \leftrightarrow N_2(X,v=36) + CO(X,v=7)$	nitrogenCO2VV  36.8595, -106.396, 24.1797
$N_2(X,v=38) + CO(X,v=6) \leftrightarrow N_2(X,v=37) + CO(X,v=7)$	nitrogenCO2VV  46.8282, -277.12, 734.321
$N_2(X,v=39) + CO(X,v=6) \leftrightarrow N_2(X,v=38) + CO(X,v=7)$	nitrogenCO2VV  31.8877, -3.12846, -529.045
$N_2(X,v=40) + CO(X,v=6) \leftrightarrow N_2(X,v=39) + CO(X,v=7)$	nitrogenCO2VV  29.9481, 26.7825, -652.65
$N_2(X,v=41) + CO(X,v=6) \leftrightarrow N_2(X,v=40) + CO(X,v=7)$	nitrogenCO2VV  33.2985, -40.1377, -336.278
$N_2(X,v=42) + CO(X,v=6) \leftrightarrow N_2(X,v=41) + CO(X,v=7)$	nitrogenCO2VV  36.1251, -95.1832, -85.9054
$N_2(X,v=43) + CO(X,v=6) \leftrightarrow N_2(X,v=42) + CO(X,v=7)$	nitrogenCO2VV  36.8802, -110.098, -29.5854
$N_2(X,v=44) + CO(X,v=6) \leftrightarrow N_2(X,v=43) + CO(X,v=7)$	nitrogenCO2VV  36.8386, -109.739, -46.3032
$N_2(X,v=45) + CO(X,v=6) \leftrightarrow N_2(X,v=44) + CO(X,v=7)$	nitrogenCO2VV  36.7837, -109.055, -64.8792
$N_2(X,v=46) + CO(X,v=6) \leftrightarrow N_2(X,v=45) + CO(X,v=7)$	nitrogenCO2VV  36.5184, -104.538, -100.884
$N_2(X,v=47) + CO(X,v=6) \leftrightarrow N_2(X,v=46) + CO(X,v=7)$	nitrogenCO2VV  48.6711, -316.493, 803.532
$N_2(X,v=48) + CO(X,v=6) \leftrightarrow N_2(X,v=47) + CO(X,v=7)$	nitrogenCO2VV  26.6562, 92.2293, -1099.18
$N_2(X,v=49) + CO(X,v=6) \leftrightarrow N_2(X,v=48) + CO(X,v=7)$	nitrogenCO2VV  29.0355, 40.8556, -840.891
$N_2(X,v=50) + CO(X,v=6) \leftrightarrow N_2(X,v=49) + CO(X,v=7)$	nitrogenCO2VV  34.2851, -61.8945, -355.602
$N_2(X,v=51) + CO(X,v=6) \leftrightarrow N_2(X,v=50) + CO(X,v=7)$	nitrogenCO2VV  36.5601, -105.948, -159.832



$N_2(X,v=52) + CO(X,v=6) \leftrightarrow N_2(X,v=51) + CO(X,v=7)$	nitrogenCO2VV  36.8119, -110.96, -152.24
$N_2(X,v=53) + CO(X,v=6) \leftrightarrow N_2(X,v=52) + CO(X,v=7)$	nitrogenCO2VV  36.8352, -111.593, -165.661
$N_2(X,v=54) + CO(X,v=6) \leftrightarrow N_2(X,v=53) + CO(X,v=7)$	nitrogenCO2VV  36.8689, -112.427, -178.155
$N_2(X,v=55) + CO(X,v=6) \leftrightarrow N_2(X,v=54) + CO(X,v=7)$	nitrogenCO2VV  36.717, -109.873, -206.119
$N_2(X,v=56) + CO(X,v=6) \leftrightarrow N_2(X,v=55) + CO(X,v=7)$	nitrogenCO2VV  51.3191, -367.91, 914.139
$N_2(X,v=57) + CO(X,v=6) \leftrightarrow N_2(X,v=56) + CO(X,v=7)$	nitrogenCO2VV  23.1465, 158.071, -1545.9
$N_2(X,v=58) + CO(X,v=6) \leftrightarrow N_2(X,v=57) + CO(X,v=7)$	nitrogenCO2VV  29.7568, 25.4383, -898.339
$N_2(X,v=59) + CO(X,v=6) \leftrightarrow N_2(X,v=58) + CO(X,v=7)$	nitrogenCO2VV  35.767, -91.902, -343.573

$N_2(X,v=1) + CO(X,v=7) \leftrightarrow N_2(X,v=0) + CO(X,v=8)$	nitrogenCO2VV  31.403, -73.1946, 89.3921
$N_2(X,v=2) + CO(X,v=7) \leftrightarrow N_2(X,v=1) + CO(X,v=8)$	nitrogenCO2VV  -1.09366, 483.763, -2217.19
$N_2(X,v=3) + CO(X,v=7) \leftrightarrow N_2(X,v=2) + CO(X,v=8)$	nitrogenCO2VV  15.9983, 187.669, -896.943
$N_2(X,v=4) + CO(X,v=7) \leftrightarrow N_2(X,v=3) + CO(X,v=8)$	nitrogenCO2VV  24.3359, 51.1143, -308.805
$N_2(X,v=5) + CO(X,v=7) \leftrightarrow N_2(X,v=4) + CO(X,v=8)$	nitrogenCO2VV  28.4318, -11.1314, -48.3867
$N_2(X,v=6) + CO(X,v=7) \leftrightarrow N_2(X,v=5) + CO(X,v=8)$	nitrogenCO2VV  31.0518, -48.7321, 107.383
$N_2(X,v=7) + CO(X,v=7) \leftrightarrow N_2(X,v=6) + CO(X,v=8)$	nitrogenCO2VV  32.6924, -70.9723, 202.432
$N_2(X,v=8) + CO(X,v=7) \leftrightarrow N_2(X,v=7) + CO(X,v=8)$	nitrogenCO2VV  33.4399, -79.4918, 244.777
$N_2(X,v=9) + CO(X,v=7) \leftrightarrow N_2(X,v=8) + CO(X,v=8)$	nitrogenCO2VV  32.0391, -52.9934, 145.584
$N_2(X,v=10) + CO(X,v=7) \leftrightarrow N_2(X,v=9) + CO(X,v=8)$	nitrogenCO2VV  31.0821, -36.1486, 93.5398
$N_2(X,v=11) + CO(X,v=7) \leftrightarrow N_2(X,v=10) + CO(X,v=8)$	nitrogenCO2VV  29.6858, -15.7056, 37.761
$N_2(X,v=12) + CO(X,v=7) \leftrightarrow N_2(X,v=11) + CO(X,v=8)$	nitrogenCO2VV  29.8717, -18.3125, 60.406
$N_2(X,v=13) + CO(X,v=7) \leftrightarrow N_2(X,v=12) + CO(X,v=8)$	nitrogenCO2VV  30.4619, -26.2484, 96.5757
$N_2(X,v=14) + CO(X,v=7) \leftrightarrow N_2(X,v=13) + CO(X,v=8)$	nitrogenCO2VV  31.2853, -37.0287, 137.264
$N_2(X,v=15) + CO(X,v=7) \leftrightarrow N_2(X,v=14) + CO(X,v=8)$	nitrogenCO2VV  32.4019, -51.4844, 184.048
$N_2(X,v=16) + CO(X,v=7) \leftrightarrow N_2(X,v=15) + CO(X,v=8)$	nitrogenCO2VV  32.4456, -51.1992, 179.52
$N_2(X,v=17) + CO(X,v=7) \leftrightarrow N_2(X,v=16) + CO(X,v=8)$	nitrogenCO2VV  32.0192, -40.4821, 124.433
$N_2(X,v=18) + CO(X,v=7) \leftrightarrow N_2(X,v=17) + CO(X,v=8)$	nitrogenCO2VV  33.628, -67.1309, 231.619
$N_2(X,v=19) + CO(X,v=7) \leftrightarrow N_2(X,v=18) + CO(X,v=8)$	nitrogenCO2VV  32.1268, -40.8926, 112.737
$N_2(X,v=20) + CO(X,v=7) \leftrightarrow N_2(X,v=19) + CO(X,v=8)$	nitrogenCO2VV  33.1611, -53.886, 140.427
$N_2(X,v=21) + CO(X,v=7) \leftrightarrow N_2(X,v=20) + CO(X,v=8)$	nitrogenCO2VV  33.477, -55.6677, 123.2
$N_2(X,v=22) + CO(X,v=7) \leftrightarrow N_2(X,v=21) + CO(X,v=8)$	nitrogenCO2VV  33.0088, -44.6233, 52.9067
$N_2(X,v=23) + CO(X,v=7) \leftrightarrow N_2(X,v=22) + CO(X,v=8)$	nitrogenCO2VV  31.091, -9.35236, -118.151
$N_2(X,v=24) + CO(X,v=7) \leftrightarrow N_2(X,v=23) + CO(X,v=8)$	nitrogenCO2VV  29.1411, 25.6512, -285.811
$N_2(X,v=25) + CO(X,v=7) \leftrightarrow N_2(X,v=24) + CO(X,v=8)$	nitrogenCO2VV  29.7958, 14.281, -250.581
$N_2(X,v=26) + CO(X,v=7) \leftrightarrow N_2(X,v=25) + CO(X,v=8)$	nitrogenCO2VV  31.9249, -22.4412, -109.584

$N_2(X,v=27) + CO(X,v=7) \leftrightarrow N_2(X,v=26) + CO(X,v=8)$	nitrogenCO2VV  32.3506, -27.5512, -115.949
$N_2(X,v=28) + CO(X,v=7) \leftrightarrow N_2(X,v=27) + CO(X,v=8)$	nitrogenCO2VV  32.1526, -21.9488, -168.877
$N_2(X,v=29) + CO(X,v=7) \leftrightarrow N_2(X,v=28) + CO(X,v=8)$	nitrogenCO2VV  39.5474, -142.616, 298.567
$N_2(X,v=30) + CO(X,v=7) \leftrightarrow N_2(X,v=29) + CO(X,v=8)$	nitrogenCO2VV  34.2218, -43.754, -172.586
$N_2(X,v=31) + CO(X,v=7) \leftrightarrow N_2(X,v=30) + CO(X,v=8)$	nitrogenCO2VV  26.4597, 96.2157, -815.085
$N_2(X,v=32) + CO(X,v=7) \leftrightarrow N_2(X,v=31) + CO(X,v=8)$	nitrogenCO2VV  28.5025, 55.0507, -626.504
$N_2(X,v=33) + CO(X,v=7) \leftrightarrow N_2(X,v=32) + CO(X,v=8)$	nitrogenCO2VV  32.4165, -18.9942, -296.016
$N_2(X,v=34) + CO(X,v=7) \leftrightarrow N_2(X,v=33) + CO(X,v=8)$	nitrogenCO2VV  34.6992, -61.4968, -117.97
$N_2(X,v=35) + CO(X,v=7) \leftrightarrow N_2(X,v=34) + CO(X,v=8)$	nitrogenCO2VV  35.7018, -80.1762, -50.3015
$N_2(X,v=36) + CO(X,v=7) \leftrightarrow N_2(X,v=35) + CO(X,v=8)$	nitrogenCO2VV  36.2946, -91.526, -14.9103
$N_2(X,v=37) + CO(X,v=7) \leftrightarrow N_2(X,v=36) + CO(X,v=8)$	nitrogenCO2VV  36.8791, -102.784, 20.7499
$N_2(X,v=38) + CO(X,v=7) \leftrightarrow N_2(X,v=37) + CO(X,v=8)$	nitrogenCO2VV  46.7606, -271.676, 721.151
$N_2(X,v=39) + CO(X,v=7) \leftrightarrow N_2(X,v=38) + CO(X,v=8)$	nitrogenCO2VV  32.4215, -9.09216, -488.489
$N_2(X,v=40) + CO(X,v=7) \leftrightarrow N_2(X,v=39) + CO(X,v=8)$	nitrogenCO2VV  30.1236, 27.3981, -642.395
$N_2(X,v=41) + CO(X,v=7) \leftrightarrow N_2(X,v=40) + CO(X,v=8)$	nitrogenCO2VV  33.3636, -37.4769, -335.703
$N_2(X,v=42) + CO(X,v=7) \leftrightarrow N_2(X,v=41) + CO(X,v=8)$	nitrogenCO2VV  36.2177, -93.123, -82.2962
$N_2(X,v=43) + CO(X,v=7) \leftrightarrow N_2(X,v=42) + CO(X,v=8)$	nitrogenCO2VV  37.0878, -110.31, -14.9449
$N_2(X,v=44) + CO(X,v=7) \leftrightarrow N_2(X,v=43) + CO(X,v=8)$	nitrogenCO2VV  37.0604, -110.303, -29.6788
$N_2(X,v=45) + CO(X,v=7) \leftrightarrow N_2(X,v=44) + CO(X,v=8)$	nitrogenCO2VV  36.9931, -109.461, -48.7041
$N_2(X,v=46) + CO(X,v=7) \leftrightarrow N_2(X,v=45) + CO(X,v=8)$	nitrogenCO2VV  36.7056, -104.603, -85.9879
$N_2(X,v=47) + CO(X,v=7) \leftrightarrow N_2(X,v=46) + CO(X,v=8)$	nitrogenCO2VV  48.5902, -311.483, 794.502
$N_2(X,v=48) + CO(X,v=7) \leftrightarrow N_2(X,v=47) + CO(X,v=8)$	nitrogenCO2VV  27.3632, 82.2188, -1036.81
$N_2(X,v=49) + CO(X,v=7) \leftrightarrow N_2(X,v=48) + CO(X,v=8)$	nitrogenCO2VV  29.2092, 40.9804, -826.585
$N_2(X,v=50) + CO(X,v=7) \leftrightarrow N_2(X,v=49) + CO(X,v=8)$	nitrogenCO2VV  34.2811, -58.3949, -357.294
$N_2(X,v=51) + CO(X,v=7) \leftrightarrow N_2(X,v=50) + CO(X,v=8)$	nitrogenCO2VV  36.6672, -104.596, -151.149
$N_2(X,v=52) + CO(X,v=7) \leftrightarrow N_2(X,v=51) + CO(X,v=8)$	nitrogenCO2VV  36.9543, -110.294, -140.223
$N_2(X,v=53) + CO(X,v=7) \leftrightarrow N_2(X,v=52) + CO(X,v=8)$	nitrogenCO2VV  36.9733, -110.85, -153.964
$N_2(X,v=54) + CO(X,v=7) \leftrightarrow N_2(X,v=53) + CO(X,v=8)$	nitrogenCO2VV  37.0039, -111.629, -166.685
$N_2(X,v=55) + CO(X,v=7) \leftrightarrow N_2(X,v=54) + CO(X,v=8)$	nitrogenCO2VV  36.8502, -109.049, -194.728
$N_2(X,v=56) + CO(X,v=7) \leftrightarrow N_2(X,v=55) + CO(X,v=8)$	nitrogenCO2VV  51.2108, -362.507, 903.89
$N_2(X,v=57) + CO(X,v=7) \leftrightarrow N_2(X,v=56) + CO(X,v=8)$	nitrogenCO2VV  23.6017, 152.696, -1504.7
$N_2(X,v=58) + CO(X,v=7) \leftrightarrow N_2(X,v=57) + CO(X,v=8)$	nitrogenCO2VV  29.7725, 28.5361, -897.909
$N_2(X,v=59) + CO(X,v=7) \leftrightarrow N_2(X,v=58) + CO(X,v=8)$	nitrogenCO2VV  35.7783, -88.7268, -343.463
$N_2(X,v=1) + CO(X,v=8) \leftrightarrow N_2(X,v=0) + CO(X,v=9)$	nitrogenCO2VV  32.3618, -88.3454, 140.387

$N_2(X,v=2) + CO(X,v=8) \leftrightarrow N_2(X,v=1) + CO(X,v=9)$	nitrogenCO2VV  -3.73436, 533.706, -2459.22
$N_2(X,v=3) + CO(X,v=8) \leftrightarrow N_2(X,v=2) + CO(X,v=9)$	nitrogenCO2VV  15.912, 191.598, -932.546
$N_2(X,v=4) + CO(X,v=8) \leftrightarrow N_2(X,v=3) + CO(X,v=9)$	nitrogenCO2VV  25.2813, 37.4707, -270.39
$N_2(X,v=5) + CO(X,v=8) \leftrightarrow N_2(X,v=4) + CO(X,v=9)$	nitrogenCO2VV  29.6215, -28.2553, 1.66105
$N_2(X,v=6) + CO(X,v=8) \leftrightarrow N_2(X,v=5) + CO(X,v=9)$	nitrogenCO2VV  32.032, -61.9251, 139.847
$N_2(X,v=7) + CO(X,v=8) \leftrightarrow N_2(X,v=6) + CO(X,v=9)$	nitrogenCO2VV  33.1967, -76.1716, 202.899
$N_2(X,v=8) + CO(X,v=8) \leftrightarrow N_2(X,v=7) + CO(X,v=9)$	nitrogenCO2VV  33.4787, -77.0806, 216.061
$N_2(X,v=9) + CO(X,v=8) \leftrightarrow N_2(X,v=8) + CO(X,v=9)$	nitrogenCO2VV  31.9344, -48.1254, 107.766
$N_2(X,v=10) + CO(X,v=8) \leftrightarrow N_2(X,v=9) + CO(X,v=9)$	nitrogenCO2VV  31.0228, -32.201, 61.8396
$N_2(X,v=11) + CO(X,v=8) \leftrightarrow N_2(X,v=10) + CO(X,v=9)$	nitrogenCO2VV  29.3031, -7.14863, -7.77146
$N_2(X,v=12) + CO(X,v=8) \leftrightarrow N_2(X,v=11) + CO(X,v=9)$	nitrogenCO2VV  29.5279, -10.9223, 23.6776
$N_2(X,v=13) + CO(X,v=8) \leftrightarrow N_2(X,v=12) + CO(X,v=9)$	nitrogenCO2VV  30.1699, -20.215, 69.4873
$N_2(X,v=14) + CO(X,v=8) \leftrightarrow N_2(X,v=13) + CO(X,v=9)$	nitrogenCO2VV  31.0208, -31.9396, 118.412
$N_2(X,v=15) + CO(X,v=8) \leftrightarrow N_2(X,v=14) + CO(X,v=9)$	nitrogenCO2VV  32.0295, -45.3682, 167.699
$N_2(X,v=16) + CO(X,v=8) \leftrightarrow N_2(X,v=15) + CO(X,v=9)$	nitrogenCO2VV  32.8678, -55.2454, 196.072
$N_2(X,v=17) + CO(X,v=8) \leftrightarrow N_2(X,v=16) + CO(X,v=9)$	nitrogenCO2VV  32.8027, -53.8685, 188.364
$N_2(X,v=18) + CO(X,v=8) \leftrightarrow N_2(X,v=17) + CO(X,v=9)$	nitrogenCO2VV  33.9073, -69.9873, 251.113
$N_2(X,v=19) + CO(X,v=8) \leftrightarrow N_2(X,v=18) + CO(X,v=9)$	nitrogenCO2VV  32.4666, -44.9351, 140.834
$N_2(X,v=20) + CO(X,v=8) \leftrightarrow N_2(X,v=19) + CO(X,v=9)$	nitrogenCO2VV  33.1698, -53.2823, 155.337
$N_2(X,v=21) + CO(X,v=8) \leftrightarrow N_2(X,v=20) + CO(X,v=9)$	nitrogenCO2VV  33.4986, -55.5803, 143.452
$N_2(X,v=22) + CO(X,v=8) \leftrightarrow N_2(X,v=21) + CO(X,v=9)$	nitrogenCO2VV  33.2677, -48.7401, 93.0705
$N_2(X,v=23) + CO(X,v=8) \leftrightarrow N_2(X,v=22) + CO(X,v=9)$	nitrogenCO2VV  32.0049, -24.8499, -27.8647
$N_2(X,v=24) + CO(X,v=8) \leftrightarrow N_2(X,v=23) + CO(X,v=9)$	nitrogenCO2VV  30.042, 10.3659, -195.065
$N_2(X,v=25) + CO(X,v=8) \leftrightarrow N_2(X,v=24) + CO(X,v=9)$	nitrogenCO2VV  29.8201, 14.6561, -228.041
$N_2(X,v=26) + CO(X,v=8) \leftrightarrow N_2(X,v=25) + CO(X,v=9)$	nitrogenCO2VV  31.6916, -17.5779, -105.225
$N_2(X,v=27) + CO(X,v=8) \leftrightarrow N_2(X,v=26) + CO(X,v=9)$	nitrogenCO2VV  32.517, -29.8576, -78.6974
$N_2(X,v=28) + CO(X,v=8) \leftrightarrow N_2(X,v=27) + CO(X,v=9)$	nitrogenCO2VV  32.0567, -19.5722, -151.69
$N_2(X,v=29) + CO(X,v=8) \leftrightarrow N_2(X,v=28) + CO(X,v=9)$	nitrogenCO2VV  38.6269, -125.262, 248.641
$N_2(X,v=30) + CO(X,v=8) \leftrightarrow N_2(X,v=29) + CO(X,v=9)$	nitrogenCO2VV  34.8377, -54.0826, -98.4217
$N_2(X,v=31) + CO(X,v=8) \leftrightarrow N_2(X,v=30) + CO(X,v=9)$	nitrogenCO2VV  26.8297, 90.8501, -765.404
$N_2(X,v=32) + CO(X,v=8) \leftrightarrow N_2(X,v=31) + CO(X,v=9)$	nitrogenCO2VV  27.8804, 68.4718, -665.245
$N_2(X,v=33) + CO(X,v=8) \leftrightarrow N_2(X,v=32) + CO(X,v=9)$	nitrogenCO2VV  31.7351, -4.18328, -342.516
$N_2(X,v=34) + CO(X,v=8) \leftrightarrow N_2(X,v=33) + CO(X,v=9)$	nitrogenCO2VV  34.2136, -49.9261, -151.515
$N_2(X,v=35) + CO(X,v=8) \leftrightarrow N_2(X,v=34) + CO(X,v=9)$	nitrogenCO2VV  35.2671, -69.1465, -83.5518
$N_2(X,v=36) + CO(X,v=8) \leftrightarrow N_2(X,v=35) + CO(X,v=9)$	nitrogenCO2VV  35.972, -82.2682, -41.7865
$N_2(X,v=37) + CO(X,v=8) \leftrightarrow N_2(X,v=36) + CO(X,v=9)$	nitrogenCO2VV  36.7554, -96.9259, 7.83565

$N_2(X,v=38) + CO(X,v=8) \leftrightarrow N_2(X,v=37) + CO(X,v=9)$	nitrogenCO2VV  46.5894, -264.667, 701.364
$N_2(X,v=39) + CO(X,v=8) \leftrightarrow N_2(X,v=38) + CO(X,v=9)$	nitrogenCO2VV  32.8274, -12.9261, -457.74
$N_2(X,v=40) + CO(X,v=8) \leftrightarrow N_2(X,v=39) + CO(X,v=9)$	nitrogenCO2VV  30.1723, 30.1307, -641.936
$N_2(X,v=41) + CO(X,v=8) \leftrightarrow N_2(X,v=40) + CO(X,v=9)$	nitrogenCO2VV  33.3654, -33.8782, -339.516
$N_2(X,v=42) + CO(X,v=8) \leftrightarrow N_2(X,v=41) + CO(X,v=9)$	nitrogenCO2VV  36.2567, -90.28, -82.5366
$N_2(X,v=43) + CO(X,v=8) \leftrightarrow N_2(X,v=42) + CO(X,v=9)$	nitrogenCO2VV  37.2602, -110.071, -2.68413
$N_2(X,v=44) + CO(X,v=8) \leftrightarrow N_2(X,v=43) + CO(X,v=9)$	nitrogenCO2VV  37.2675, -110.81, -13.6114
$N_2(X,v=45) + CO(X,v=8) \leftrightarrow N_2(X,v=44) + CO(X,v=9)$	nitrogenCO2VV  37.1955, -109.964, -32.3401
$N_2(X,v=46) + CO(X,v=8) \leftrightarrow N_2(X,v=45) + CO(X,v=9)$	nitrogenCO2VV  36.8942, -104.931, -70.0985
$N_2(X,v=47) + CO(X,v=8) \leftrightarrow N_2(X,v=46) + CO(X,v=9)$	nitrogenCO2VV  48.5121, -306.762, 786.572
$N_2(X,v=48) + CO(X,v=8) \leftrightarrow N_2(X,v=47) + CO(X,v=9)$	nitrogenCO2VV  28.0918, 71.5555, -971.601
$N_2(X,v=49) + CO(X,v=8) \leftrightarrow N_2(X,v=48) + CO(X,v=9)$	nitrogenCO2VV  29.3963, 40.5812, -809.933
$N_2(X,v=50) + CO(X,v=8) \leftrightarrow N_2(X,v=49) + CO(X,v=9)$	nitrogenCO2VV  34.2713, -55.0634, -358.291
$N_2(X,v=51) + CO(X,v=8) \leftrightarrow N_2(X,v=50) + CO(X,v=9)$	nitrogenCO2VV  36.7601, -103.258, -142.477
$N_2(X,v=52) + CO(X,v=8) \leftrightarrow N_2(X,v=51) + CO(X,v=9)$	nitrogenCO2VV  37.0864, -109.721, -127.82
$N_2(X,v=53) + CO(X,v=8) \leftrightarrow N_2(X,v=52) + CO(X,v=9)$	nitrogenCO2VV  37.0995, -110.175, -141.985
$N_2(X,v=54) + CO(X,v=8) \leftrightarrow N_2(X,v=53) + CO(X,v=9)$	nitrogenCO2VV  37.1256, -110.875, -155.04
$N_2(X,v=55) + CO(X,v=8) \leftrightarrow N_2(X,v=54) + CO(X,v=9)$	nitrogenCO2VV  36.9683, -108.236, -183.307
$N_2(X,v=56) + CO(X,v=8) \leftrightarrow N_2(X,v=55) + CO(X,v=9)$	nitrogenCO2VV  51.0817, -357.009, 893.191
$N_2(X,v=57) + CO(X,v=8) \leftrightarrow N_2(X,v=56) + CO(X,v=9)$	nitrogenCO2VV  24.0612, 146.943, -1461.72
$N_2(X,v=58) + CO(X,v=8) \leftrightarrow N_2(X,v=57) + CO(X,v=9)$	nitrogenCO2VV  29.7843, 31.4039, -896.377
$N_2(X,v=59) + CO(X,v=8) \leftrightarrow N_2(X,v=58) + CO(X,v=9)$	nitrogenCO2VV  35.7668, -85.4168, -344.006

$N_2(X,v=1) + CO(X,v=9) \leftrightarrow N_2(X,v=0) + CO(X,v=10)$	nitrogenCO2VV  33.2204, -102.447, 189.316
$N_2(X,v=2) + CO(X,v=9) \leftrightarrow N_2(X,v=1) + CO(X,v=10)$	nitrogenCO2VV  -5.6317, 569.782, -2637.94
$N_2(X,v=3) + CO(X,v=9) \leftrightarrow N_2(X,v=2) + CO(X,v=10)$	nitrogenCO2VV  16.3071, 186.471, -927.03
$N_2(X,v=4) + CO(X,v=9) \leftrightarrow N_2(X,v=3) + CO(X,v=10)$	nitrogenCO2VV  26.4668, 19.1097, -210.435
$N_2(X,v=5) + CO(X,v=9) \leftrightarrow N_2(X,v=4) + CO(X,v=10)$	nitrogenCO2VV  30.9276, -47.9501, 63.8296
$N_2(X,v=6) + CO(X,v=9) \leftrightarrow N_2(X,v=5) + CO(X,v=10)$	nitrogenCO2VV  33.0599, -76.5064, 179.239
$N_2(X,v=7) + CO(X,v=9) \leftrightarrow N_2(X,v=6) + CO(X,v=10)$	nitrogenCO2VV  33.7306, -82.2853, 207.325
$N_2(X,v=8) + CO(X,v=9) \leftrightarrow N_2(X,v=7) + CO(X,v=10)$	nitrogenCO2VV  33.523, -74.9006, 186.907
$N_2(X,v=9) + CO(X,v=9) \leftrightarrow N_2(X,v=8) + CO(X,v=10)$	nitrogenCO2VV  31.8635, -43.8771, 70.5171
$N_2(X,v=10) + CO(X,v=9) \leftrightarrow N_2(X,v=9) + CO(X,v=10)$	nitrogenCO2VV  31.018, -29.1196, 31.0993
$N_2(X,v=11) + CO(X,v=9) \leftrightarrow N_2(X,v=10) + CO(X,v=10)$	nitrogenCO2VV  28.8321, 2.99391, -62.8544
$N_2(X,v=12) + CO(X,v=9) \leftrightarrow N_2(X,v=11) + CO(X,v=10)$	nitrogenCO2VV  29.1205, -2.32015, -21.3736

$N_2(X,v=13) + CO(X,v=9) \leftrightarrow N_2(X,v=12) + CO(X,v=10)$	nitrogenCO2VV  29.8514, -13.5554, 36.1305
$N_2(X,v=14) + CO(X,v=9) \leftrightarrow N_2(X,v=13) + CO(X,v=10)$	nitrogenCO2VV  30.7857, -27.1095, 96.3588
$N_2(X,v=15) + CO(X,v=9) \leftrightarrow N_2(X,v=14) + CO(X,v=10)$	nitrogenCO2VV  31.8973, -42.6205, 157.965
$N_2(X,v=16) + CO(X,v=9) \leftrightarrow N_2(X,v=15) + CO(X,v=10)$	nitrogenCO2VV  32.9819, -56.9686, 209.272
$N_2(X,v=17) + CO(X,v=9) \leftrightarrow N_2(X,v=16) + CO(X,v=10)$	nitrogenCO2VV  33.1225, -56.1964, 198.935
$N_2(X,v=18) + CO(X,v=9) \leftrightarrow N_2(X,v=17) + CO(X,v=10)$	nitrogenCO2VV  34.1266, -72.9717, 269.1
$N_2(X,v=19) + CO(X,v=9) \leftrightarrow N_2(X,v=18) + CO(X,v=10)$	nitrogenCO2VV  32.7486, -48.0928, 162.049
$N_2(X,v=20) + CO(X,v=9) \leftrightarrow N_2(X,v=19) + CO(X,v=10)$	nitrogenCO2VV  33.1203, -51.818, 164.014
$N_2(X,v=21) + CO(X,v=9) \leftrightarrow N_2(X,v=20) + CO(X,v=10)$	nitrogenCO2VV  33.5025, -55.2404, 159.984
$N_2(X,v=22) + CO(X,v=9) \leftrightarrow N_2(X,v=21) + CO(X,v=10)$	nitrogenCO2VV  33.4518, -51.6074, 125.475
$N_2(X,v=23) + CO(X,v=9) \leftrightarrow N_2(X,v=22) + CO(X,v=10)$	nitrogenCO2VV  32.6541, -35.7329, 40.0799
$N_2(X,v=24) + CO(X,v=9) \leftrightarrow N_2(X,v=23) + CO(X,v=10)$	nitrogenCO2VV  30.9868, -5.67572, -103.473
$N_2(X,v=25) + CO(X,v=9) \leftrightarrow N_2(X,v=24) + CO(X,v=10)$	nitrogenCO2VV  30.0975, 10.3894, -186.584
$N_2(X,v=26) + CO(X,v=9) \leftrightarrow N_2(X,v=25) + CO(X,v=10)$	nitrogenCO2VV  31.4012, -11.8884, -105.723
$N_2(X,v=27) + CO(X,v=9) \leftrightarrow N_2(X,v=26) + CO(X,v=10)$	nitrogenCO2VV  32.7705, -33.9485, -34.4103
$N_2(X,v=28) + CO(X,v=9) \leftrightarrow N_2(X,v=27) + CO(X,v=10)$	nitrogenCO2VV  32.0509, -19.1746, -125.744
$N_2(X,v=29) + CO(X,v=9) \leftrightarrow N_2(X,v=28) + CO(X,v=10)$	nitrogenCO2VV  37.7578, -109.427, 206.721
$N_2(X,v=30) + CO(X,v=9) \leftrightarrow N_2(X,v=29) + CO(X,v=10)$	nitrogenCO2VV  35.3059, -62.2261, -33.2488
$N_2(X,v=31) + CO(X,v=9) \leftrightarrow N_2(X,v=30) + CO(X,v=10)$	nitrogenCO2VV  27.6315, 76.9357, -675.108
$N_2(X,v=32) + CO(X,v=9) \leftrightarrow N_2(X,v=31) + CO(X,v=10)$	nitrogenCO2VV  27.4622, 77.5115, -682.173
$N_2(X,v=33) + CO(X,v=9) \leftrightarrow N_2(X,v=32) + CO(X,v=10)$	nitrogenCO2VV  31.0404, 10.261, -385.5
$N_2(X,v=34) + CO(X,v=9) \leftrightarrow N_2(X,v=33) + CO(X,v=10)$	nitrogenCO2VV  33.7322, -39.0703, -179.677
$N_2(X,v=35) + CO(X,v=9) \leftrightarrow N_2(X,v=34) + CO(X,v=10)$	nitrogenCO2VV  34.7918, -57.9553, -115.578
$N_2(X,v=36) + CO(X,v=9) \leftrightarrow N_2(X,v=35) + CO(X,v=10)$	nitrogenCO2VV  35.5545, -71.7656, -72.7516
$N_2(X,v=37) + CO(X,v=9) \leftrightarrow N_2(X,v=36) + CO(X,v=10)$	nitrogenCO2VV  36.4783, -88.6724, -14.7636
$N_2(X,v=38) + CO(X,v=9) \leftrightarrow N_2(X,v=37) + CO(X,v=10)$	nitrogenCO2VV  46.2905, -255.678, 673.509
$N_2(X,v=39) + CO(X,v=9) \leftrightarrow N_2(X,v=38) + CO(X,v=10)$	nitrogenCO2VV  33.1156, -14.8287, -435.521
$N_2(X,v=40) + CO(X,v=9) \leftrightarrow N_2(X,v=39) + CO(X,v=10)$	nitrogenCO2VV  30.0684, 35.4771, -653.336
$N_2(X,v=41) + CO(X,v=9) \leftrightarrow N_2(X,v=40) + CO(X,v=10)$	nitrogenCO2VV  33.2786, -28.8421, -349.83
$N_2(X,v=42) + CO(X,v=9) \leftrightarrow N_2(X,v=41) + CO(X,v=10)$	nitrogenCO2VV  36.228, -86.3459, -87.9188
$N_2(X,v=43) + CO(X,v=9) \leftrightarrow N_2(X,v=42) + CO(X,v=10)$	nitrogenCO2VV  37.3816, -109.034, 5.63488
$N_2(X,v=44) + CO(X,v=9) \leftrightarrow N_2(X,v=43) + CO(X,v=10)$	nitrogenCO2VV  37.4509, -111.026, 0.820871
$N_2(X,v=45) + CO(X,v=9) \leftrightarrow N_2(X,v=44) + CO(X,v=10)$	nitrogenCO2VV  37.3873, -110.424, -16.465
$N_2(X,v=46) + CO(X,v=9) \leftrightarrow N_2(X,v=45) + CO(X,v=10)$	nitrogenCO2VV  37.0877, -105.513, -53.3103
$N_2(X,v=47) + CO(X,v=9) \leftrightarrow N_2(X,v=46) + CO(X,v=10)$	nitrogenCO2VV  48.4428, -302.366, 779.847
$N_2(X,v=48) + CO(X,v=9) \leftrightarrow N_2(X,v=47) + CO(X,v=10)$	nitrogenCO2VV  28.8408, 60.34, -904.086

$N_2(X,v=49) + CO(X,v=9) \leftrightarrow N_2(X,v=48) + CO(X,v=10)$	nitrogenCO2VV   29.6015, 39.645, -790.914
$N_2(X,v=50) + CO(X,v=9) \leftrightarrow N_2(X,v=49) + CO(X,v=10)$	nitrogenCO2VV   34.2623, -51.9532, -358.373
$N_2(X,v=51) + CO(X,v=9) \leftrightarrow N_2(X,v=50) + CO(X,v=10)$	nitrogenCO2VV   36.8435, -101.954, -133.755
$N_2(X,v=52) + CO(X,v=9) \leftrightarrow N_2(X,v=51) + CO(X,v=10)$	nitrogenCO2VV   37.2134, -109.272, -114.909
$N_2(X,v=53) + CO(X,v=9) \leftrightarrow N_2(X,v=52) + CO(X,v=10)$	nitrogenCO2VV   37.2188, -109.595, -129.61
$N_2(X,v=54) + CO(X,v=9) \leftrightarrow N_2(X,v=53) + CO(X,v=10)$	nitrogenCO2VV   37.2385, -110.184, -143.131
$N_2(X,v=55) + CO(X,v=9) \leftrightarrow N_2(X,v=54) + CO(X,v=10)$	nitrogenCO2VV   37.0752, -107.442, -171.815
$N_2(X,v=56) + CO(X,v=9) \leftrightarrow N_2(X,v=55) + CO(X,v=10)$	nitrogenCO2VV   50.9359, -351.43, 882.095
$N_2(X,v=57) + CO(X,v=9) \leftrightarrow N_2(X,v=56) + CO(X,v=10)$	nitrogenCO2VV   24.5304, 140.774, -1416.81
$N_2(X,v=58) + CO(X,v=9) \leftrightarrow N_2(X,v=57) + CO(X,v=10)$	nitrogenCO2VV   29.7967, 34.0224, -893.654
$N_2(X,v=59) + CO(X,v=9) \leftrightarrow N_2(X,v=58) + CO(X,v=10)$	nitrogenCO2VV   35.7364, -81.9823, -345.153

ii.  $N_2$ -CO<sub>2</sub> V-V:

The process:

$CO_2(00^0v_i1) + N_2(w_i) \leftrightarrow CO_2(00^0v_f1) + N_2(w_f)$  | KustovaScaling\_CO2v3\_N2 |  $v_i \cdot w_f$  | has a rate coefficient of  $k = v_i \cdot w_f \cdot 1.66 \cdot 10^{-30} \cdot \exp(27.221 + 10.8178 \cdot T^{-1/3} - 224.158 \cdot T^{-2/3})$  in  $m^3s^{-1}$ .

$CO_2(X,v=00011) + N_2(X,v=0) \leftrightarrow CO_2(X,v=00001) + N_2(X,v=1)$ %k=k0*(v3+1)(w+1)	nitrogenCO2VV   43.8, -306, 1288
$CO_2(X,v=00011) + N_2(X,v=1) \leftrightarrow CO_2(X,v=00021) + N_2(X,v=0)$	nitrogenCO2VV   46.953, -349.851, 1482
$CO_2(X,v=00021) + N_2(X,v=1) \leftrightarrow CO_2(X,v=00031) + N_2(X,v=0)$	nitrogenCO2VV   41.6815, -239.359, 944.929
$CO_2(X,v=00031) + N_2(X,v=1) \leftrightarrow CO_2(X,v=00041) + N_2(X,v=0)$	KustovaScaling_CO2v3_N2   4
$CO_2(X,v=00041) + N_2(X,v=1) \leftrightarrow CO_2(X,v=00051) + N_2(X,v=0)$	KustovaScaling_CO2v3_N2   5
$CO_2(X,v=00011) + N_2(X,v=1) \leftrightarrow CO_2(X,v=00001) + N_2(X,v=2)$	nitrogenCO2VV   35.8752, -138.147, 471.585
$CO_2(X,v=00021) + N_2(X,v=1) \leftrightarrow CO_2(X,v=00011) + N_2(X,v=2)$	nitrogenCO2VV   44.8346, -294.813, 1213.08
$CO_2(X,v=00021) + N_2(X,v=2) \leftrightarrow CO_2(X,v=00031) + N_2(X,v=1)$	nitrogenCO2VV   48.0886, -350.201, 1481.91
$CO_2(X,v=00031) + N_2(X,v=2) \leftrightarrow CO_2(X,v=00041) + N_2(X,v=1)$	nitrogenCO2VV   44.0283, -265.507, 1069.99
$CO_2(X,v=00041) + N_2(X,v=2) \leftrightarrow CO_2(X,v=00051) + N_2(X,v=1)$	KustovaScaling_CO2v3_N2   10
$CO_2(X,v=00011) + N_2(X,v=2) \leftrightarrow CO_2(X,v=00001) + N_2(X,v=3)$	KustovaScaling_CO2v3_N2   3
$CO_2(X,v=00021) + N_2(X,v=2) \leftrightarrow CO_2(X,v=00011) + N_2(X,v=3)$	KustovaScaling_CO2v3_N2   6
$CO_2(X,v=00031) + N_2(X,v=2) \leftrightarrow CO_2(X,v=00021) + N_2(X,v=3)$	nitrogenCO2VV   45.2075, -286.167, 1170.46
$CO_2(X,v=00041) + N_2(X,v=2) \leftrightarrow CO_2(X,v=00031) + N_2(X,v=3)$	nitrogenCO2VV   48.6965, -348.305, 1471.57
$CO_2(X,v=00041) + N_2(X,v=3) \leftrightarrow CO_2(X,v=00051) + N_2(X,v=2)$	nitrogenCO2VV   45.8051, -287.873, 1178.84

CO2(X,v=00011) + N2(X,v=3) ↔ CO2(X,v=00001) + N2(X,v=4) | KustovaScaling\_CO2v3\_N2 | 4 |  
 CO2(X,v=00021) + N2(X,v=3) ↔ CO2(X,v=00011) + N2(X,v=4) | KustovaScaling\_CO2v3\_N2 | 8 |  
 CO2(X,v=00031) + N2(X,v=3) ↔ CO2(X,v=00021) + N2(X,v=4) | KustovaScaling\_CO2v3\_N2 | 12 |  
 CO2(X,v=00041) + N2(X,v=3) ↔ CO2(X,v=00031) + N2(X,v=4) | nitrogenCO2VV | 44.6275, -263.695, 1061.25 |  
 CO2(X,v=00051) + N2(X,v=3) ↔ CO2(X,v=00041) + N2(X,v=4) | nitrogenCO2VV | 49.2916, -350.245, 1482.44 |

CO2(X,v=00011) + N2(X,v=4) ↔ CO2(X,v=00001) + N2(X,v=5) | KustovaScaling\_CO2v3\_N2 | 5 |  
 CO2(X,v=00021) + N2(X,v=4) ↔ CO2(X,v=00011) + N2(X,v=5) | KustovaScaling\_CO2v3\_N2 | 10 |  
 CO2(X,v=00031) + N2(X,v=4) ↔ CO2(X,v=00021) + N2(X,v=5) | KustovaScaling\_CO2v3\_N2 | 15 |  
 CO2(X,v=00041) + N2(X,v=4) ↔ CO2(X,v=00031) + N2(X,v=5) | KustovaScaling\_CO2v3\_N2 | 20 |  
 CO2(X,v=00051) + N2(X,v=4) ↔ CO2(X,v=00041) + N2(X,v=5) | nitrogenCO2VV | 43.6765, -236.98, 933.642 |

CO2(X,v=00011) + N2(X,v=5) ↔ CO2(X,v=00001) + N2(X,v=6) | KustovaScaling\_CO2v3\_N2 | 6 |  
 CO2(X,v=00021) + N2(X,v=5) ↔ CO2(X,v=00011) + N2(X,v=6) | KustovaScaling\_CO2v3\_N2 | 12 |  
 CO2(X,v=00031) + N2(X,v=5) ↔ CO2(X,v=00021) + N2(X,v=6) | KustovaScaling\_CO2v3\_N2 | 18 |  
 CO2(X,v=00041) + N2(X,v=5) ↔ CO2(X,v=00031) + N2(X,v=6) | KustovaScaling\_CO2v3\_N2 | 24 |  
 CO2(X,v=00051) + N2(X,v=5) ↔ CO2(X,v=00041) + N2(X,v=6) | KustovaScaling\_CO2v3\_N2 | 30 |

CO2(X,v=00011) + N2(X,v=6) ↔ CO2(X,v=00001) + N2(X,v=7) | KustovaScaling\_CO2v3\_N2 | 7 |  
 CO2(X,v=00021) + N2(X,v=6) ↔ CO2(X,v=00011) + N2(X,v=7) | KustovaScaling\_CO2v3\_N2 | 14 |  
 CO2(X,v=00031) + N2(X,v=6) ↔ CO2(X,v=00021) + N2(X,v=7) | KustovaScaling\_CO2v3\_N2 | 21 |  
 CO2(X,v=00041) + N2(X,v=6) ↔ CO2(X,v=00031) + N2(X,v=7) | KustovaScaling\_CO2v3\_N2 | 28 |  
 CO2(X,v=00051) + N2(X,v=6) ↔ CO2(X,v=00041) + N2(X,v=7) | KustovaScaling\_CO2v3\_N2 | 35 |

CO2(X,v=00011) + N2(X,v=7) ↔ CO2(X,v=00001) + N2(X,v=8) | KustovaScaling\_CO2v3\_N2 | 8 |  
 CO2(X,v=00021) + N2(X,v=7) ↔ CO2(X,v=00011) + N2(X,v=8) | KustovaScaling\_CO2v3\_N2 | 16 |  
 CO2(X,v=00031) + N2(X,v=7) ↔ CO2(X,v=00021) + N2(X,v=8) | KustovaScaling\_CO2v3\_N2 | 24 |  
 CO2(X,v=00041) + N2(X,v=7) ↔ CO2(X,v=00031) + N2(X,v=8) | KustovaScaling\_CO2v3\_N2 | 32 |  
 CO2(X,v=00051) + N2(X,v=7) ↔ CO2(X,v=00041) + N2(X,v=8) | KustovaScaling\_CO2v3\_N2 | 40 |

CO2(X,v=00011) + N2(X,v=8) ↔ CO2(X,v=00001) + N2(X,v=9) | KustovaScaling\_CO2v3\_N2 | 9 |  
 CO2(X,v=00021) + N2(X,v=8) ↔ CO2(X,v=00011) + N2(X,v=9) | KustovaScaling\_CO2v3\_N2 | 18 |  
 CO2(X,v=00031) + N2(X,v=8) ↔ CO2(X,v=00021) + N2(X,v=9) | KustovaScaling\_CO2v3\_N2 | 27 |  
 CO2(X,v=00041) + N2(X,v=8) ↔ CO2(X,v=00031) + N2(X,v=9) | KustovaScaling\_CO2v3\_N2 | 36 |  
 CO2(X,v=00051) + N2(X,v=8) ↔ CO2(X,v=00041) + N2(X,v=9) | KustovaScaling\_CO2v3\_N2 | 45 |

CO2(X,v=00011) + N2(X,v=9) ↔ CO2(X,v=00001) + N2(X,v=10) | KustovaScaling\_CO2v3\_N2 | 10 |  
CO2(X,v=00021) + N2(X,v=9) ↔ CO2(X,v=00011) + N2(X,v=10) | KustovaScaling\_CO2v3\_N2 | 20 |  
CO2(X,v=00031) + N2(X,v=9) ↔ CO2(X,v=00021) + N2(X,v=10) | KustovaScaling\_CO2v3\_N2 | 30 |  
CO2(X,v=00041) + N2(X,v=9) ↔ CO2(X,v=00031) + N2(X,v=10) | KustovaScaling\_CO2v3\_N2 | 40 |  
CO2(X,v=00051) + N2(X,v=9) ↔ CO2(X,v=00041) + N2(X,v=10) | KustovaScaling\_CO2v3\_N2 | 50 |

CO2(X,v=00011) + N2(X,v=10) ↔ CO2(X,v=00001) + N2(X,v=11) | KustovaScaling\_CO2v3\_N2 | 11 |  
CO2(X,v=00021) + N2(X,v=10) ↔ CO2(X,v=00011) + N2(X,v=11) | KustovaScaling\_CO2v3\_N2 | 22 |  
CO2(X,v=00031) + N2(X,v=10) ↔ CO2(X,v=00021) + N2(X,v=11) | KustovaScaling\_CO2v3\_N2 | 33 |  
CO2(X,v=00041) + N2(X,v=10) ↔ CO2(X,v=00031) + N2(X,v=11) | KustovaScaling\_CO2v3\_N2 | 44 |  
CO2(X,v=00051) + N2(X,v=10) ↔ CO2(X,v=00041) + N2(X,v=11) | KustovaScaling\_CO2v3\_N2 | 55 |

CO2(X,v=00011) + N2(X,v=11) ↔ CO2(X,v=00001) + N2(X,v=12) | KustovaScaling\_CO2v3\_N2 | 12 |  
CO2(X,v=00021) + N2(X,v=11) ↔ CO2(X,v=00011) + N2(X,v=12) | KustovaScaling\_CO2v3\_N2 | 24 |  
CO2(X,v=00031) + N2(X,v=11) ↔ CO2(X,v=00021) + N2(X,v=12) | KustovaScaling\_CO2v3\_N2 | 36 |  
CO2(X,v=00041) + N2(X,v=11) ↔ CO2(X,v=00031) + N2(X,v=12) | KustovaScaling\_CO2v3\_N2 | 48 |  
CO2(X,v=00051) + N2(X,v=11) ↔ CO2(X,v=00041) + N2(X,v=12) | KustovaScaling\_CO2v3\_N2 | 60 |

CO2(X,v=00011) + N2(X,v=12) ↔ CO2(X,v=00001) + N2(X,v=13) | KustovaScaling\_CO2v3\_N2 | 13 |  
CO2(X,v=00021) + N2(X,v=12) ↔ CO2(X,v=00011) + N2(X,v=13) | KustovaScaling\_CO2v3\_N2 | 26 |  
CO2(X,v=00031) + N2(X,v=12) ↔ CO2(X,v=00021) + N2(X,v=13) | KustovaScaling\_CO2v3\_N2 | 39 |  
CO2(X,v=00041) + N2(X,v=12) ↔ CO2(X,v=00031) + N2(X,v=13) | KustovaScaling\_CO2v3\_N2 | 52 |  
CO2(X,v=00051) + N2(X,v=12) ↔ CO2(X,v=00041) + N2(X,v=13) | KustovaScaling\_CO2v3\_N2 | 65 |

CO2(X,v=00011) + N2(X,v=13) ↔ CO2(X,v=00001) + N2(X,v=14) | KustovaScaling\_CO2v3\_N2 | 14 |  
CO2(X,v=00021) + N2(X,v=13) ↔ CO2(X,v=00011) + N2(X,v=14) | KustovaScaling\_CO2v3\_N2 | 28 |  
CO2(X,v=00031) + N2(X,v=13) ↔ CO2(X,v=00021) + N2(X,v=14) | KustovaScaling\_CO2v3\_N2 | 42 |  
CO2(X,v=00041) + N2(X,v=13) ↔ CO2(X,v=00031) + N2(X,v=14) | KustovaScaling\_CO2v3\_N2 | 56 |  
CO2(X,v=00051) + N2(X,v=13) ↔ CO2(X,v=00041) + N2(X,v=14) | KustovaScaling\_CO2v3\_N2 | 70 |

CO2(X,v=00011) + N2(X,v=14) ↔ CO2(X,v=00001) + N2(X,v=15) | KustovaScaling\_CO2v3\_N2 | 15 |  
CO2(X,v=00021) + N2(X,v=14) ↔ CO2(X,v=00011) + N2(X,v=15) | KustovaScaling\_CO2v3\_N2 | 30 |  
CO2(X,v=00031) + N2(X,v=14) ↔ CO2(X,v=00021) + N2(X,v=15) | KustovaScaling\_CO2v3\_N2 | 45 |  
CO2(X,v=00041) + N2(X,v=14) ↔ CO2(X,v=00031) + N2(X,v=15) | KustovaScaling\_CO2v3\_N2 | 60 |  
CO2(X,v=00051) + N2(X,v=14) ↔ CO2(X,v=00041) + N2(X,v=15) | KustovaScaling\_CO2v3\_N2 | 75 |

















$\text{CO}_2(\text{X},\text{v}=00011) + \text{N}_2(\text{X},\text{v}=57) \leftrightarrow \text{CO}_2(\text{X},\text{v}=00001) + \text{N}_2(\text{X},\text{v}=58) \mid \text{KustovaScaling\_CO2v3\_N2} \mid 58 \mid$   
 $\text{CO}_2(\text{X},\text{v}=00021) + \text{N}_2(\text{X},\text{v}=57) \leftrightarrow \text{CO}_2(\text{X},\text{v}=00011) + \text{N}_2(\text{X},\text{v}=58) \mid \text{KustovaScaling\_CO2v3\_N2} \mid 116 \mid$   
 $\text{CO}_2(\text{X},\text{v}=00031) + \text{N}_2(\text{X},\text{v}=57) \leftrightarrow \text{CO}_2(\text{X},\text{v}=00021) + \text{N}_2(\text{X},\text{v}=58) \mid \text{KustovaScaling\_CO2v3\_N2} \mid 174 \mid$   
 $\text{CO}_2(\text{X},\text{v}=00041) + \text{N}_2(\text{X},\text{v}=57) \leftrightarrow \text{CO}_2(\text{X},\text{v}=00031) + \text{N}_2(\text{X},\text{v}=58) \mid \text{KustovaScaling\_CO2v3\_N2} \mid 232 \mid$   
 $\text{CO}_2(\text{X},\text{v}=00051) + \text{N}_2(\text{X},\text{v}=57) \leftrightarrow \text{CO}_2(\text{X},\text{v}=00041) + \text{N}_2(\text{X},\text{v}=58) \mid \text{KustovaScaling\_CO2v3\_N2} \mid 290 \mid$

$\text{CO}_2(\text{X},\text{v}=00011) + \text{N}_2(\text{X},\text{v}=58) \leftrightarrow \text{CO}_2(\text{X},\text{v}=00001) + \text{N}_2(\text{X},\text{v}=59) \mid \text{KustovaScaling\_CO2v3\_N2} \mid 59 \mid$   
 $\text{CO}_2(\text{X},\text{v}=00021) + \text{N}_2(\text{X},\text{v}=58) \leftrightarrow \text{CO}_2(\text{X},\text{v}=00011) + \text{N}_2(\text{X},\text{v}=59) \mid \text{KustovaScaling\_CO2v3\_N2} \mid 118 \mid$   
 $\text{CO}_2(\text{X},\text{v}=00031) + \text{N}_2(\text{X},\text{v}=58) \leftrightarrow \text{CO}_2(\text{X},\text{v}=00021) + \text{N}_2(\text{X},\text{v}=59) \mid \text{KustovaScaling\_CO2v3\_N2} \mid 177 \mid$   
 $\text{CO}_2(\text{X},\text{v}=00041) + \text{N}_2(\text{X},\text{v}=58) \leftrightarrow \text{CO}_2(\text{X},\text{v}=00031) + \text{N}_2(\text{X},\text{v}=59) \mid \text{KustovaScaling\_CO2v3\_N2} \mid 236 \mid$   
 $\text{CO}_2(\text{X},\text{v}=00051) + \text{N}_2(\text{X},\text{v}=58) \leftrightarrow \text{CO}_2(\text{X},\text{v}=00041) + \text{N}_2(\text{X},\text{v}=59) \mid \text{KustovaScaling\_CO2v3\_N2} \mid 295 \mid$



## B. Calculated concentrations of all the species considered in the model

Table 4: Densities in  $m^{-3}$  of all the species included in the model, at 2 Torr and 50 mA, for different  $CO_2-N_2$  mixtures for the short tube (length 0.23 cm) where the  $CO_2$  dissociation fraction and NO densities are measured.

CO <sub>2</sub> fraction	2 Torr					
	short tube 0.23 cm					
	0.1	0.25	0.5	0.75	0.9	1
species density ( $m^{-3}$ )						
O <sub>2</sub> (X <sup>3</sup> Σ <sub>g</sub> <sup>-</sup> )	1.59E+20	5.81E+20	1.37E+21	2.14E+21	2.59E+21	2.95E+21
O <sub>2</sub> (a <sup>1</sup> Δ <sub>g</sub> )	1.98E+19	5.22E+19	1.05E+20	1.67E+20	2.10E+20	2.46E+20
O <sub>2</sub> (b <sup>1</sup> Σ <sub>g</sub> <sup>+</sup> )	5.12E+17	6.52E+17	7.00E+17	8.11E+17	9.15E+17	1.04E+18
O <sub>2</sub> (A <sup>3</sup> Δ <sub>u</sub> , A <sup>3</sup> Σ <sub>u</sub> <sup>+</sup> , c <sup>1</sup> Σ <sub>u</sub> <sup>-</sup> )	2.32E+16	4.29E+16	8.00E+16	1.22E+17	1.49E+17	1.66E+17
O <sub>2</sub> <sup>+</sup>	2.45E+15	2.17E+15	1.54E+15	1.56E+15	2.23E+15	9.23E+15
O( <sup>3</sup> P)	1.34E+21	2.00E+21	2.24E+21	2.44E+21	2.61E+21	2.85E+21
O( <sup>1</sup> D)	1.65E+17	7.42E+16	4.17E+16	3.55E+16	3.56E+16	3.80E+16
O <sup>+</sup>	6.16E+13	1.74E+13	6.47E+12	3.89E+12	3.31E+12	3.40E+12
O <sup>-</sup>	3.87E+13	5.39E+13	8.22E+13	1.13E+14	1.34E+14	1.47E+14
O <sub>3</sub>	9.12E+14	3.25E+15	6.29E+15	8.80E+15	1.01E+16	1.18E+16
O <sub>3</sub> <sup>*</sup>	6.58E+11	8.55E+12	4.15E+13	9.22E+13	1.28E+14	1.64E+14
CO <sub>2</sub> (X <sup>1</sup> Σ <sub>g</sub> <sup>+</sup> )	1.20E+21	3.77E+21	8.31E+21	1.26E+22	1.49E+22	1.63E+22
CO <sub>2</sub> <sup>+</sup>	2.86E+14	2.11E+14	1.81E+14	1.61E+14	1.54E+14	1.56E+14
C( <sup>3</sup> P)	4.25E+16	1.73E+16	9.45E+15	7.56E+15	7.22E+15	7.38E+15
CO(a <sup>3</sup> Π <sub>r</sub> )	4.07E+16	3.63E+16	3.54E+16	3.74E+16	3.95E+16	4.18E+16
CO(X <sup>1</sup> Σ <sup>+</sup> )	1.78E+21	3.39E+21	5.37E+21	7.24E+21	8.35E+21	9.24E+21
CO <sup>+</sup>	3.21E+13	9.01E+12	3.43E+12	2.12E+12	1.83E+12	1.91E+12
N <sub>2</sub> (X <sup>1</sup> Σ <sub>g</sub> <sup>+</sup> )	2.68E+22	2.14E+22	1.36E+22	6.53E+21	2.53E+21	
N <sub>2</sub> (A <sup>3</sup> Σ <sub>u</sub> <sup>+</sup> )	1.59E+18	5.62E+17	1.62E+17	4.68E+16	1.45E+16	
N <sub>2</sub> (B <sup>3</sup> Π <sub>g</sub> )	6.89E+16	2.08E+16	9.23E+15	4.00E+15	1.55E+15	
N <sub>2</sub> (C <sup>3</sup> Π <sub>u</sub> )	2.17E+14	1.16E+14	5.32E+13	2.10E+13	7.63E+12	
N <sub>2</sub> (w <sup>1</sup> Δ <sub>u</sub> )	1.15E+16	7.55E+15	4.01E+15	1.73E+15	6.47E+14	
N <sub>2</sub> (a <sup>1</sup> Π <sub>g</sub> )	1.37E+16	7.25E+15	2.70E+15	8.63E+14	2.76E+14	
N <sub>2</sub> (a <sup>1</sup> Σ <sub>u</sub> <sup>-</sup> )	2.49E+17	7.33E+16	1.46E+16	3.81E+15	1.35E+15	
N <sub>2</sub> <sup>+</sup>	4.01E+14	1.23E+14	3.63E+13	1.08E+13	3.59E+12	
N <sub>2</sub> <sup>+</sup> (B <sup>2</sup> Σ <sub>u</sub> <sup>+</sup> )	8.11E+10	2.17E+10	6.37E+09	1.80E+09	5.77E+08	
N( <sup>4</sup> S)	6.21E+18	1.26E+18	2.66E+17	7.85E+16	3.11E+16	
N( <sup>2</sup> D)	1.38E+18	4.57E+17	9.19E+16	2.37E+16	7.89E+15	
N( <sup>2</sup> P)	5.14E+16	5.30E+15	4.44E+14	9.03E+13	3.49E+13	
N <sup>+</sup>	1.64E+12	1.26E+11	7.22E+09	9.67E+08	2.61E+08	
N <sub>4</sub> <sup>+</sup>	1.53E+13	1.56E+12	1.27E+11	7.61E+09	4.10E+08	
N <sub>3</sub> <sup>+</sup>	1.06E+13	6.19E+11	2.98E+10	1.95E+09	1.87E+08	
NO(X <sup>2</sup> Π <sub>r</sub> )	7.91E+19	1.18E+20	1.87E+20	1.88E+20	1.25E+20	
NO(A <sup>2</sup> Σ <sup>+</sup> )	1.83E+15	9.45E+14	4.22E+14	1.20E+14	2.43E+13	
NO(B <sup>2</sup> Π <sub>r</sub> )	7.56E+10	1.81E+10	2.73E+09	5.01E+08	1.28E+08	
NO <sup>+</sup>	7.14E+15	7.71E+15	8.09E+15	7.84E+15	7.08E+15	

NO <sub>2</sub> (X <sup>2</sup> A <sub>1</sub> )	8.92E+15	1.10E+16	1.28E+16	8.55E+15	4.09E+15	
NO <sub>2</sub> (a <sup>4</sup> A <sub>2</sub> )	6.44E+13	1.42E+14	2.52E+14	2.71E+14	1.87E+14	
CN(X <sup>2</sup> Σ <sup>+</sup> )	1.61E+11	5.15E+10	1.66E+10	5.25E+09	1.39E+09	
CN(B <sup>2</sup> Σ <sup>+</sup> )	6.98E+08	2.51E+07	2.65E+06	5.49E+05	1.63E+05	
n <sub>e</sub>	1.04E+16	1.02E+16	9.78E+15	9.46E+15	9.34E+15	9.24E+15

Table 5: Densities in m<sup>-3</sup> of all the species included in the model, at 2 Torr and 50 mA, for different CO<sub>2</sub>-N<sub>2</sub> mixtures for the long tube (length 0.67 cm) where the O density is measured.

CO <sub>2</sub> fraction	2 Torr					
	long tube 0.67 cm					
	0.1	0.25	0.5	0.75	0.9	1
species density (m <sup>-3</sup> )						
O <sub>2</sub> (X <sup>3</sup> Σ <sub>g</sub> <sup>-</sup> )	2.38E+20	9.65E+20	2.18E+21	3.26E+21	3.83E+21	4.25E+21
O <sub>2</sub> (a <sup>1</sup> Δ <sub>g</sub> )	3.10E+19	8.72E+19	1.69E+20	2.53E+20	3.06E+20	3.47E+20
O <sub>2</sub> (b <sup>1</sup> Σ <sub>g</sub> <sup>+</sup> )	1.29E+18	1.70E+18	1.68E+18	1.77E+18	1.88E+18	2.05E+18
O <sub>2</sub> (A <sup>3</sup> Δ <sub>u</sub> , A <sup>3</sup> Σ <sub>u</sub> <sup>+</sup> , c <sup>1</sup> Σ <sub>u</sub> <sup>-</sup> )	2.79E+16	5.79E+16	1.03E+17	1.44E+17	1.67E+17	1.80E+17
O <sub>2</sub> <sup>+</sup>	2.20E+15	1.69E+15	1.21E+15	1.22E+15	1.67E+15	9.44E+15
O( <sup>3</sup> P)	1.70E+21	2.46E+21	2.71E+21	2.95E+21	3.15E+21	3.43E+21
O( <sup>1</sup> D)	3.19E+17	1.25E+17	6.38E+16	5.08E+16	4.95E+16	5.18E+16
O <sup>+</sup>	1.27E+14	2.93E+13	9.59E+12	5.43E+12	4.49E+12	4.54E+12
O <sup>-</sup>	3.23E+13	5.01E+13	7.41E+13	9.57E+13	1.09E+14	1.19E+14
O <sub>3</sub>	1.31E+15	5.38E+15	1.00E+16	1.34E+16	1.49E+16	1.73E+16
O <sub>3</sub> *	1.49E+12	2.26E+13	9.83E+13	1.98E+14	2.60E+14	3.21E+14
CO <sub>2</sub> (X <sup>1</sup> Σ <sub>g</sub> <sup>+</sup> )	5.95E+20	2.20E+21	5.30E+21	8.35E+21	9.98E+21	1.09E+22
CO <sub>2</sub> <sup>+</sup>	1.96E+14	1.43E+14	1.24E+14	1.09E+14	1.03E+14	1.04E+14
C( <sup>3</sup> P)	3.89E+16	1.48E+16	8.44E+15	6.86E+15	6.54E+15	6.62E+15
CO(a <sup>3</sup> Π <sub>r</sub> )	4.34E+16	3.96E+16	3.83E+16	3.90E+16	4.03E+16	4.17E+16
CO(X <sup>1</sup> Σ <sup>+</sup> )	2.34E+21	4.74E+21	7.68E+21	1.02E+22	1.16E+22	1.26E+22
CO <sup>+</sup>	7.94E+13	2.05E+13	7.57E+12	4.50E+12	3.76E+12	3.79E+12
N <sub>2</sub> (X <sup>1</sup> Σ <sub>g</sub> <sup>+</sup> )	2.64E+22	2.07E+22	1.29E+22	6.06E+21	2.31E+21	
N <sub>2</sub> (A <sup>3</sup> Σ <sub>u</sub> <sup>+</sup> )	1.19E+18	3.37E+17	8.76E+16	2.46E+16	7.58E+15	
N <sub>2</sub> (B <sup>3</sup> Π <sub>g</sub> )	5.51E+16	1.59E+16	6.42E+15	2.54E+15	9.32E+14	
N <sub>2</sub> (C <sup>3</sup> Π <sub>u</sub> )	2.01E+14	1.02E+14	4.54E+13	1.74E+13	6.15E+12	
N <sub>2</sub> (w <sup>1</sup> Δ <sub>u</sub> )	1.09E+16	6.09E+15	2.70E+15	1.03E+15	3.65E+14	
N <sub>2</sub> (a <sup>1</sup> Π <sub>g</sub> )	1.25E+16	5.14E+15	1.58E+15	4.77E+14	1.51E+14	
N <sub>2</sub> (a <sup>1</sup> Σ <sub>u</sub> <sup>-</sup> )	1.88E+17	3.85E+16	7.27E+15	2.03E+15	7.28E+14	
N <sub>2</sub> <sup>+</sup>	3.14E+14	9.22E+13	2.81E+13	8.51E+12	2.78E+12	
N <sub>2</sub> <sup>+</sup> (B <sup>2</sup> Σ <sub>u</sub> <sup>+</sup> )	7.17E+10	2.24E+10	7.44E+09	2.27E+09	7.25E+08	
N( <sup>4</sup> S)	5.23E+18	7.42E+17	1.48E+17	4.57E+16	1.82E+16	
N( <sup>2</sup> D)	1.11E+18	2.44E+17	4.29E+16	1.09E+16	3.58E+15	
N( <sup>2</sup> P)	3.27E+16	1.79E+15	1.40E+14	3.02E+13	1.16E+13	
N <sup>+</sup>	1.07E+12	4.25E+10	2.15E+09	2.93E+08	7.94E+07	
N <sub>4</sub> <sup>+</sup>	7.87E+12	6.74E+11	5.88E+10	3.50E+09	1.68E+08	
N <sub>3</sub> <sup>+</sup>	5.28E+12	1.93E+11	8.81E+09	5.80E+08	5.45E+07	
NO(X <sup>2</sup> Π <sub>r</sub> )	9.61E+19	1.68E+20	2.58E+20	2.55E+20	1.80E+20	
NO(A <sup>2</sup> Σ <sup>+</sup> )	1.66E+15	7.99E+14	3.05E+14	8.22E+13	1.76E+13	

NO( $B^2\Pi_r$ )	7.88E+10	1.24E+10	1.72E+09	3.51E+08	1.00E+08	
NO <sup>+</sup>	7.47E+15	8.36E+15	8.68E+15	8.47E+15	7.90E+15	
NO <sub>2</sub> ( $X^2A_1$ )	6.90E+15	1.14E+16	1.39E+16	8.94E+15	4.23E+15	
NO <sub>2</sub> ( $a^4A_2$ )	1.89E+14	3.73E+14	5.14E+14	4.92E+14	3.43E+14	
CN( $X^2\Sigma^+$ )	1.45E+11	4.29E+10	1.45E+10	4.87E+09	1.39E+09	
CN( $B^2\Sigma^+$ )	5.14E+08	1.46E+07	1.43E+06	3.07E+05	9.25E+04	
ne	1.04E+16	1.03E+16	9.99E+15	9.73E+15	9.58E+15	9.44E+15

Table 6: Densities in  $m^{-3}$  of all the species included in the model, at 2 Torr and 50mA, for different CO<sub>2</sub>-N<sub>2</sub> mixtures and including the reactions with N<sub>2</sub>(A,B) from section III.1.1. for the short tube (length 0.23 cm) where the CO<sub>2</sub> dissociation fraction and NO densities are measured.

CO <sub>2</sub> fraction	2 Torr				
	short tube 0.23 cm				
	0.1	0.25	0.5	0.75	0.9
species density ( $m^{-3}$ )					
O <sub>2</sub> ( $X^3\Sigma_g^-$ )	2.49E+20	8.16E+20	1.65E+21	2.31E+21	2.66E+21
O <sub>2</sub> ( $a^1\Delta_g$ )	3.01E+19	7.03E+19	1.25E+20	1.80E+20	2.16E+20
O <sub>2</sub> ( $b^1\Sigma_g^+$ )	1.15E+18	1.07E+18	9.23E+17	9.01E+17	9.48E+17
O <sub>2</sub> ( $A^3\Delta_u, A^3\Sigma_u^+, c^1\Sigma_u^-$ )	3.17E+16	5.69E+16	9.51E+16	1.31E+17	1.52E+17
O <sub>2</sub> <sup>+</sup>	2.33E+15	2.12E+15	1.62E+15	1.61E+15	2.17E+15
O( $^3P$ )	1.56E+21	2.11E+21	2.26E+21	2.42E+21	2.60E+21
O( $^1D$ )	2.63E+17	8.93E+16	4.54E+16	3.61E+16	3.58E+16
O <sup>+</sup>	1.01E+14	2.06E+13	6.87E+12	3.91E+12	3.31E+12
O <sup>-</sup>	3.71E+13	5.61E+13	8.43E+13	1.14E+14	1.33E+14
O <sub>3</sub>	1.39E+15	4.53E+15	7.59E+15	9.50E+15	1.04E+16
O <sub>3</sub> *	1.61E+12	1.62E+13	5.78E+13	1.05E+14	1.34E+14
CO <sub>2</sub> ( $X^1\Sigma_g^+$ )	7.33E+20	3.06E+21	7.53E+21	1.22E+22	1.47E+22
CO <sub>2</sub> <sup>+</sup>	2.21E+14	1.83E+14	1.69E+14	1.57E+14	1.52E+14
C( $^3P$ )	3.49E+16	1.47E+16	8.79E+15	7.32E+15	7.15E+15
CO( $a^3\Pi_r$ )	4.38E+16	3.88E+16	3.72E+16	3.80E+16	3.97E+16
CO( $X^1\Sigma^+$ )	2.21E+21	4.00E+21	5.99E+21	7.59E+21	8.49E+21
CO <sup>+</sup>	6.27E+13	1.28E+13	4.21E+12	2.29E+12	1.88E+12
N <sub>2</sub> ( $X^1\Sigma_g^+$ )	2.65E+22	2.11E+22	1.34E+22	6.50E+21	2.52E+21
N <sub>2</sub> ( $A^3\Sigma_u^+$ )	1.10E+18	3.78E+17	1.23E+17	4.20E+16	1.48E+16
N <sub>2</sub> ( $B^3\Pi_g$ )	3.69E+16	9.00E+15	3.04E+15	1.06E+15	3.71E+14
N <sub>2</sub> ( $C^3\Pi_u$ )	2.01E+14	1.08E+14	5.10E+13	2.05E+13	7.54E+12
N <sub>2</sub> ( $w^1\Delta_u$ )	1.09E+16	6.68E+15	3.52E+15	1.59E+15	6.25E+14
N <sub>2</sub> ( $a^1\Pi_g$ )	1.25E+16	5.91E+15	2.24E+15	7.83E+14	2.66E+14
N <sub>2</sub> ( $a^1\Sigma_u^-$ )	1.99E+17	5.52E+16	1.25E+16	3.60E+15	1.30E+15
N <sub>2</sub> <sup>+</sup>	3.39E+14	1.11E+14	3.52E+13	1.07E+13	3.56E+12
N <sub>2</sub> <sup>+</sup> ( $B^2\Sigma_u^+$ )	7.54E+10	2.20E+10	6.65E+09	1.84E+09	5.81E+08
N( $^4S$ )	5.41E+18	9.63E+17	2.32E+17	7.47E+16	3.01E+16
N( $^2D$ )	9.82E+17	2.87E+17	6.64E+16	2.06E+16	7.86E+15
N( $^2P$ )	3.14E+16	2.82E+15	3.15E+14	7.89E+13	3.34E+13
N <sup>+</sup>	9.71E+11	6.14E+10	4.56E+09	7.87E+08	2.51E+08
N <sub>4</sub> <sup>+</sup>	8.94E+12	1.07E+12	1.08E+11	7.12E+09	3.96E+08

$N_3^+$	5.33E+12	3.12E+11	1.98E+10	1.66E+09	1.85E+08
$NO(X^2\Pi_r)$	8.89E+19	1.24E+20	1.79E+20	1.81E+20	1.30E+20
$NO(A^2\Sigma^+)$	1.42E+15	6.64E+14	3.03E+14	1.03E+14	2.58E+13
$NO(B^2\Pi_r)$	7.55E+10	1.44E+10	2.40E+09	4.80E+08	1.25E+08
$NO^+$	7.33E+15	7.80E+15	8.10E+15	7.79E+15	7.14E+15
$NO_2(X^2A_1)$	9.88E+15	1.13E+16	1.13E+16	6.59E+15	2.75E+15
$NO_2(a^4A_2)$	8.43E+13	1.58E+14	2.43E+14	2.59E+14	1.92E+14
$CN(X^2\Sigma^+)$	1.30E+11	4.28E+10	1.51E+10	4.98E+09	1.35E+09
$CN(B^2\Sigma^+)$	5.01E+08	1.69E+07	2.05E+06	4.92E+05	1.58E+05
$n_e$	1.04E+16	1.02E+16	9.86E+15	9.46E+15	9.34E+15

Table 7: Densities in  $m^{-3}$  of all the species included in the model, for a 50 %  $CO_2$  50 %  $N_2$  initial gas mixture, for different pressures, at 50mA and including the reactions with  $N_2(A,B)$  from section III.1.1. for the short tube (length 0.23 cm) where the  $CO_2$  dissociation fraction and  $NO$  densities are measured.

	50 % $CO_2$ 50 % $N_2$			
	short tube 0.23 cm			
	0.6	1	2	4
Pressure (Torr)	0.6	1	2	4
species density ( $m^{-3}$ )				
$O_2(X^3\Sigma_g^-)$	4.98E+20	6.34E+20	1.36E+21	3.11E+21
$O_2(a^1\Delta_g)$	4.37E+19	5.42E+19	1.05E+20	2.03E+20
$O_2(b^1\Sigma_g^+)$	6.30E+17	6.20E+17	6.97E+17	6.50E+17
$O_2(A'^3\Delta_u, A^3\Sigma_u^+, c^1\Sigma_u^-)$	8.50E+16	6.63E+16	7.93E+16	1.26E+17
$O_2^+$	3.74E+15	2.97E+15	1.54E+15	7.86E+14
$O(^3P)$	1.04E+21	1.60E+21	2.25E+21	2.29E+21
$O(^1D)$	6.21E+16	5.90E+16	4.18E+16	2.35E+16
$O^+$	3.59E+13	2.09E+13	6.49E+12	1.62E+12
$O^-$	1.14E+14	8.73E+13	8.17E+13	9.04E+13
$O_3$	9.48E+15	5.48E+15	6.27E+15	7.67E+15
$O_3^*$	1.21E+13	1.35E+13	4.13E+13	1.19E+14
$CO_2(X^1\Sigma_g^+)$	3.77E+21	5.03E+21	8.31E+21	1.41E+22
$CO_2^+$	9.17E+14	4.60E+14	1.81E+14	8.53E+13
$C(^3P)$	2.49E+16	2.03E+16	9.48E+15	4.25E+15
$CO(a^3\Pi_r)$	5.69E+16	4.65E+16	3.54E+16	2.76E+16
$CO(X^1\Sigma^+)$	2.22E+21	3.10E+21	5.37E+21	9.16E+21
$CO^+$	2.01E+13	1.05E+13	3.43E+12	1.05E+12
$N_2(X^1\Sigma_g^+)$	5.95E+21	8.07E+21	1.36E+22	2.31E+22
$N_2(A^3\Sigma_u^+)$	3.60E+17	2.80E+17	1.62E+17	8.71E+16
$N_2(B^3\Pi_g)$	1.86E+16	1.49E+16	9.25E+15	5.24E+15
$N_2(C^3\Pi_u)$	7.46E+13	6.66E+13	5.32E+13	4.06E+13
$N_2(w^1\Delta_u)$	9.32E+15	7.34E+15	4.02E+15	1.99E+15
$N_2(a^1\Pi_g)$	6.59E+15	5.28E+15	2.71E+15	1.25E+15
$N_2(a'^1\Sigma_u^-)$	3.15E+16	2.60E+16	1.46E+16	8.05E+15
$N_2^+$	1.78E+14	9.74E+13	3.62E+13	1.48E+13
$N_2^+(B^2\Sigma_u^+)$	3.78E+10	1.95E+10	6.37E+09	2.04E+09
$N(^4S)$	5.58E+17	4.52E+17	2.67E+17	1.37E+17
$N(^2D)$	1.99E+17	1.85E+17	9.25E+16	2.94E+16

$N(^2P)$	2.20E+15	1.47E+15	4.46E+14	9.14E+13
$N^+$	1.59E+11	7.00E+10	7.29E+09	4.45E+08
$N_4^+$	5.09E+11	2.79E+11	1.27E+11	7.56E+10
$N_3^+$	2.92E+11	1.53E+11	2.98E+10	4.06E+09
$NO(X^2\Pi_r)$	9.12E+19	1.20E+20	1.87E+20	2.40E+20
$NO(A^2\Sigma^+)$	4.71E+14	4.82E+14	4.23E+14	2.75E+14
$NO(B^2\Pi_r)$	2.16E+09	2.67E+09	2.75E+09	1.75E+09
$NO^+$	3.51E+15	5.38E+15	8.09E+15	9.79E+15
$NO_2(X^2A_1)$	9.96E+14	2.67E+15	1.01E+16	3.11E+16
$NO_2(a^4A_2)$	7.55E+13	1.49E+14	3.09E+14	3.80E+14
$CN(X^2\Sigma^+)$	1.90E+10	2.12E+10	1.67E+10	1.26E+10
$CN(B^2\Sigma^+)$	2.49E+07	1.11E+07	2.67E+06	5.87E+05
$ne$	8.29E+15	8.86E+15	9.78E+15	1.06E+16

Table 8: Densities in  $m^{-3}$  of all the species included in the model, for a 50 %  $CO_2$  50 %  $N_2$  initial gas mixture, for different pressures, at 50mA and including the reactions with  $N_2(A,B)$  from section III.1.1. for the long tube (length 0.67 cm) where the O density is measured.

Pressure (Torr)	50 % $CO_2$ 50 % $N_2$			
	long tube 0.67 cm			
	0.6	1	2	4
species density ( $m^{-3}$ )				
$O_2(X^3\Sigma_g^-)$	8.46E+20	1.08E+21	2.18E+21	4.63E+21
$O_2(a^1\Delta_g)$	7.70E+19	9.45E+19	1.69E+20	2.97E+20
$O_2(b^1\Sigma_g^+)$	1.65E+18	1.64E+18	1.68E+18	1.35E+18
$O_2(A^2\Sigma_u^-, A^3\Sigma_u^+, c^1\Sigma_u^-)$	1.16E+17	8.89E+16	1.03E+17	1.57E+17
$O_2^+$	3.26E+15	2.41E+15	1.21E+15	6.56E+14
$O(^3P)$	1.34E+21	2.03E+21	2.71E+21	2.63E+21
$O(^1D)$	1.02E+17	9.67E+16	6.38E+16	3.31E+16
$O^+$	5.78E+13	3.35E+13	9.59E+12	2.14E+12
$O^-$	1.01E+14	7.66E+13	7.41E+13	8.26E+13
$O_3$	1.46E+16	8.89E+15	1.00E+16	1.13E+16
$O_3^*$	3.51E+13	3.77E+13	9.83E+13	2.34E+14
$CO_2(X^1\Sigma_g^+)$	2.33E+21	3.10E+21	5.30E+21	9.45E+21
$CO_2^+$	6.14E+14	3.07E+14	1.24E+14	5.95E+13
$C(^3P)$	2.17E+16	1.75E+16	8.44E+15	3.98E+15
$CO(a^3\Pi_r)$	6.28E+16	5.09E+16	3.83E+16	2.94E+16
$CO(X^1\Sigma^+)$	3.32E+21	4.55E+21	7.68E+21	1.28E+22
$CO^+$	4.80E+13	2.47E+13	7.57E+12	2.16E+12
$N_2(X^1\Sigma_g^+)$	5.58E+21	7.57E+21	1.29E+22	2.21E+22
$N_2(A^3\Sigma_u^+)$	1.91E+17	1.48E+17	8.76E+16	4.91E+16
$N_2(B^3\Pi_g)$	1.24E+16	1.02E+16	6.42E+15	3.71E+15
$N_2(C^3\Pi_u)$	6.20E+13	5.60E+13	4.54E+13	3.50E+13
$N_2(w^1\Delta_u)$	6.13E+15	4.89E+15	2.70E+15	1.37E+15
$N_2(a^1\Pi_g)$	3.71E+15	3.00E+15	1.58E+15	7.66E+14
$N_2(a^1\Sigma_u^-)$	1.46E+16	1.20E+16	7.27E+15	4.49E+15
$N_2^+$	1.31E+14	7.23E+13	2.81E+13	1.20E+13

$N_2^+(B^2\Sigma_u^+)$	4.02E+10	2.16E+10	7.44E+09	2.47E+09
$N(^4S)$	3.50E+17	2.56E+17	1.48E+17	8.21E+16
$N(^2D)$	1.00E+17	8.90E+16	4.29E+16	1.41E+16
$N(^2P)$	7.82E+14	4.74E+14	1.40E+14	3.23E+13
$N^+$	5.29E+10	2.12E+10	2.15E+09	1.45E+08
$N_4^+$	1.83E+11	1.04E+11	5.88E+10	4.01E+10
$N_3^+$	9.66E+10	4.68E+10	8.81E+09	1.31E+09
$NO(X^2\Pi_r)$	1.32E+20	1.75E+20	2.58E+20	3.02E+20
$NO(A^2\Sigma^+)$	3.59E+14	3.64E+14	3.05E+14	1.86E+14
$NO(B^2\Pi_r)$	1.67E+09	1.81E+09	1.72E+09	1.13E+09
$NO^+$	4.29E+15	6.19E+15	8.68E+15	1.03E+16
$NO_2(X^2A_1)$	1.38E+15	3.76E+15	1.39E+16	3.94E+16
$NO_2(a^4A_2)$	1.43E+14	2.78E+14	5.14E+14	5.49E+14
$CN(X^2\Sigma^+)$	1.62E+10	1.77E+10	1.45E+10	1.17E+10
$CN(B^2\Sigma^+)$	1.61E+07	6.22E+06	1.43E+06	3.42E+05
$n_e$	8.30E+15	8.95E+15	9.99E+15	1.09E+16